INFORMATION TO USERS

This manuscript has been reproduced from the microfilm master. UMI films the text directly from the original or copy submitted. Thus, some thesis and dissertation copies are in typewriter face, while others may be from any type of computer printer.

The quality of this reproduction is dependent upon the quality of the copy submitted. Broken or indistinct print, colored or poor quality illustrations and photographs, print bleedthrough, substandard margins, and improper alignment can adversely affect reproduction.

In the unlikely event that the author did not send UMI a complete manuscript and there are missing pages, these will be noted. Also, if unauthorized copyright material had to be removed, a note will indicate the deletion.

Oversize materials (e.g., maps, drawings, charts) are reproduced by sectioning the original, beginning at the upper left-hand corner and continuing from left to right in equal sections with small overlaps. Each original is also photographed in one exposure and is included in reduced form at the back of the book.

Photographs included in the original manuscript have been reproduced xerographically in this copy. Higher quality 6" x 9" black and white photographic prints are available for any photographs or illustrations appearing in this copy for an additional charge. Contact UMI directly to order.

UMI

A Bell & Howell Information Company
300 North Zeeb Road, Ann Arbor MI 48106-1346 USA
313/761-4700 800/521-0600

INTERBUBBLE GAS DIFFUSION AND THE STABILITY OF FOAMS

by

FRANÇOIS GÉRARD GANDOLFO

A dissertation submitted to the Graduate Faculty in Chemistry in partial fulfillment of the requirements for the degree of Doctor of Philosophy, The City University of New York

1998

This manuscript has been read and accepted for the Graduate Faculty in Chemistry in satisfaction of the dissertation requirements for the degree of Doctor of Philosophy.

12/19/1997
Date

Helen L. Rosano
Chair of Examining Committee

Dec. 23, 1997
Date

Executive Officer

Prof. Arents

Prof. Locke

Dr. Cante

Dr. Saleeb

Dr. Habif

Supervisory Committee

The City University of New York

Abstract

INTERBUBBLE GAS DIFFUSION AND THE STABILITY OF FOAMS

by

François Gérard Gandolfo

Adviser: Professor Henri Louis Rosano

Powders consisting of solid microspheres, produced by spray-drying a feed composed of a surfactant and a shell-forming substance, have many applications in the medical and food industries, one of the most familiar being foaming coffee-creamer powders. These are typically dissolved in an aqueous solution (coffee at near boiling temperatures) and produce a foam in addition to adding a creamlike flavor. The present study discusses (i) the role played by the physico-chemical properties of the feed, and by the spray-drying process itself, in determining the characteristics of the powder; (ii) factors affecting the foamability, i.e., the ability to form a liquid film, of various aqueous solutions; and (iii) the stability and decay of the resulting foam.

The external and internal structure of foaming creamer powders was investigated with an electron scanning microscope. Next, the surface tension and foamability of various aqueous solutions were determined using the tensiolaminometric technique. An investigation of the foamability of a mixture of a milk protein and sucrose ester showed a synergistic effect.

After the microspheres of the powder are dissolved, the resulting foam may undergo decay arising either from liquid drainage, whether gravitational or due to interbubble gas diffusion, or from rupture of the interbubble liquid lamellae. In studying factors affecting foam stability, I focused on interbubble gas diffusion, which works against stability even given a stable lamella. I show that liquid drainage from the foam due to such diffusion (as distinct from that due to gravitation) can often be greatly reduced by adding a water-insoluble vapor to the foam-generating gas: the presence of such a vapor counterbalances the Ostwald ripening, thus stabilizing the system. The rate of disproportionation is governed not only by differences in Laplace pressure but also by the gas composition and the rheological behavior of the liquid-gas interface. The permeability of the interbubble lamellae also plays an important role.

Acknowledgments

My first thanks go to Professor Henri Louis Rosano, my mentor, who took me into his laboratory and provided me with the essentials for my success in graduate school: partial financial support, confidence, knowledge, and ever-exciting research topics. His insights into practical problem-solving in chemistry have been invaluable in my development as a chemist.

I would also like to thank the members of my thesis committee--these were, besides Professor Rosano, Professors John Arents and David Locke of The City University of New York; Dr. Charles Cante and Dr. Fouad Saleeb, Kraft Foods, Tarrytown, New York; and Dr. Stéphane Habif, Unilever Research U.S., Edgewater, New Jersey--for their help and support.

I feel the deepest gratitude for the financial support provided by Alliance Pharmaceutical Corp., San Diego, California. I would particularly like to thank Duane Roth (President and CEO), Jeff Weers, Alexey Kabalnov, and Leo Trevino, for making my work more efficient.

Similarly, I would like to acknowledge the financial and technical support of Kraft Foods. There Peter Wilson, Fouad Saleeb, Gail Conti, Ken Kale, and Lou Anne Blanchard taught me a lot about foaming creamers (Maxwell House's Cappuccino, in particular).

I would like to thank various members of the faculty of The City University of New York for financial support: Professor Richard Pizer (Executive Officer of the doctoral program in Chemistry), Professor Stanley Radel (Chairman of the City College Chemistry Department), Professor Michael Green (former Chairman), and Dr. Laurent Mars. Thanks to Scott Berlant, John Downey, and Hugo Schimatz for their guidance and technical support.

I would like to thank my friends: Martha Browne for her editorial help; Jean-Denis Hidrot for his collaboration in the laboratory; Javier Gomez (Columbia University) for his technical assistance; and specially Carmen Reinoso Becerra for being with me.

Last but not least, my everlasting love and gratitude to my parents, Amal and Gérard, and my brother, Frédéric, who always trusted my decisions, supported me, and let me be who I am today.

Table of contents

Copyright ii

Approval iii

Abstract iv

Acknowledgments vi

Table of contents viii

List of figures xi

List of tables xvii

Introduction 1

Chapter 1 Scanning electron microscope study of microspheres obtained by spray-drying 5

1.1 Introduction 6

1.2 The process of spray-drying 7

1.2.1 Definition 7

1.2.2 Drying of spray (moisture evaporation) 7

1.3 Foam spray-drying (a variant of spray-drying) 9

1.3.1 General considerations 9

1.3.2 Stability of the foam/gaseous emulsion 10

1.3.3 Characteristics of the product 11

1.4 Literature review of spray-dried milk powders 11

1.5 Experimental part 15

1.5.1 Materials 15

1.5.2 Methods 16

1.6 Results and discussion 17

Chapter 2 The tensiolaminometric technique for studying the foamability of solutions 36

2.1 Introduction 37

2.2 Description of the tensiolaminometer 38

2.2.1 Procedure 38

2.2.2 Influence of the speed of withdrawal 39

2.2.3 Reversibility 40

2.3 Theoretical study of the deformation of a liquid surface by a rectangular frame 41

2.4 Experimental part 45

2.4.1 Materials 45

2.4.2 Methods 45

2.5 Results and discussion 46

2.5.2 A well-known example of foam booster 47

2.5.3 Influence of sugar ester on a solution of milk protein 47

2.5.4 Foamability of a solution of milk protein with different additives 48

Chapter 3 Interbubble gas diffusion and the stability of foams 60

3.1 Introduction 61

3.2 Theory 65

3.3 Experimental part 68

3.3.1 Materials 68

3.3.2 Methods 69

3.4 Results and discussion 70

3.4.1 Influence of the gas composition in the

bubbles 70

3.4.2 Influence of the structure and permeability of the liquid lamella 74

Chapter 4 Models for the behavior of bubbles containing a gas insoluble in the continuous phase 104

4.1 Predicting changes in bubble-size distribution due to interbubble gas diffusion in foams: Lemlich's Theory 105

4.2 Bubbles containing a gas insoluble in the continuous phase : Lemlich's theory modified 108

4.3 Numerical simulation 111

4.3.1 Values for R_{21} and Φ 111

4.3.2 Curves of dR/dY as a function of R 111

4.3.3 Influence of the amount of insoluble gas 112

4.3.4 Variation of the radius as a function of time 112

4.3.5 Is the hypothesis of constant R_{21} reasonable ? 113

4.3.6 Stable equilibrium condition 113

Conclusion 122

Appendix 124

Bibliography 132

List of Figures

1.1 Schematic of the process of spray-drying 22

1.2 Rotary atomizer in operation 23

1.3 A pilot-plant spray-dryer 23

1.4 Mechanism of droplet drying illustrated in simplified manner. Droplets dry to single, misshapen particles 24

1.5 Scanning Electron Micrograph of "KFI Foaming Creamer" showing a large particle with a lot of broken pieces and holes on the surface 25

1.6 Scanning Electron Micrograph of the internal structure of the wall of a hollow microsphere of "KFI Foaming Creamer" 25

1.7 Scanning Electron Micrograph of "Non-gasified control creamer" showing small spherical particles, and no broken pieces 26

1.8 Scanning Electron Micrograph of "Non-gasified control creamer" showing wrinkled surfaces, and small particles embedded in larger particles 26

1.9 Scanning Electron Micrograph of the internal structure of "Non-gasified control creamer" showing a hollow particle with a thick wall full of voids 27

1.10 Scanning Electron Micrograph of "KFI creamer Alapro Substitution" showing wrinkled surfaces, and a lot of particles embedded in each other 27

1.11 Scanning Electron Micrograph of "KFI creamer TMP

Substitution" showing collapsed particles 28

1.12 Scanning Electron Micrograph of TMP showing collapsed particles 28

1.13 Scanning Electron Micrograph of the internal structure of "KFI creamer TMP Substitution" showing a hollow particle with a thin wall 29

1.14 Scanning Electron Micrograph of the internal structure of the wall of a "KFI creamer TMP Substitution" particle showing a wall full of small voids 29

1.15 Scanning Electron Micrograph of "KFI creamer 2% Bicarbonate" showing spherical particles 30

1.16 Scanning Electron Micrograph of the internal structure of "KFI creamer 2% Bicarbonate" showing a hollow particle with a thin wall 30

1.17 Scanning Electron Micrograph of the internal structure of "LFHP 0.132" powder 31

1.18 Scanning Electron Micrograph of the internal structure of "HFLP 0.116" powder 31

1.19 Scanning Electron Micrograph of the internal structure of "HFHP 0.152" powder 32

1.20 Scanning Electron Micrograph of the internal structure of "HFLP 0.164" powder 32

1.21 Scanning Electron Micrograph of the internal structure of "LPHF 0.163" powder 33

1.22 Scanning Electron Micrograph of Imagent US showing very small particles aggregated 33

1.23 Scanning Electron Micrograph of Imagent US 34

2.1 The tensiolaminometer 50

2.2 Theoretical shape of the curves 51

2.3 Shape of the curves given by the tensiolaminometer for reversible and irreversible surface adsorption 52

2.4 Adsorption behavior showing how the dynamic surface tension values differ from the equilibrium adsorption value γ_o 53

2.5 Experimental shape of the curves 54

2.6 Foamability and Surface Tension of Sodium Dodecyl sulfate (SDS) with Lauric diethanolamide (Ninol 96-SL) 55

2.7 Influence of different foaming agents on a solution of milk protein 56

3.1a Calculated r_a/r_b at equilibrium versus r_a/r_b initial for various values of θ 79

3.1b Graph of θ versus v for y=1.5 and 1.2 80

3.2 Experimental setup to study the drainage of a standing foam 81

3.3 Typical result of a drainage experiment and interpolation by a biphasic first-order kinetic equation. Solution : 1g/L of Pluronic F68. N_2 saturated with water or with PFH, Foam surface velocity=0.22 cm/s, V_O=50ml, Temperature=30°C. Curve I: Correlation by a biphasic first-order kinetic equation (τ_g=276s and τ_d=190s). Curve II: Correlation by a biphasic first-order kinetic equation (τ_g=243s and τ_d=4203s) 82

3.4 Effect of the addition of various perfluorocarbon vapors to the air of the bubbles. Solution : 1g/L of Pluronic F68.

V_O=50ml, Temperature=20°C 83

3.5 Effect of initial insoluble vapor percentage (FC104) in the CO_2 Foam-generating gas on liquid drainage. Solution : 1g/L of Pluronic F68. V_O=50ml, Temperature=25°C, Rate of foam formation=0.22 cm/s 84

3.6 Photograph at 1900 seconds of a foam containing 3.75% of FC104 in the CO_2-generating gas 85

3.7 Photograph at 220 seconds of a foam containing 0.203 % FC104 in the CO_2-generating gas 86

3.8 Comparison between two gases, CO_2 and N_2, with and without PFH. Solution : 1g/L of Pluronic F68. V_O=50ml, Temperature =30°C, Rate of foam formation=0.22 cm/s 87

3.9 Difference between the % of water retained in the foam in experiments with and without PFH at various temperatures. Solution: 1g/L of Pluronic F68. V_O=50ml, Rate of foam formation=0.22 cm/s 88

3.10a Drainage curve and foam height of a milk protein foam as a function of time, when the foam generating gas is air. Solution: Alapro milk protein 0.5%, V_O=50ml, Temperature= 80°C 89

3.10b Drainage curve and foam height of a milk protein foam as a function of time, when the foam generating gas is air with PFH. Solution: Alapro milk protein 0.5%, V_O=50ml, Temperature=80°C 90

3.11 a) Results of drainage experiments for formulation A. b) Foam heights of drainage experiments for formulation A. Solution : 1g/100ml of formulation A. CO_2 saturated with water or with PFH, Foam surface velocity=0.35 cm/s, V_O=50ml,

Temperature =21°C 91

3.12 a) Results of drainage experiments for formulation B. b) Foam heights of drainage experiments for formulation B. Solution : 1g/100ml of formulation B. CO_2 saturated with water or with PFH, Foam surface velocity=0.35 cm/s, V_O=50ml, Temperature =21°C 93

3.13 a) Results of drainage experiments for formulation C. b) Foam heights of drainage experiments for formulation C. Solution : 1g/100ml of formulation C. CO_2 saturated with water or with PFH, Foam surface velocity=0.35 cm/s, V_O=50ml, Temperature=21°C 95

3.14 a) Results of drainage experiments for formulation D. b) Foam heights of drainage experiments for formulation D. Solution : 1g/100ml of formulation D. CO_2 saturated with water or with PFH, Foam surface velocity=0.35 cm/s, V_O=50ml, Temperature=21°C 97

3.15 Difference between the % of water retained in the foam in experiments with and without PFH. Solutions : 1g/100ml of Pluronic F68, formulation A, B, C and D. V_O=50ml, Rate of foam formation=0.35 cm/s, Temperature=21°C 99

3.16 Drainage curves for Sodium dodecyl sulfate (0.2% w/v) alone and with Lauryl alcohol (0.012% w/v). Vo=50ml, Rate of foam formation 0.44 cm/sec, T=25°C, CO_2 foam 100

3.17 Drainage curves for Sodium dodecyl sulfate (0.2% w/v) alone and with Xanthan Gum (0.025% w/v). Vo=50ml, Rate of foam formation 0.44 cm/sec, T=25°C, CO_2 foam 101

4.1 Distribution of de Vries 115

4.2 Distribution of Bayens

4.3 Plot of dR/dY as a function of the radius R for $\Phi = 0.05$, $R_{21} = 1.5$, $R_o = 0.6$ 116

4.4 Plot of dR/dY for several initial radii (R_o) and with $\Phi = 0.05$, $R_{21} = 1.5$ 117

4.5 Effect of increasing the osmotic pressure ($\Phi = 0.05, 0.1, 0.2, 1, 5$) for $R_{21} = 1.5$ and $R_o = 0.4$ 118

4.6 Radius at equilibrium versus initial radius R_o 119

4.7 Curves of radius versus time for a bubble with and without an osmotic pressure, with $R_o = 0.8$, $R_{21} = 1.5$ and $\Phi = 0, 0.05, 0.2, 0.5$ 120

4.8 Plot of dR/dY for different R_{21} (1.5, 1.7, 2) and $\Phi = 0.05$, $R_o = 0.5$, and $R_{21o} = 1.5$ 121

List of Tables

1.1 Description of the morphology of the foaming creamer (L: low, H: high, F: fat, P: protein) 35

2.1 Foamability and surface tension of various solutions measured at 30°C with a glass frame according to procedure #2. (CS: cleaning the surface, NCS: without cleaning the surface) 57

2.2 Foamability and surface tension of various solutions measured at 80°C with a platinum frame according to procedure #3 without cleaning the surface 58

2.3 Foamability and surface tension of various solutions measured at 80°C with a platinum frame according to procedure #3 after cleaning the surface 59

3.1 Physical characteristics of Fluorinert 102

3.2 Vapor pressure of FC104 as a function of the temperature 103

INTRODUCTION

This thesis is not just about the "Interbubble gas diffusion and the stability of foams" referred to in the title. It is really the story of a scientific investigation of a practical problem. Indeed, when I first arrived in Professor Henri Rosano's laboratory from France in August 1994, one of the goals of his research team was an enhanced understanding of the workings of coffee creamers--more formally, of the phenomena occurring when a powder consisting of hollow microspheres is dissolved in an aqueous solution to produce a dispersion of bubbles and thus generate a certain amount of stable foam. (This investigation was carried out under contract with Kraft Foods and Alliance Pharmaceutical.)

As I rapidly learned in my first days on the project, powders consisting of solid microspheres -- produced by spray-drying a solution composed of one or more surfactants and a shell-forming substance -- have wide applications in medical and food industries, with coffee creamers among the most well-known.

Spray-drying is a widely used technique to facilitate storage and handling of food products. In a spray-dried food powder, the fat is in many cases the component which is most sensitive to oxidation. It is therefore often desirable to encapsulate the fat to protect it from oxidation.

In addition, the presence of fat on a powder surface reduces the wettability and the dispersibility of the powder in water.

In the case of a powdered coffee foaming creamer, the powder will eventually be dispersed into coffee or hot water, and the objective (given consumer preferences) is the formation of a fine and lasting foam. The microspheres must be rigid enough not to break during storage in the packaged mix, and the rate of dissolution of the powder in hot liquid must be slow enough to allow the formation of a foaming solution in which the gas entrapped within the microspheres will be released as foam bubbles.

I started to work on the project right away, with one principle in mind. When we want to find out something that we do not know, there are two ways to proceed: by seeking expert advice, either in conversation or by reading the works of recognized scholars (an excellent plan if anyone happens to have answered precisely the question we are asking), or by devising an experiment and finding out ourselves.[1] The second way, I have found, often has the added benefit of showing not just *what* but *how*. And in the present case, my search for answers to the coffee creamer problem led to a deeper theoretical understanding of the problems of foam stability and interbubble gas diffusion that are the subject of this thesis.

Adopting the "do-it-yourself" method, I sought first of all to characterize the appearance of powders resulting from gasified, spray-dried protein/carbohydrate systems. The characterization of these powders was achieved by examining the microstructures of several foaming

---

[1] Boys, C.V., Soap-bubbles, Dover Publications, Inc., New York (1959), p 14

creamers with a scanning electron microscope both as is (to determine external structure) and crushed (to determine internal structure). Chapter 1 reviews the process of spray-drying and shows our results on the microstructure of these microspheres.

Then, using the tensiolaminometric technique, I determined the surface tension and the foamability, defined as the ability to form a liquid film, of several mixtures of foaming and shell-forming compounds. I measured the foaming behavior of milk protein solutions and the "foaming potential" both alone and in combination with the milk protein of different ingredients that could be added to the aqueous carbohydrate/systems before spray-drying. Chapter 2 presents this technique and gives results on different systems investigated.

But besides the properties of the interfaces, another important factor to consider when analyzing foam stability is the role of the diffusion of gas between gas bubbles. I built a device to study the stability of a foam by measuring the rate of drainage. With this apparatus, I was able to show that it was possible to stabilize a foam regarding interbubble gas diffusion (Ostwald ripening) by adding a vapor of an insoluble compound to the gas used to generate the foam. The stabilization effect of this insoluble vapor is explained theoretically. Furthermore, the reduction of gas diffusion by changing the permeability and the rheological properties of the interface is demonstrated. Chapter 3 thus describes my investigation of gas diffusion and presents ways to reduce it.

Finally, Chapter 4 presents the theory of Lemlich, which describes the effect of gas diffusion on a distribution of bubbles. I add to this theory a consideration of the effect of adding an insoluble compound to the gas of the bubbles.

Chapter 1

Scanning electron microscope study of microspheres obtained by spray-drying

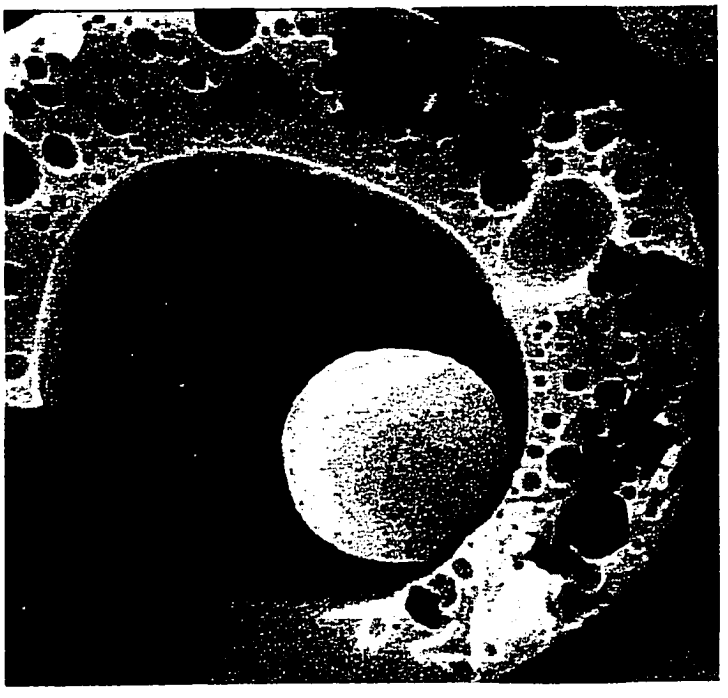

1.1 Introduction

As a first step in my investigation of spray-dried powders, I undertook to characterize several foaming creamers from Kraft Foods and powders from Alliance Pharmaceutical Corporation, studying both their external structure and their internal structure with a scanning electron microscope. (Scanning electron microscopy (S.E.M.) has traditionally been used to characterize powders, especially food powders[2] The reasons for using it are numerous: high resolution providing details several nanometers in diameter, ability to study surfaces as well as internal structure, and ability to examine samples in the frozen hydrated state. Scientific papers on electron microscopy of milk powders may be found in various journals, particularly *Food Structure*, *Journal of Dairy Science*, and *Journal of Dairy Research.*) In interpretating these micrographs a basic grasp of the process of formation of these powders is indispensable; I accordingly present a review of the process of spray-drying and the mechanism of drying of a droplet. I also describe foam spray-drying, since most powders under investigation are obtained by this variant of spray-drying that allows the density of the powder to be controlled. Finally, the pictures I obtained are compared with S.E.M. investigations described in the literature on protein/carbohydrate systems, to better understand the effect of the different constituents in the powders I studied.

---

[2] Kaláb, M., Food Struct., **12**, 95 (1993).

1.2 The process of spray-drying[3]

1.2.1 Definition.

Spray-drying, as illustrated in Figure 1.1, is by definition the transformation of feed (such as preconcentrated milk) from a fluid to a dried state by spraying it into a hot drying medium. It is a one-step continuous suspended particle processing operation. The resulting dried product consists of a granular powder, the precise form of which depends both on the physical and chemical properties of the feed and on the dryer design and operation. The dried particles that result from spray-drying can have highly diverse forms, range in size from 10μm to 300μm, and can exhibit greater or lesser degrees of structural uniformity.

Two essential steps of the spray-drying process are the **atomization** of feed into a spray of fine droplets 10 to 250 μm in diameter, and **contact** between the spray and a drying medium (usually air), with resultant moisture evaporation. The drying of the spray proceeds until the desired moisture content in the dried particles is obtained, and the product is recovered from the air. The atomizer usually consists of a centrifugal disc or a pressure nozzle. Figure 1.2 shows the atomization of the feed by a centrifugal disc. Figure 1.3 shows a pilot-plant spray-dryer.

1.2.2 Drying of spray (moisture evaporation)

---

[3] Masters, K., Spray Drying Handbook, 5th ed., John Wiley & Sons Inc., New York (1991).

The drying history of the droplets is very important to an understanding of the structure of the microspheres. As soon as the droplets of the spray come into contact with the drying air, evaporation takes place from the saturated vapor film that is quickly established at the droplet surface. The temperature at the droplet surface approximates the wet-bulb temperature of the drying air. Evaporation takes place in two stages. At first there is sufficient moisture within the droplet to replenish that lost at the surface. Diffusion of moisture from within the droplet maintains saturated surface conditions, and as long as this lasts, evaporation takes place at a constant rate. This is termed the first, or "constant rate," period of drying. When the moisture content becomes too low to maintain saturated conditions, the so-called critical point is reached and a dried shell forms at the droplet surface. Evaporation is now dependent upon the rate of moisture diffusion through the dried surface shell. The thickness of the dried shell increases with time, causing a decrease in the rate of evaporation. This is termed the second, or "falling rate," period of drying. Different products exhibit different evaporation characteristics. Some tend to expand, while others collapse, fracture, or disintegrate, leading to porous, irregularly shaped particles, as illustrated in Figure 1.4.

In a simplified manner, we can say that the shape of the particles depends on the properties of the crust. If it is pervious to water then the particle will collapse and shrink. If the crust is impervious to water then the particle will explode, leading to a lot of broken pieces. Thus the particle shape is closely connected to the drying history and the properties of the crust.

1.3 Foam spray-drying (a variant of spray-drying)[4,5]

1.3.1 General considerations.

On occasion, it is advantageous to introduce gases into the feed stock prior to atomization. The feed is then dried in the form of already foamed droplets, with foam formation occurring either before, during, or after atomization and before or during the drying itself. The presence of such gases, or of their precursors, has been reported to influence directly the drying characteristics of the drops, the properties of the dried particles, and the operation of the dryer itself.

Foams are generally considered to be dispersions of large volumes of gas in small amounts of liquid, whereas gaseous emulsions are dispersions of small volumes of gas in large amounts of liquid. Such foams have a distinct structure, and resemble, in some respects, moldable bodies in which the gas particles are polyhedral in shape and are separated by relatively thin liquid films. Emulsions, in which the gas bubbles are small and spherical, have little or no structure and usually resemble liquids. The foams generated during spray-drying generally lie between these two extremes. With the methods used to mix dispersed and dissolved gases with the feed stock, it is extremely doubtful that a uniform dispersion or solution of the gas ever reaches the atomizer because of poor bulk mixing, nonuniformity of the generated dispersion, and/or incomplete dissolution. The relationship between volume-fraction of gas in a foam, α_v, and the volume-ratio of gas to feed stock, v_v, is given by $\alpha_v = v_v/(1+v_v)$. The

---

[4] Crosby, E.J. and Weyl, R.W., AIChE Symp. Ser., **73**, 82 (1977).
[5] Frey, D.D. and King, C.J., Ind. Eng. Chem. Fundam., **25**, 723 (1986).

effective mixing of 40 volumes of gas with 1 volume of liquid results in the volume-fraction of gas in the final foam being 0.98. A decrease in mixing effectiveness reduces the volume-fraction of the gas.

The three basic ways to form dispersions of gases in liquids are (i) direct mixing, (ii) desorption from solution, and (iii) chemical generation. Direct mixing involves the intimate mechanical blending of two immiscible bulk phases. Desorption involves the supersaturation of a liquid containing a dissolved gas with subsequent bubble formation and growth by either reduction of pressure or increase in temperature. In chemical generation, also a desorption process, the gas in question is produced by a chemical reaction within the drop. Foaming can be expected from the decomposition of an aqueous solution of sodium bicarbonate. All three methods have found use in spray-drying.

1.3.2 Stability of the foam/gaseous emulsion

As long as the continuous phase in a foam or emulsion is fluid, the system is essentially unstable.

In the case of very dilute, gaseous emulsions, the steady-state motion of the bubbles relative to the continuous Newtonian liquid phase is probably described reasonably well by Stoke's law. When the drop is not experiencing any acceleration, the bubbles will not migrate within the drop, and the emulsion will be stable in this respect regardless of the viscosity of the feed stock. This is approximately the situation in a spray-

dryer, except very near the atomizer. Any tendency for bubbles to migrate in foams or concentrated emulsions will be retarded by hindrance effects.

In the case of rich foams, where the volume fraction of gas is high, instability can result from a change in bubble sizes, film thinning, and film rupture. As in most situations involving particulate matter at equilibrium with its surroundings, the larger bubbles grow at the expense of the smaller ones. The gas is under a higher pressure in the smaller bubbles than in the larger bubbles, leading to pressure diffusion of the gas through the film separating a smaller bubble from a larger bubble. Gas dissolution from the smaller bubbles (where the capillarity pressure is high) into the solution and desorption into the larger bubbles or out of the liquid (where the capillarity pressure is low) is called disproportionation or Ostwald ripening. *This form of instability will occur as long as the film is liquid and will be inhibited by the rapid drying of the drops.*

1.3.3 Characteristics of the product

The physical appearance of various foam spray-dried products and the photographic histories of single macrodrops undergoing drying while containing dissolved and dispersed gases indicate that foam spray-dried particles (i) may resemble thin- or thick-shelled hollow spheres, (ii) may contain rather small, uniformly dispersed voids, or (iii) may contain a large number of small voids together with a few voids of much larger size.

1.4 Literature review of spray-dried milk powders.

Buma[6] and **Buma & Henstra**[7] completed the most comprehensive study of spray-dried milk structure by S.E.M. and explained many phenomena observed in dried milk, such as the particle structure and size distribution, the fat globule size distribution in the powder particles, and the occurrence of fat in four forms in the powder particles.

Electron micrographs may help to explain some of the processes that occur in the spray-drying chamber. In some powders, such as spray-dried buttermilk, small particles surrounded by rims were observed on the surfaces of larger particles whereas shallow depressions in particles surfaces were observed in spray-dried retentates obtained from the ultrafiltration of milk[8]. These differences have been explained as follows: small droplets dry and solidify sooner than the larger droplets. If these small droplets collide with the larger particles while these latter particles are still viscous, the small particles become embedded in the larger particles and the impact forms the rim around the small particles. If, however, the larger particles are no longer sticky but are not yet hard, the collisions with the small particles result in the formation of depressions while the small particles rebound after the collisions.

Most powder particles contain air in the form of vacuoles. Their development and prevention were extensively studied by **Verhey**[9], who investigated the development of vacuoles during spray-drying of skim milk

---

[6] Buma, T.J., Neth. Milk Dairy J., **25**, 33, (1971).
[7] Buma, T.J. and Henstra S., Neth. Milk Dairy J., **25**, 75, (1971).
[8] Kaláb, M., Caric, M. and S. Milanovic, Food Struct., **10**, 327, (1991).
[9] Verhey J.G.P., Neth. Milk Dairy J., **26**, 186, (1972).

particles by measuring the volumes of air and vacuoles present in powders produced under various processing conditions. This process of air incorporation in the feed liquid is a surface phenomenon that may well be related to the foaming properties of the liquid, such as surface tension and foam stability. The well-known practical observation that whole milk powders usually exhibit a smaller vacuole volume than do skim milk powders may be explained by the better foaming properties of skim milk and its concentrates. Verhey's results lend strong support to a hypothesis of vacuole formation comprising two stages, viz., air incorporation into the liquid during droplet formation (in the atomizer) and expansion of air bubbles due to case hardening (increasing resistance against shrinkage) during drying. He showed that by using CO_2 to spray-dry the feed, CO_2 was then isolated from the resulting powders instead of the air normally present in the drying chamber. The volume of the vacuoles produced was furthermore decreased, as CO_2 is highly soluble in water[10].

Mistry and **Hassan**[11] examined by S.E.M. a delactosed, high milk protein powder. This powder was characterized by smooth surface and dents, whereas particles of skim milk powder had wrinkled surface. Commercial casein products had a structure similar to the high milk protein powders. **Mistry, Hassan,** and **Robison**[12] showed that lactose and protein content of dried milk considerably affected surface structure of powder particles. The surface of skim milk powder particles containing 51.4% lactose and 35.6% protein was extremely wrinkled. Particles of dried ultrafiltered/diafiltered skim milk had a smooth surface with no

---

[10] Verhey J.G.P., Neth. Milk Dairy J., **26**, 203, (1972).
[11] Mistry, V.V. and Hassan, H.N., J. Dairy Sci., **11**, 3716, (1991).
[12] Mistry, V.V., Hassan, H.N. and Robison, D.J., Food Struct., **11**, 73, (1992).

wrinkles. These powders contained 3.1 to 19.9% lactose and 66 to 81.5% protein. Particles of a commercial caseinate containing less than 1% lactose and 88% protein (mainly casein) were also smooth. When lactose was added to diafiltered skim milk and dried, the resulting powder particles became wrinkly.

Fäldt and **Bergenståhl**[13] studied the surface composition of spray-dried mixtures of lactose-protein (Sodium Caseinate and Bovine Albumin) and lactose-glycine by means of electron spectroscopy for chemical analysis (E.S.C.A.). The results show that the protein starts to appear on the powder surface even when it is present at a concentration as low as 0.1% of dry material. At a protein/lactose ratio of 20/80 (by weight), about 70% of the surface is covered by protein. The results are similar for the protein sodium caseinate and bovine albumin. In the case of spray-drying of mixtures of lactose and glycine, the surface composition of the powder reflects the composition of the mixture to be dried. This is explained by the higher surface activity of the proteins than lactose. Glycine affects the surface tension to a minor extent. Thus, *the composition of the air-water interface of the drying droplets is reflected in the surface composition of the dried powder.* In addition, scanning electron micrographs show that the particles obtained when a pure lactose solution is spray-dried are spherical and have a smooth surface. At a minor addition of 0.1% protein to the lactose solution, dents start to appear at the particle surfaces. Thus, the changes in the powder structure when protein is added to the solution are associated with the presence of protein on the surface.

---

[13] Fäldt, P. and Bergenståhl, B., Colloids Surfaces A: Physicochem. Eng. Aspects, **90**, 183, (1994).

When the surface coverage of the protein increases, dents start to appear in the particles.

Recently, **Fäldt** and **Bergenståhl**[14] showed that the presence of lactose is important in obtaining complete encapsulation of the fat after spray-drying of sodium-caseinate-stabilized soybean oil emulsions. The following explanation is suggested. In the emulsion before drying, the protein is the most surface-active component present and accumulates at the air-water interface of the drying droplets. The protein in the surface film in the emulsion is completely hydrated, however, and the loss of water during drying would cause shrinkage of the film. If the emulsion contains lactose, the lactose may replace the water to some extent and keep the protein solubilized after drying and thereby reduce the shrinkage. This increases the stability of the sodium caseinate film on the powder surface, and less fat leaks out onto the powder surface during the drying process. But the presence of lactose in a powder requires that the powder be well protected from humidity, since lactose is the component responsible for the release of fat onto the powder surface when lactose-containing powders are stored in a humid atmosphere.

1.5 Experimental part

1.5.1 Materials.

Foaming creamers were supplied from Kraft Foods (Tarrytown, N.Y.): "KFI Foaming Creamer," "Non-gasified control creamer," "KFI creamer Alapro Substitution," "KFI creamer TMP Substitution," "KFI

[14] Fäldt, P. and Bergenståhl, B., JAOCS, **72**, n° 2, 171, (1995).

creamer 2% Bicarbonate," and 16 creamers referred to by a combination of 4 letters, H, L, F, P (which stand respectively for High, Low, Fat, and Protein). All the creamers were made with different proportions of the following compounds: soybean oil (fat), lactose (carbohydrate), disodium phosphate, and dried milk (proteins). The dried milk powders used in the preparation of the foaming creamers were either: Non-Fat Dry Milk (NFDM) from Kraft Foods; Total Milk Protein (TMP) isolate containing casein and soluble whey protein, milk protein concentrate containing 56-82 % protein (Alapro), and sodium caseinate (Alanate 180) from New Zealand Milk Products (North America Inc.).

The powders for imaging, *Imagent US* , were from Alliance Pharmaceuticals (San Diego, California). The composition of these powders was essentially Hydroxyethyl Starch from Ajinomoto Inc. (Tokyo, Japan), Pluronic F68 (a block copolymer of ethylene oxide and propylene oxide condensate) from Alliance Pharmaceutical Corporation (San Diego, California), and Sucrose Stearate (Ryoto Sugar Ester S1570) from Mitsubishi-Kasei Food Corporation.

1.5.2 Methods

Preparation of a foaming creamer (non-gasified control creamer).

The foaming creamer (non-gasified control creamer) is prepared by first preparing an emulsion of soybean oil in an aqueous solution of lactose with a mixture of sodium caseinate (Alanate 180) and Non-Fat Dry Milk

(NFDM). The mixture is homogenized and finally spray-dried on a pilot plant spray-dryer. The role of the sodium caseinate is twofold: it acts both as the emulsifying agent (encapsulating agent for the fat) and as the foaming agent in the end product. Disodium phosphate is also present to stabilize the emulsion against coagulation at low pH and at high temperature. The lactose is used to ensure good wetting of the creamer. The fat confers the whitening power as well as a creamy appearance.

Scanning electron microscope.

The samples were mounted on S.E.M. stubs secured by double-sided adhesive tape. Samples were then coated with a thin layer (10 to 20 nm) of gold using a sputter and were examined with a Carl Zeiss DSM 940 instrument operating at 15kV. The observation time was kept as short as possible in order to prevent cracks in the metal-carbon layer and in the particles.

1.6 Results and discussion.

Several foaming creamers were investigated with a scanning electron microscope both as is and crushed with a mortar to characterize the external and internal morphology of the powder. Figure 1.5, illustrating the microstructure of "KFI foaming creamer" powder, shows a large particle (300 μm in diameter) with a lot of broken pieces around it and holes on the surface. "KFI foaming creamer" is the foam-generating "ingredient" in the composition of the commercial foaming creamer. This powder is obtained with a factory-size spray-dryer. The solution to be

spray-dried is composed of NFDM, fat, lactose, and sodium caseinate. Figure 1.6 is a micrograph showing the internal structure of the wall of a particle. The wall is thin (8 μm) compared to the size of the particles with big voids (5 μm in diameter) and a lot of small voids (0.2 μm in diameter). Figure 1.7 illustrates the microstructure of the "Non-gasified control creamer," which has the same composition as "KFI foaming creamer" but was spray-dried with a pilot plant spray-dryer. As we notice, the "Non-gasified control creamer" is composed of small spherical particles (10 to 50 μm in diameter) without any broken pieces. Figure 1.8 illustrates the microstructure of the surface of the particles. The powder particles have wrinkled surfaces, and we observe small particles embedded in larger particles, proving that during the process of drying, small droplets collide with larger particles while these latter particles are still viscous. These results show that a change of process changes the morphology of the particles in the powder. Figure 1.9 shows the internal structure of a particle of "Non-gasified control creamer." This micrograph shows a hollow particle with a thick shell compared to the size of the particle, full of small voids. The cavity contains a particle that might have been incorporated during the preparation of the sample for the observation.

Influence of the nature of the dried milk on the powder's structure

Several powders were prepared by varying the nature of the dried milk in the composition of the foaming creamer before spray-drying. Instead of using NFDM, to prepare the feed, Alapro or TMP was used consecutively at the same level of milk protein.

Figure 1.10 illustrates the microstructure of "KFI creamer Alapro Substitution." The powder particles have wrinkled surfaces, and we observe a lot of particles embedded in each other. Figure 1.11 illustrates the microstructure of "KFI creamer TMP Substitution." In the case of the milk protein, TMP, the fat of the cow's milk is removed by centrifugation, and lactose and minerals are removed by ultrafiltration. This process is done at low temperature. The powder shows spherical particles and collapsed particles resembling blood cells, with smooth surfaces. This type of structure is characteristic of a powder with a high protein content. Figure 1.12 shows the microstructure of TMP milk protein. The particles are all collapsed with a lot of dents and smooth surfaces. Figure 1.13 illustrates the internal structure of "KFI creamer TMP Substitution" showing a hollow particle with a thin wall. Figure 1.14 illustrates the internal structure of the wall of a "KFI creamer TMP Substitution" particle showing a wall full of small voids. Figure 1.15 illustrates the microstructure of "KFI creamer 2% Bicarbonate" showing nice spherical particles. Figure 1.16 illustrates the internal structure of "KFI creamer 2% Bicarbonate" showing a hollow particle with a thin wall.

All these microstructures lead to the conclusion that, in most cases, we are looking at hollow particles capable of entrapping gas. The best way to encapsulate the gas is to use either NFDM or Alapro, both of which give nice spherical hollow particles, whereas with TMP most particles collapsed.

Influence of the fat and protein composition on the structure of foam spray-dried powder

Table 1.1 summarizes the results of these observations of powders obtained by foam spray-drying. The density of the powders was varied, as were the amounts of fat and of milk protein. The particles' diameters vary, ranging from 25 to 400 μm. In some cases the particles are well-shaped, regular spheres; in other cases they are misshapen. The surface is rough or smooth, some particles have a large cavity as their internal structure, while others have several voids. Finally, we notice that some powders give an amorphous structure when they are crushed with a mortar. At low density, the surface is rough, characteristic of the drying of a foamed droplet. As the density increases, we see smaller particles with smoother surfaces.

Figure 1.17 is a micrograph of the internal structure of "LFHP 0.132" powder. We notice a large cavity in the center and a thick wall full of large voids. Figure 1.18 is a micrograph of "HFLP 0.116" powder. As can be seen, the particle has a rough surface with a brittle wall structure. Furthermore, we notice a large cavity inside the particle. Figure 1.19 is a micrograph of the internal structure of "HFHP 0.152" powder. In this case, we have a hollow sphere with a thin wall with small voids. These microspheres have a strong wall structure. It seems that in those cases, the foamed droplet must have internal bubbles that coarsen at a rate higher than the drying rate, forming a large central bubble. The resulting powder has a large cavity. Figure 1.20 is a micrograph of the internal structure of "HFLP 0.164" powder. In this case, we notice that the internal structure consists of a lot of voids. The structure resembles a dry foam with plateau borders. The coarsening of the foamed droplets is inhibited by the rapid drying of the droplets. We observe a "foam-type" internal structure.

Figure 1.21 is a micrograph of the internal structure of "LPHF 0.163" powder, again illustrating the "foam-type" internal structure.

Figure 1.22 is a micrograph of *Imagent US.*, a product developed by Alliance Pharmaceutical Corporation for use in ultrasonographic medical imaging. (Ultrasonography, one of the most widely used imaging methods due to its safe, non-invasive nature and its low cost compared to such competing methods as X rays, computed tomography, or magnetic resonance techniques, is based on the measurement of sound waves transmitted through the body and reflected to varying extents by various anatomical structures. Air-filled bubbles, which are excellent reflectors of sound waves, can be injected into the bloodstream as a way of enhancing the sound-reflecting power of flowing blood, but the rapid dissipation of air from the bubbles previously limited the usefulness of this technique. Underlying the development of Imagent U.S. was the desire to stabilize the bubbles enough to allow for a longer, more useful imaging period; when injectable microbubbles are prepared by dissolving solid microspheres of Imagent into a saline solution, the perfluorohexane (PFH)/gas mixture that substitutes for air has the desired stabilizing effect.) This micrograph shows that this powder is constituted of aggregated very small particles. The size of those spherical particles is about 10 μm in diameter, as illustrated in the micrograph of Figure 1.23. The size of these microspheres is very important, given the injectability constraints on the size of the microbbubles they produce.

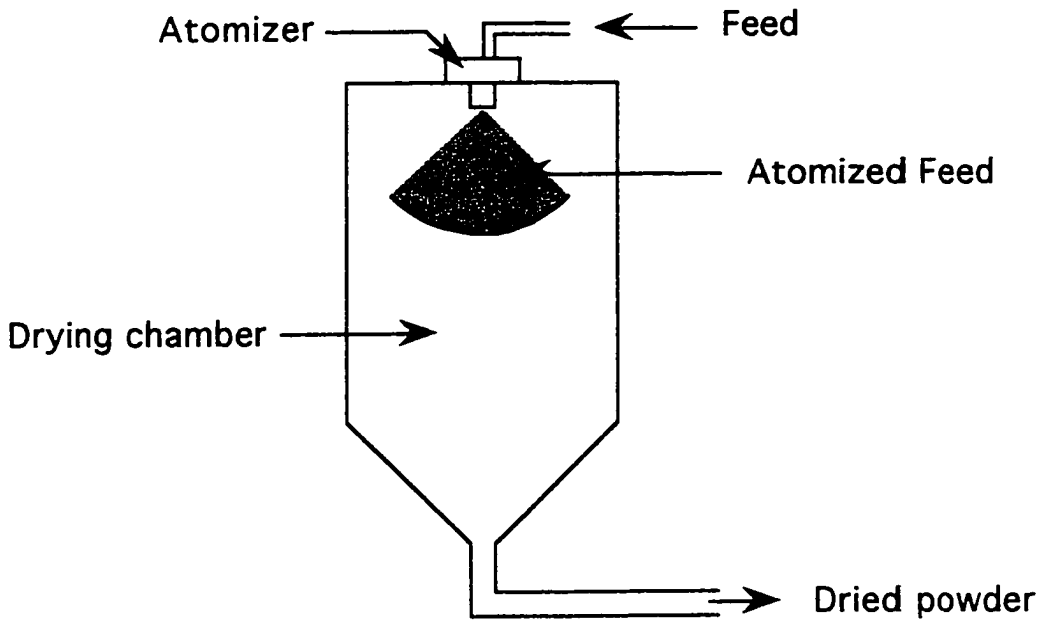

Figure 1.1 : Schematic of the process of spray-drying.

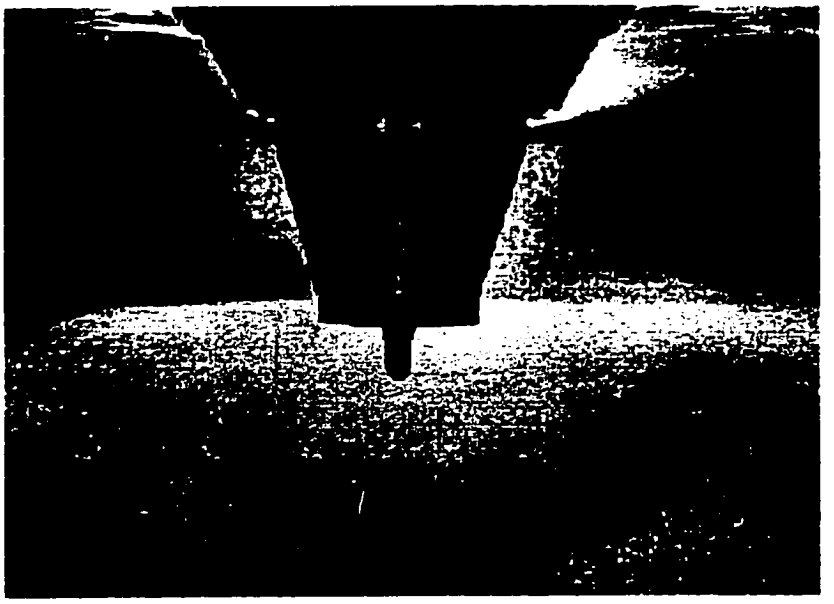

Figure 1.2 : Rotary atomizer in operation

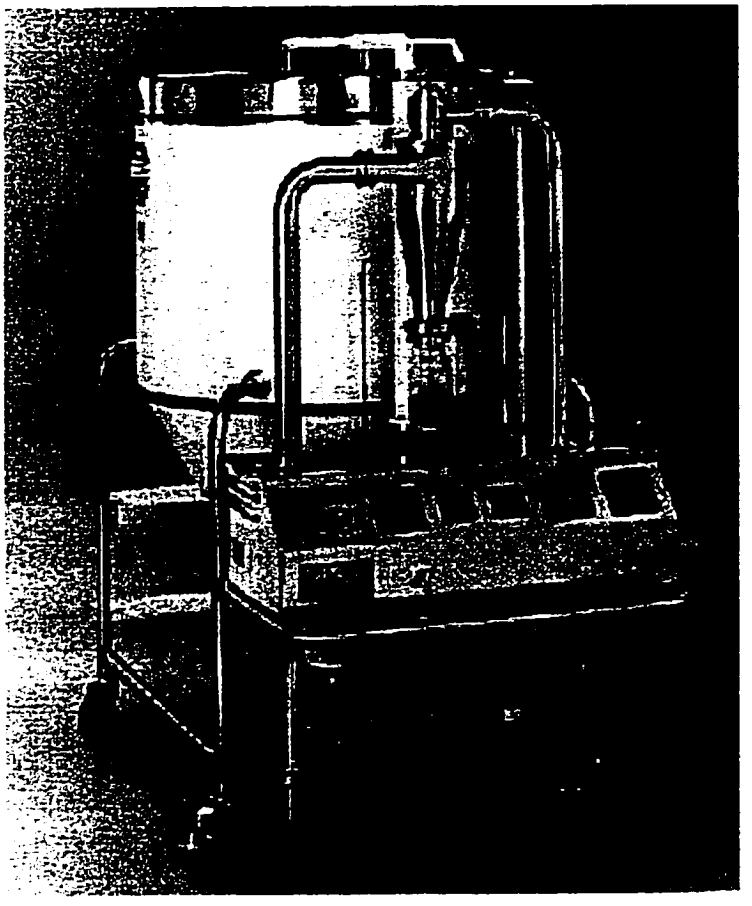

Figure 1.3 : A pilot-plant spray-dryer.

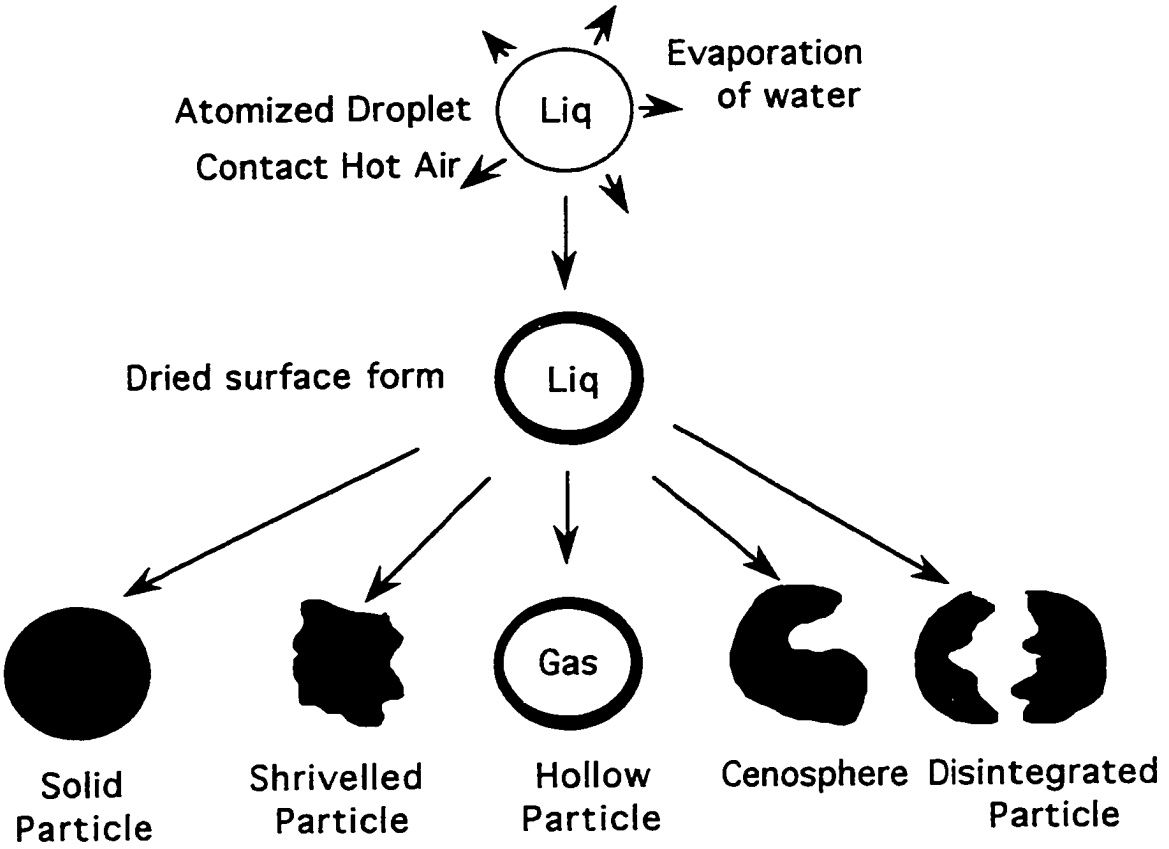

Figure 1.4 : Mechanism of droplet drying illustrated in simplified manner. Droplets dry to single, misshapen particles.

Figure 1.5 : Scanning Electron Micrograph of "KFI Foaming Creamer" showing a large particle with a lot of broken pieces and holes on the surface.

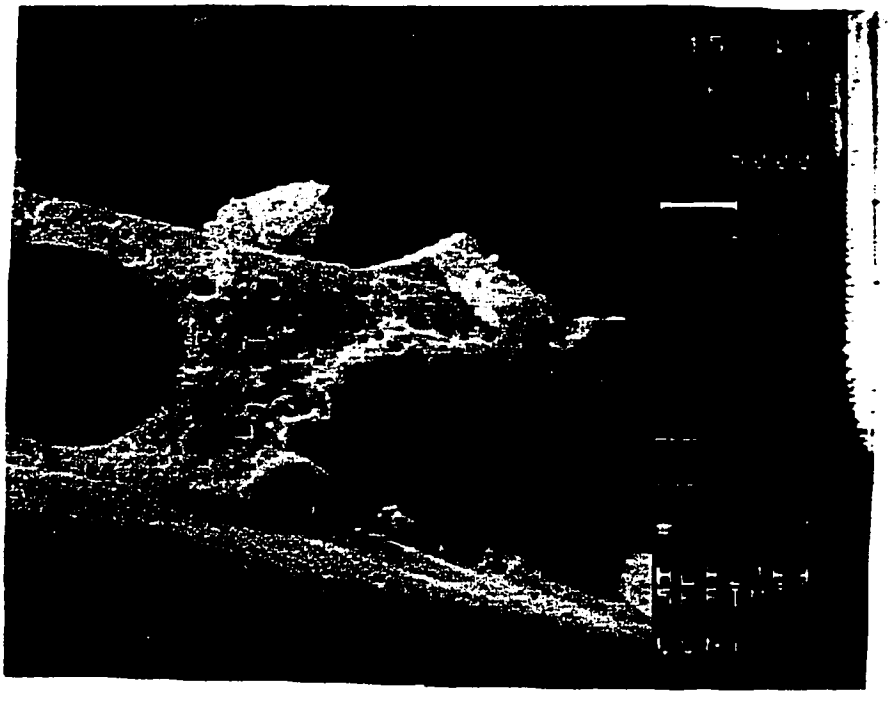

Figure 1.6 : Scanning Electron Micrograph of the internal structure of the wall of a hollow microsphere of "KFI Foaming Creamer".

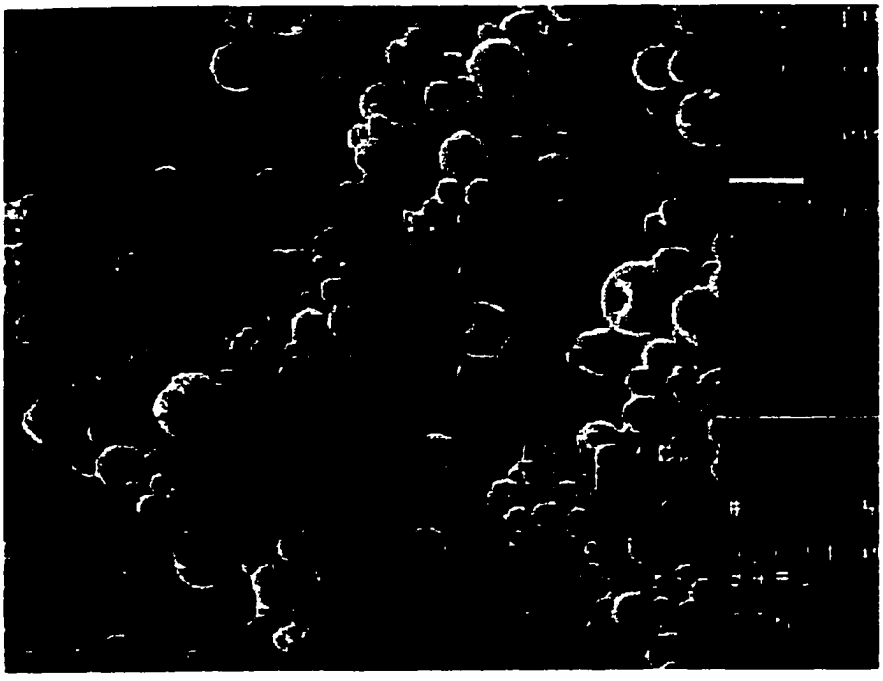

Figure 1.7 : Scanning Electron Micrograph of "Non-gasified control creamer" showing small spherical particles, and no broken pieces.

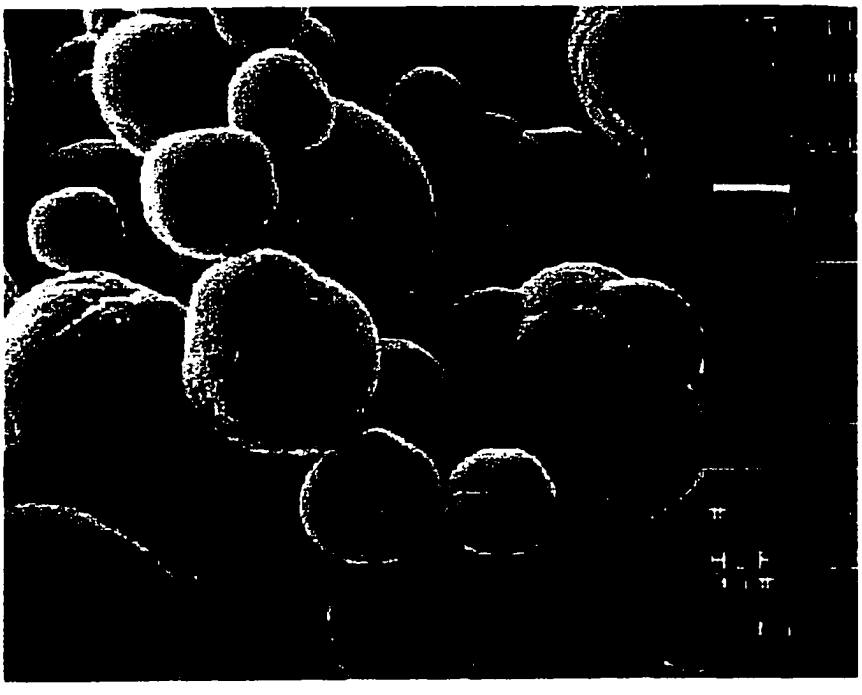

Figure 1.8 : Scanning Electron Micrograph of "Non-gasified control creamer" showing wrinkled surfaces, and small particles embedded in larger particles.

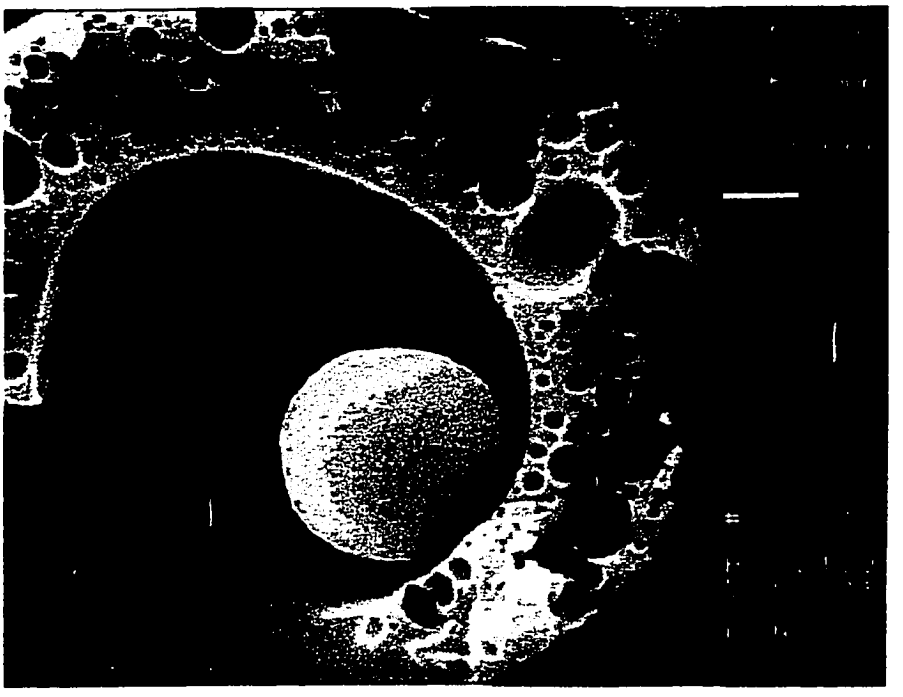

Figure 1.9 : Scanning Electron Micrograph of the internal structure of "Non-gasified control creamer" showing a hollow particle with a thick wall full of voids.

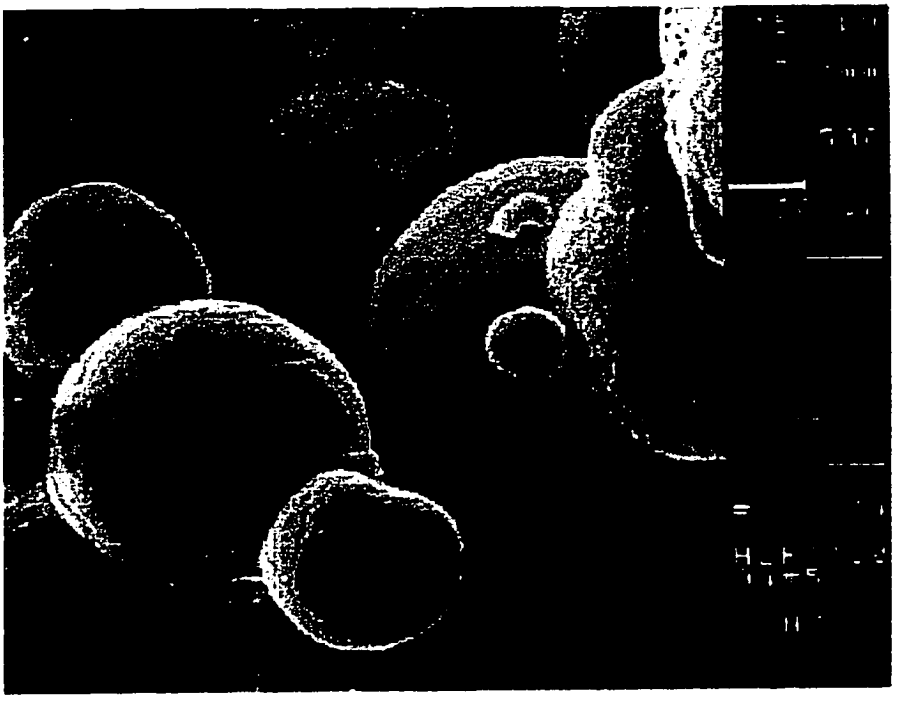

Figure 1.10 : Scanning Electron Micrograph of "KFI creamer Alapro Substitution" showing wrinkled surfaces, and a lot of particles embedded in each other.

Figure 1.11 : Scanning Electron Micrograph of "KFI creamer TMP Substitution" showing collapsed particles

Figure 1.12 : Scanning Electron Micrograph of TMP showing collapsed particles

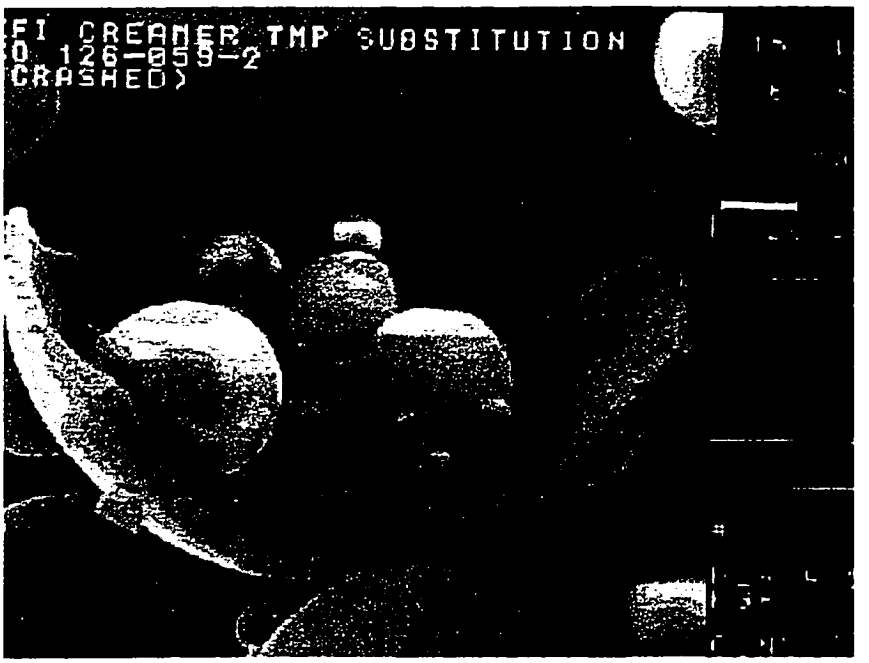

Figure 1.13 : Scanning Electron Micrograph of the internal structure of "KFI creamer TMP Substitution" showing a hollow particle with a thin wall.

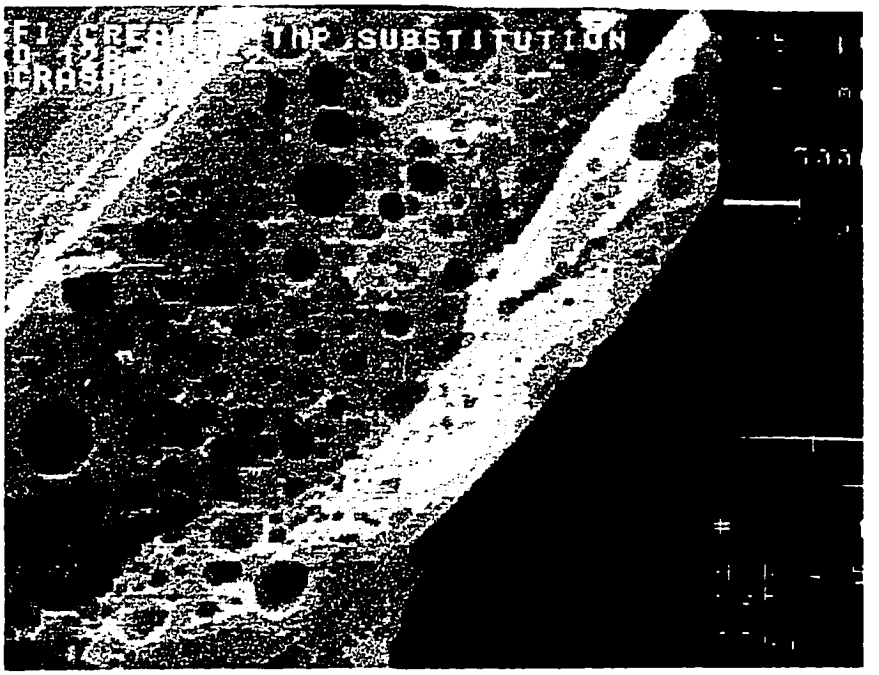

Figure 1.14 : Scanning Electron Micrograph of the internal structure of the wall of a "KFI creamer TMP Substitution" particle showing a wall full of small voids.

Figure 1.15 : Scanning Electron Micrograph of "KFI creamer 2% Bicarbonate" showing spherical particles.

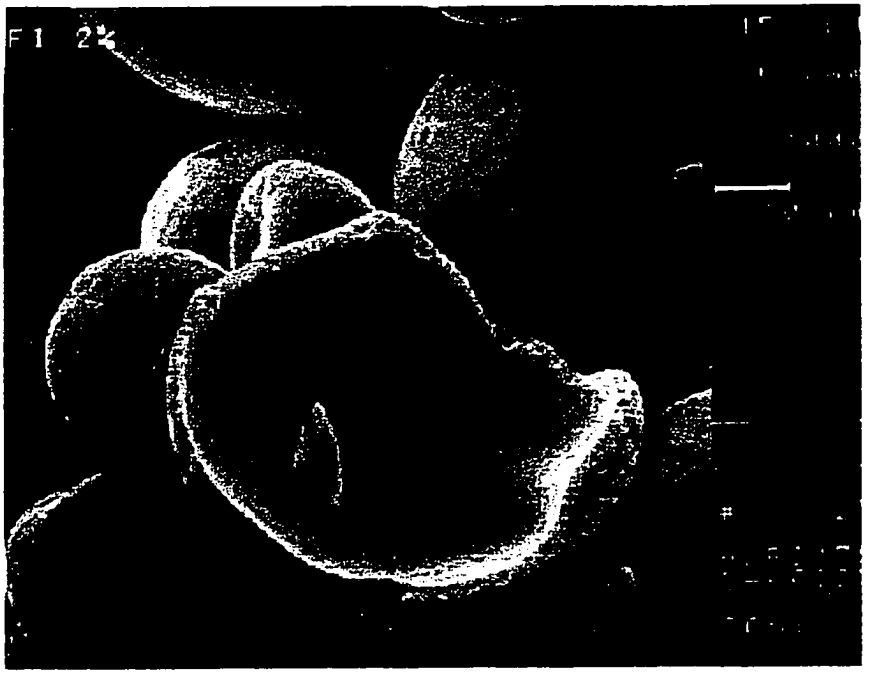

Figure 1.16 : Scanning Electron Micrograph of the internal structure of "KFI creamer 2% Bicarbonate" showing a hollow particle with a thin wall.

Figure 1.17 : Scanning Electron Micrograph of the internal structure of "LFHP 0.132" powder.

Figure 1.18 : Scanning Electron Micrograph of the internal structure of "HFLP 0.116" powder.

Figure 1.19 : Scanning Electron Micrograph of the internal structure of "HFHP 0.152" powder.

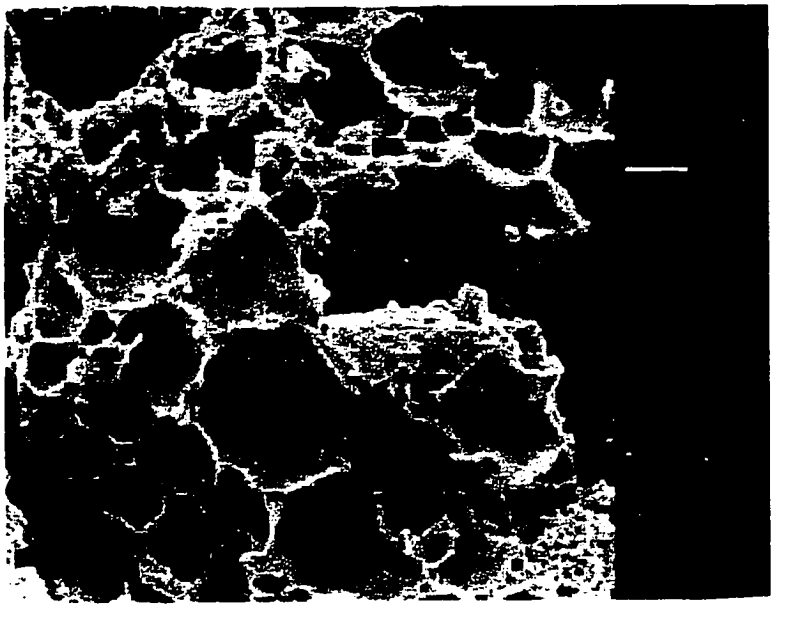

Figure 1.20 : Scanning Electron Micrograph of the internal structure of "HFLP 0.164" powder.

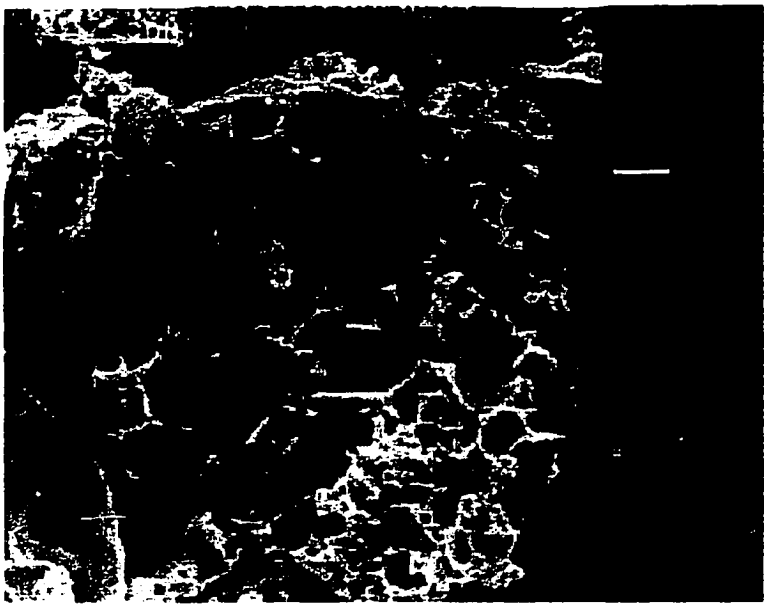

Figure 1.21 : Scanning Electron Micrograph of the internal structure of "LPHF 0.163" powder.

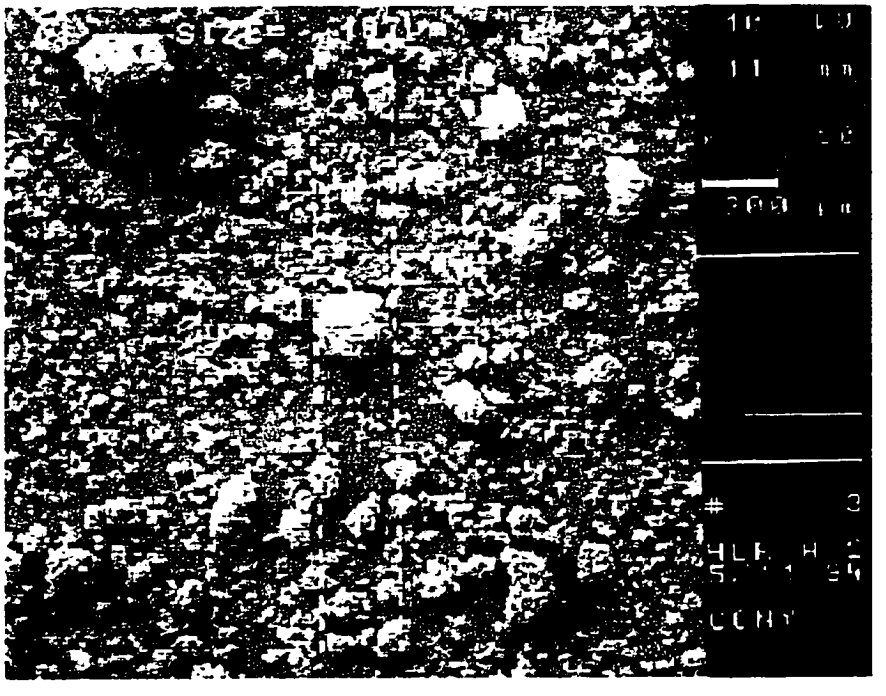

Figure 1.22 : Scanning Electron Micrograph of Imagent US showing very small particles aggregated.

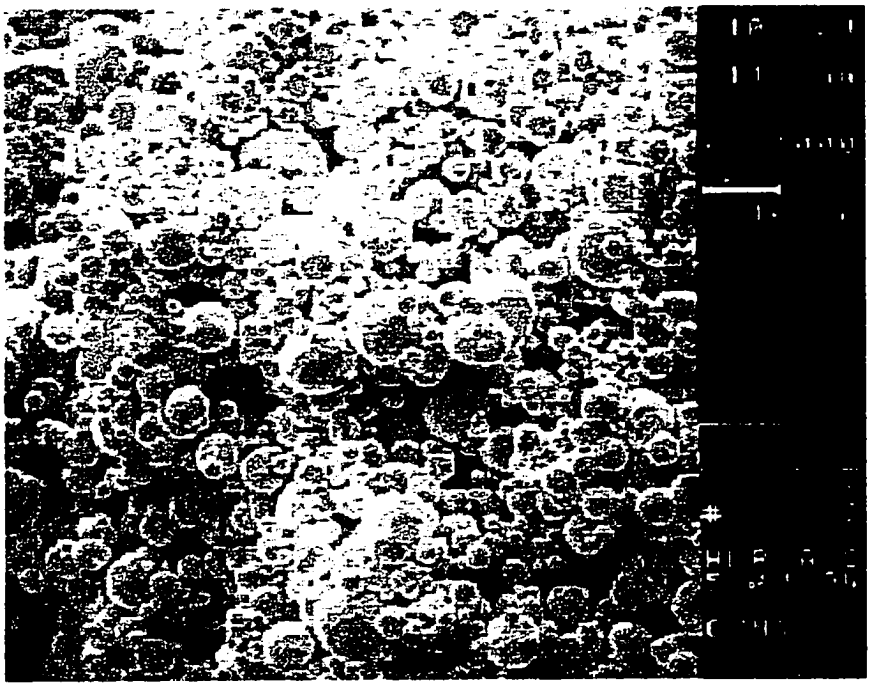

Figure 1.23 : Scanning Electron Micrograph of Imagent US.

Sample (density g/cm^3)	Diameter (μm)	Shape	Surface	Internal structure
LFHP Control (0.090)	50-200	spherical	rough with holes	Thin wall, large cavity
LFHP Control (0.132)	50-200	spherical	smooth with holes	Thick wall with voids, large cavity
LFHP Control (0.163)	50-200	spherical	smooth with holes	large number of voids (foam type)
LFLP (0.089)	100-250	misshapen	very rough	large cavity
LFLP (0.124)	50-400	misshapen	rough	Thin wall, large cavity, amorphous when crushed
LFLP (0.169)	50-250	misshapen, broken pieces	smooth	
MFMP (0.093)	100-400	misshapen, broken pieces	rough	Thin wall, large cavity, amorphous when crushed
MFMP (0.099)	80-300	misshapen, broken pieces	rough	Thin wall, large cavity, amorphous when crushed
MFMP (0.150)	50-250	spherical, misshappen	large rough, small smooth	Thick wall (strong), large cavity
HFLP (0.116)	100-400	misshapen, broken pieces	rough	Thin wall, large cavity, amorphous when crushed
HFLP (0.164)	25-300	spherical	rough	Large number of voids (foam type)
HFLP (0.232)	25-200	misshapen	rough	Amorphous when crushed
HFHP (0.077)	80-400	misshapen, broken pieces	rough	Thin wall, large cavity
HFHP (0.152)	25-200	misshapen, spherical	smooth	Thin wall, large cavity
HFHP (0.213)	15-200	misshapen, spherical	smooth	Thin wall, large cavity

Table 1.1 : Description of the morphology of the foaming creamer.

(L: low, H: high, F: fat, P: protein)

Chapter 2

The tensiolaminometric technique for studying the foamability of solutions

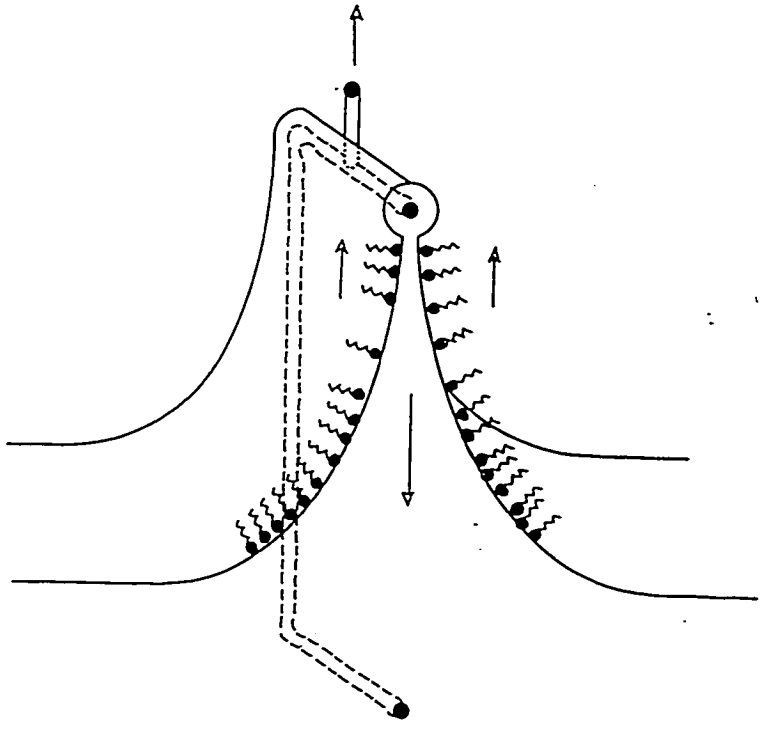

2.1 Introduction

The hollow microspheres produced by spray-drying are eventually dispersed into a liquid, in the case of creamers hot coffee or hot water. The shell dissolves, releasing the gas entrapped into the aqueous phase; as noted above, with creamers the formation of a fine foam is desirable. Therefore the intrinsic foamability of the initial solution is important.

In any study of the foamability of surfactant solutions, two main properties must be distinguished: first, the ease of formation of the thin liquid lamellae that form the walls of the gas bubbles; and second, the stability of these lamellae. The first property depends upon the lowering of the surface free energy by the adsorption of the dissolved surface-active agents at the gas-water interface. The second is a function of the behavior of the lamellae during aging, as they change both in surface structure and in the interlaminar liquid composition. These changes largely determine the work opposing surface reduction. It should always be kept in mind that a liquid foam can never be thermodynamically stable, since any reduction in surface corresponds to a decrease in the free energy of the system. Relative stability is achieved through the creation of an energy barrier opposing surface reduction and the thinning of the foam lamellae; such energy barriers include steric hindrance, electrostatic repulsion between

the two sides of the lamella, and increased surface viscosity, among other possibilities.

The objective of this part of my study is the determination of the physico-chemical properties of the solution produced when the microspheres are dissolved in liquid. The tensiolaminometric technique is used to determine the solution's surface tension and foamability. I then identify ways of increasing the foamability of such solutions.

2.2 Description of the tensiolaminometer[15]

The apparatus consists of a wettable wire frame attached to a platform that can be moved vertically at constant speed (Figure 2.1); as the frame is pulled out of a solution, a liquid lamella is formed inside it. The force acting upon the frame is measured with a transducer and recorded electrically via a plotter. In the present studies, the solution was in a thermostatted 250ml beaker, and a glass or platinum frame 2.5 cm in width was used. The surface tension can be measured to within ± 0.2 mN/m. The rate of film formation with this apparatus can be varied from 0.08 to 0.13 cm/sec.

2.2.1 Procedure

After complete immersion in the solution, the frame is pulled out at a constant speed. As long as the frame is entirely immersed no force is acting on it. (The wires are thin enough that buoyancy and hydrodynamic

[15] Eydt, A.J. and Rosano, H.L., Journal of the American Oil Chemists Society, **45**, 607, (1967)

effects are negligible.) When the horizontal wire of the frame reaches the air-water interface, surface tension comes into play. A liquid meniscus is formed around the wire. Once the angle formed by the plane of the frame and the liquid meniscus surface reaches zero, the surface tension acts vertically. At this point there are two possible outcomes as the frame is withdrawn further:

1) In the case of pure liquids, no liquid lamella is formed and the force drops back to zero (case (a), Figure 2.2).

2) In the case of foaming solutions, the force remains constant upon further withdrawal as a liquid lamella is formed inside the frame (case (b), Figure 2.2). (The weight of the lamella is negligible.)

The area under the force-versus-displacement curve corresponds to the work involved in forming the liquid-air surfaces inside the frame. This is a direct result of the definition of surface tension as the isothermal and reversible work of surface formation. The lower the surface tension of the solution, the easier it will be to form additional liquid-air surfaces, i.e., the easier the solution will foam, assuming the liquid lamella is stable.

2.2.3 Influence of the speed of withdrawal

With a slow rate of film formation, the solution can feed the film and there is a constant equilibrium between the surface-active material in the bulk and that absorbed in the film. The force-versus-displacement

curve has a horizontal plateau as the surface tension corresponds to the equilibrium value and the weight of the film is negligible.

When the rate of film formation is increased, the rate of adsorption of the surface-active agents will become the controlling factor (case (A), Figure 2.3). The surface tension will always be higher than the equilibrium value, because the surface concentration of the surfactants is less than the equilibrium value. If the film withdrawal is stopped, the surface tension drops to its equilibrium value (case (B), Figure 2.3). Solutions showing this type of curve tend to yield stable foams, as this behavior is related to the Marangoni effect. If, because of thermal or mechanical action, one part of the surface momentarily thins out and becomes poorer in surfactant, its surface tension increases locally and the surface tends subsequently to contract, thus bringing the film thickness to a more resistant level. This is especially the case if the surfactant concentration is not too high. At high concentrations the diffusion of the surface-active material from the bulk to the thinned section of the film exceeds the lateral diffusion in the film and no "healing" takes place.

2.2.4 Reversibility

If, after the plateau is reached, the frame is reintroduced into the solution, two distinct force-versus-displacement curves may be obtained. The curve corresponding to reentry of the frame is either completely symmetrical to, or consistently lower than, the curve corresponding to withdrawal (Figure 2.4).

In the first case, no change in surface tension accompanies the compression of the film, i.e., the surface-active material redissolves immediately in the bulk and the liquid lamella stays in continuous equilibrium with the bulk solution. The phenomenon is completely reversible (Figure 2.4, top).

In the second case, the surface-active molecules are unable to desorb from the surface with sufficient speed to keep up with the reentering frame; they crowd together in the available surface, increasing the surface pressure with a concomittant decrease in surface tension (case (C), Figure 2.3). It is interesting to note that if the frame is stopped before complete reentry into the solution, the surface tension increases slowly to its equilibrium value (case (D), Figure 2.3). A similar curve is obtained if the surfactant substance undergoes an irreversible chemical modification at the air-water interface that renders it insoluble (as happens with proteins, for example). The surface layer is solid and hard to compress.

Some generalizations are possible at this point. Solutions yielding highly dissymmetrical curves form very stable foams. Foam stability is related to the magnitude of hysteresis in film expansion and contraction, and to irreversibility of adsorption at the water-air interface, while foamability is related to the lowering of the surface tension.

2.3 Theoretical study of the deformation of a liquid surface by a rectangular frame

In order to understand more completely the stretching curves, it is necessary to recall the theoretical study of the deformation of liquid surfaces by a Proctor Hall frame assumed to be completely wettable by the liquid and to have negligible thickness.

Relationship between the position of the frame and the angle at the top of the meniscus edge

Bouasse solved Laplace's equation and derived the following expression relating the height of the meniscus edge to the surface tension and the complement of the contact angle (see Appendix 1).

$$y = \sqrt{\frac{2\gamma}{\rho g}(1-\cos\theta)} \qquad [2.1]$$

ρ=specific gravity, γ=surface tension, g=gravitational constant

This relation allows us to calculate the surface tension (Wilhelmy's method when the frame is a wettable plate) and the maximum height of the meniscus, h.

At the point N (vertical plane) $\theta = \frac{\pi}{2}$ $y = \sqrt{\frac{2\gamma}{\rho g}} = h$ (see Appendix 2)

Relationship between the acting force F and the angle at the top of the meniscus

The force F balances the total weight of the liquid in the meniscus above the liquid surface, so $F = V\rho g$, where V is the total volume of the meniscus.

Since the plane of the frame is a plane of symmetry we have

$$\frac{1}{2}V = \int_0^h y\,dx$$

but as we have already established the relationship between y and θ, by using $\frac{dy}{dx} = \tan\theta$ we get

$$dx = \frac{dy}{\tan\theta} = \frac{h\sin\theta\,d\theta}{2\sqrt{(1-\cos\theta)\tan\theta}} = \frac{h\cos\theta\,d\theta}{2\sqrt{(1-\cos\theta)}}$$

And thus

$$V = 2\int_0^\theta h\sqrt{(1-\cos\theta)}\,\frac{h\cos\theta\,d\theta}{2\sqrt{(1-\cos\theta)}}$$

$$= 2\int_0^\theta \frac{h^2\cos\theta\,d\theta}{2} = \frac{2\gamma}{\rho g}\sin\theta$$

Finally, we obtain the force for a frame of unit width:

$$F = 2\gamma\sin\theta \qquad [2.2]$$

The force reaches its maximum value when $\theta = \frac{\pi}{2}$. Then $F = 2\gamma$.

For a frame of perimeter ω (twice the width of the frame), during the formation of the liquid lamella, we get γ by the following relation:

$$\frac{F}{\omega} = \gamma$$

Relationship between F and y

From Equation [2.1] we get $\cos\theta = 1 - \frac{y^2}{h^2}$, and with Equation [2.2], $F = 2\gamma\sin\theta$. Thus:

$$F = 2\gamma\sin\theta = 2\gamma\sqrt{(1-\cos^2\theta)}$$
$$= 2\gamma\frac{y}{h}\sqrt{\left(2-\frac{y^2}{h^2}\right)} = 2\sqrt{\gamma\rho g}\; y\sqrt{\left(1-\frac{y^2}{2h^2}\right)}$$

The expression for F(y) above enables us to calculate the value of the slope of the curve at the origin:

$$\left.\frac{dF}{dy}\right)_{y=0} = 2\sqrt{\gamma\rho g}$$

This relationship shows that the slope of the curves F(y) is a function of the surface tension of the solution.

Work necessary to lift the frame from the bulk of the solution

The work W necessary to lift the frame can be shown to be the sum of two terms (see Appendix 3): (a) the work P against gravity for raising the liquid into the meniscus, where

$$P = 2\sqrt{2}\; h\gamma\left(\cos\frac{\theta}{2} - \frac{2}{3}\cos^3\frac{\theta}{2} - \frac{1}{3}\right)$$

and (b) the work S against the surface cohesion of the liquid while increasing the liquid-air interface, where

$$S = 2\sqrt{2}\; h\gamma\left(1-\cos\frac{\theta}{2}\right)$$

Thus, when the meniscus reaches its maximum height $\left(\theta = \frac{\pi}{2}\right)$ the total work required to raise the frame becomes 2γ (for a frame of unit width), since the only work remaining will be capillarity work.

2.4 Experimental part

2.4.1 Materials

The dried milk powders used in the preparation of the foaming solutions were either: Non-Fat Dry Milk (NFDM) from Kraft Foods; Total Milk Protein (TMP) isolate containing casein and soluble whey protein, milk protein concentrate containing 56-82 % protein (Alapro), or sodium caseinate (Alanate 180) from New Zealand Milk Products (North America Inc.). Sodium dodecyl sulfate (SDS) from Sigma, Lauric diethanolamide (Ninol 96-SL) from Stepan Company (Northfield, Ilinois), Pluronic F68 (a block copolymer of ethylene oxide and propylene oxide condensate) from Alliance Pharmaceutical Corporation (San Diego, California), Sucrose Stearate (Ryoto Sugar Ester S1570) from Mitsubishi-Kasei Food Corporation.

2.4.2 Methods

Procedure #1: 150ml of solution prepared at room temperature is poured into the thermostatted beaker at 30°C or 80°C. The solution is stirred for 10 minutes to reach temperature equilibrium. Then 20 paired foamability and surface-tension measurements are done. If the solution has too much foam on the surface, the surface is cleaned by suction of the

liquid at the surface. Measurements are performed 10 minutes later, so that the surface tension will have reached its equilibrium value.

Procedure #2: 150ml of milk solution is prepared at room temperature and poured into the thermostatted beaker at 30°C. The solution is stirred for 10 minutes to reach temperature equilibrium. Then 20 paired measurements are done; these serve as the control. A certain amount of a foaming or thickening agent is added to the mixture with stirring during 10 minutes before 20 paired measurements are performed.

Procedure #3: Hot distilled water at 80°C is added to the solid mixture and stirred for 2 minutes to allow dissolution of the powder. Then the solution is poured in the thermostatted beaker at 80°C and the 20 paired measurements are done.

2.5 Results and discussion

In practice, as the frame has a certain thickness, we notice a constant increase of the force due to the buoyancy effect on the vertical wires. We also notice a shoulder in the plotted force versus displacement, due to the thickness of the horizontal wire and the liquid raised under the horizontal wire. This amount of liquid disappears when the formation of the lamella (Figure 2.5). It is still possible to measure the surface tension and the foamability of the solution, however. The foamability is proportionate to the length of the plateau and will be defined as the height of the liquid lamella times a unit length (1cm).

2.5.2 A well-known example of foam booster

One well-known method of increasing foamability in a solution of sodium dodecyl sulfate (SDS) involves adding lauric diethanolamide (Ninol 96-SL). To investigate this method, I mixed, in varying ratios, two solutions containing 1g/L water of SDS and Ninol 96-SL. The foamability and the surface tension of these mixtures were measured. The speed of withdrawal was 0.13 cm/s and the temperature of the solution 30°C. From Figure 2.6, we notice a synergistic effect between the SDS and the Ninol. SDS alone gives a foamability of 1 cm^2, and Ninol alone 2 cm^2. But the correct combination of the two can give a foamability of more than 3 cm^2. We thus have a boosting effect on the foamability. Furthermore, it is important to notice that this effect is not obvious from the surface tension curve.

2.5.3 Influence of sugar ester on a solution of milk protein

The same technique was used to investigate the effect of several foaming agents on a solution of milk protein (NFDM). The different foaming agents are sugar ester (S1570), sodium caseinate, "total milk protein" (TMP), and pluronic F68. The results show that the foamability of the milk protein, whether sodium caseinate, "total milk protein" (TMP), or F68 is used as the foaming agent, remains fairly constant at around 1 cm^2. But when sugar ester is used, we can reach a foamability of more than 4 cm^2. Thus, we must assume that there is an interaction between the sugar ester and the milk protein (Figure 2.7).

2.5.4 Foamability of a solution of milk protein with different additives

I investigated the ability of different ingredients to increase the foamability of a solution of 2% (2g/100ml) milk protein (NFDM) with the tensiolaminometer with a glass frame. The various ingredients used were sodium caseinate (milk protein), sucrose ester (S1570, edible surfactant), carboxy methyl cellulose (CMC), and pectin. The experiments were carried out at 30°C with a glass frame according to procedure #2 (above), to arrive at a first approximation of the solutions' behavior. The results are given in Table 2.1. Each value is the average of 20 paired measurements of the same solution. The relative average deviation for the length of the lamella is about 25%; for the surface tension it is about 1%. As shown, for the values of sodium caseinate the results depend on whether or not the surface is cleaned before the measurements are performed. This is due to the slow rate of adsorption and denaturation at the interface of proteins. If we look at the values of the length of the lamella, which characterizes the foamability of the solution, we notice that the longest lamellae are obtained for sucrose ester and CMC. A lamella that fills the whole frame is pulled out 13 times for S1570 and 14 times for CMC. The sucrose ester lowers the surface tension of the solution, whereas the CMC does not change it. The increase of the foamability with CMC is due to an increase of the viscosity of the medium. We notice that sodium caseinate also increases the foamability of the solution of NFDM.

I used a platinum frame to study the solution at 80°C, as when the experiment was performed at this temperature the milk was sticking to the glass frame, which was difficult to clean without breaking it. The experiments were carried out according to procedure #3 (above). The results are given in Table 2.2 and Table 2.3. Once more we see that the measurements depend on whether or not the surface is cleaned. The interesting point is that when the experiment is performed, some mixtures give a very viscous, gel type of lamella after a few measurements (e.g., NFDM + sodium caseinate), whereas others give a liquid lamella (e.g., NFDM + S1570).

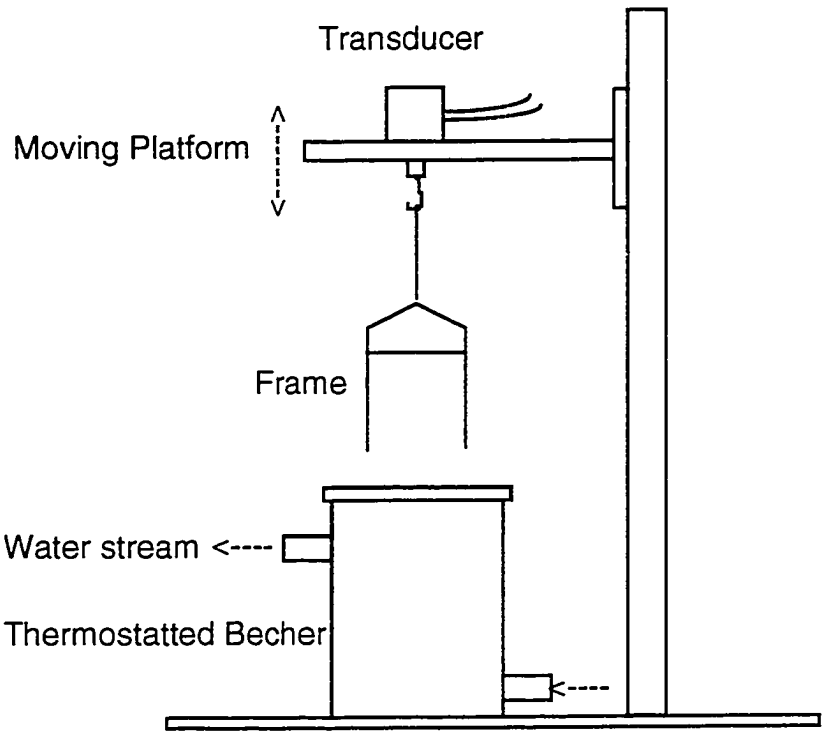

Figure 2.1 : The tensiolaminometer

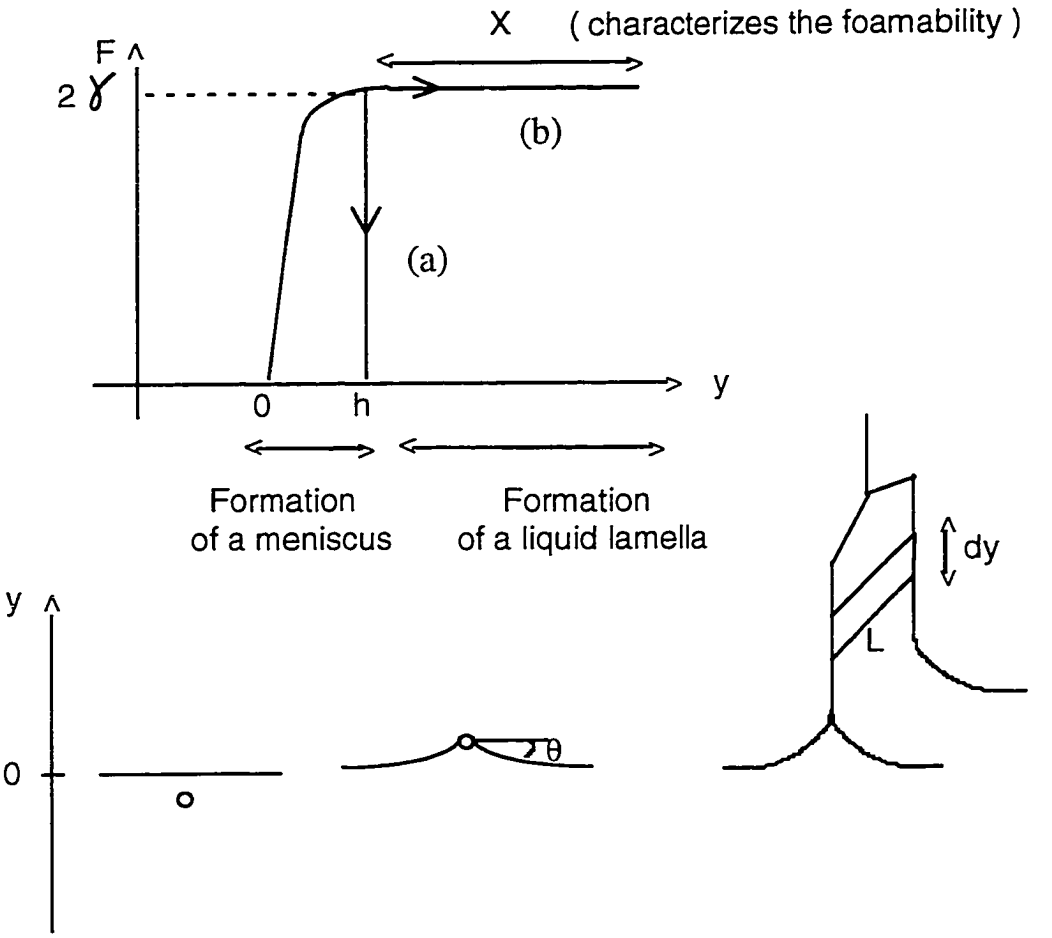

Figure 2.2 : Theoretical shape of the curves

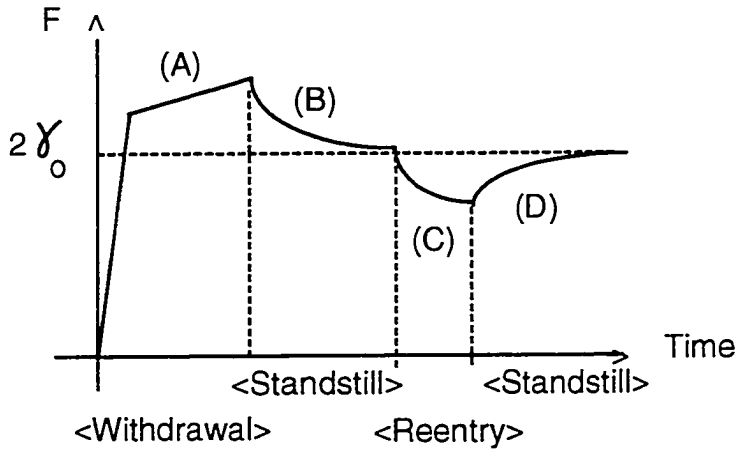

Figure 2.3 : Adsorption behavior showing how the dynamic surface tension values differ from the equilibrium adsorption value γ_o

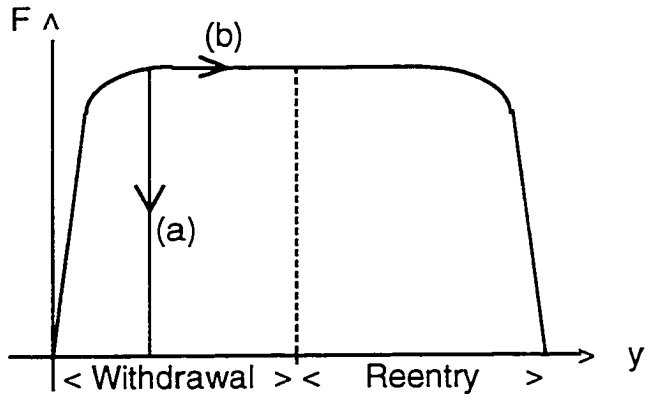

I. Reversible

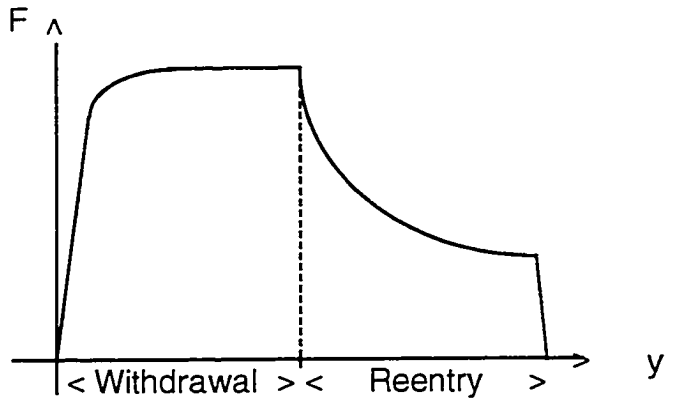

II. Irreversible

Figure 2.4 : Shape of the curves given by the tensiolaminometer for reversible and irreversible surface adsorption

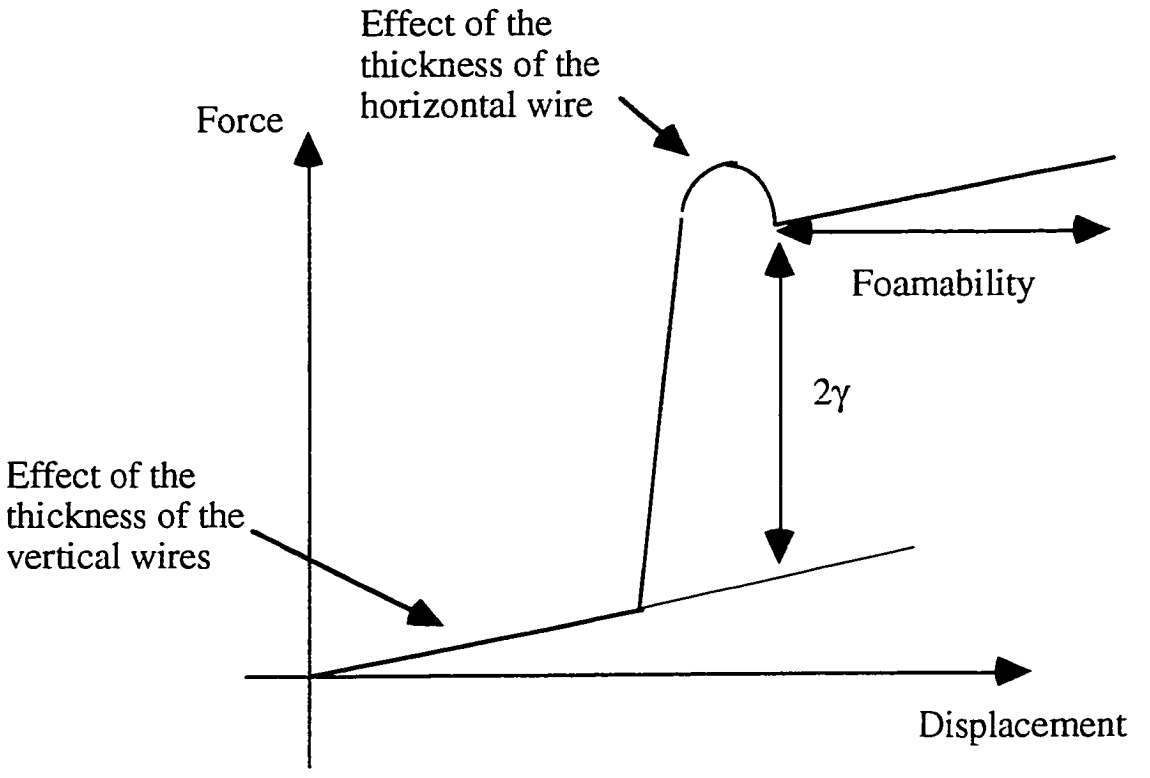

Figure 2.5 : Experimental shape of the curves

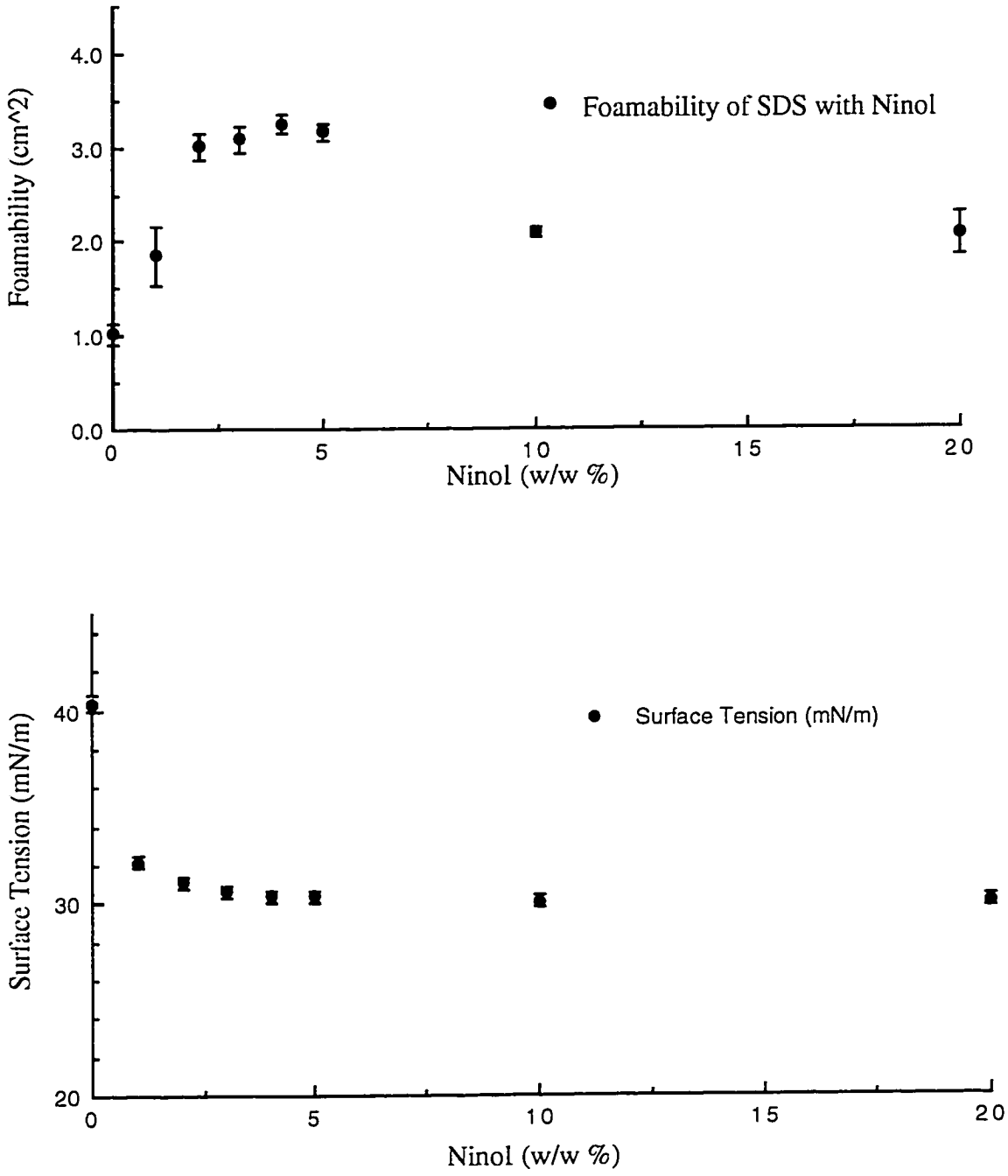

Figure 2.6 : Foamability and Surface Tension of Sodium dodecyl sulfate (SDS) with Lauric diethanolamide (Ninol 96-SL).

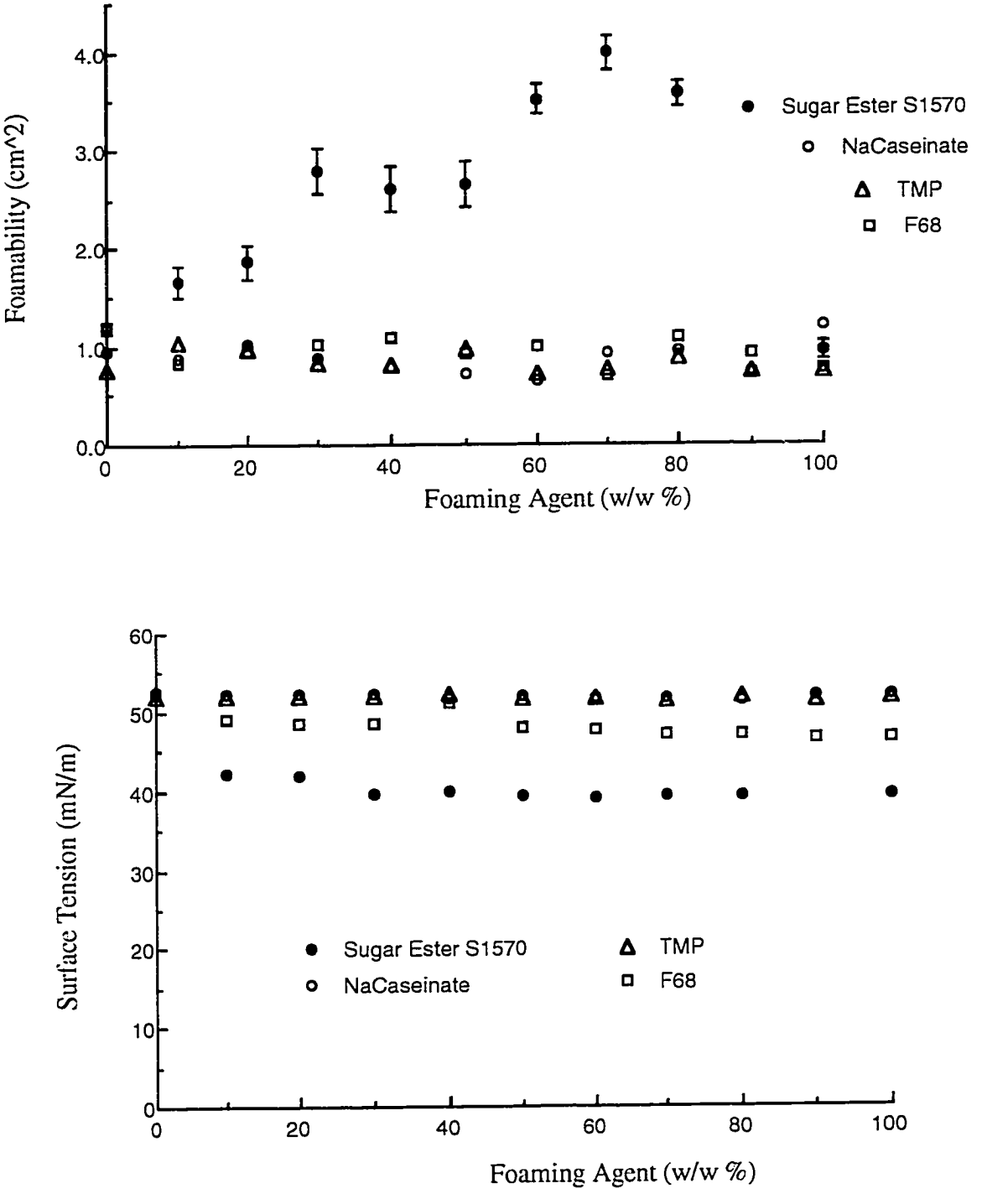

Figure 2.7 : Influence of different foaming agents on a solution of milk protein.

Solution	Average Surface Tension (mN/m)	Average Length of Lamella (cm)	max= 5.6	
Control creamer (4%)	48.92	0.00		CS
NFDM (2%)	51.04	1.74		NCS
NFDM (2%) + NaCaseinate (0.08%)	51.22	2.51		NCS
NaCaseinate (0.08%)	52.39	1.11		CS
Alapro (1.25%)	52.15	0.77		NCS
NFDM (2%) + Sucrose Ester S1570 (0.1%)	40.70	3.96	13*max	NCS
NFDM (2%) + TMP (0.08%)	45.87	3.03		CS
NFDM (2%) + Pectin (0.1%)	51.23	1.41		NCS
NFDM (2%) + CMC (0.1%)	51.83	3.75	14*max	NCS

Table 2.1 : Foamability and surface tension of various solutions measured at 30°C with a glass frame according to procedure #2. (CS: cleaning the surface, NCS: without cleaning the surface)

Solution	Average Surface Tension (mN/m)	Average Length of Lamella (cm)
Control creamer (4%)	44.84	1.40
NFDM (2%)	42.90	1.66
NFDM (2%) + NaCaseinate (0.08%)	41.99	1.38
NaCaseinate (0.08%)	45.85	0.73
Alapro (1.25%)	42.24	0.31
NFDM (2%) + Sucrose Ester S1570 (0.1%)	32.30	1.62
NFDM (2%) + TMP(0.08%)	42.10	1.39
NFDM (2%) + Pectin (0.1%)	43.60	0.97
NFDM (2%) + CMC (0.1%)	44.49	1.26

Table 2.2 : Foamability and surface tension of various solutions measured at 80°C with a platinum frame according to procedure #3 without cleaning the surface.

Solution	Surface Tension near equilibrium (mN/m)	Average Length of Lamella (cm)
Control creamer (4%)	45.49	1.41
NFDM (2%) + NaCaseinate (0.08%)	42.90	1.56
NaCaseinate (0.08%)	46.08	0.82
Alapro (1.25%)	40.29	1.33
NFDM (2%) + Sucrose Ester S1570 (0.1%)	32.30	1.67
NFDM (2%) + TMP(0.08%)	43.58	1.52
NFDM (2%) + Pectin (0.1%)	43.15	2.13
NFDM (2%) + CMC (0.1%)	43.80	2.42

Table 2.3 : Foamability and surface tension of various solutions measured at 80°C with a platinum frame according to procedure #3 after cleaning the surface.

Chapter 3

Interbubble Gas Diffusion and the Stability of Foams

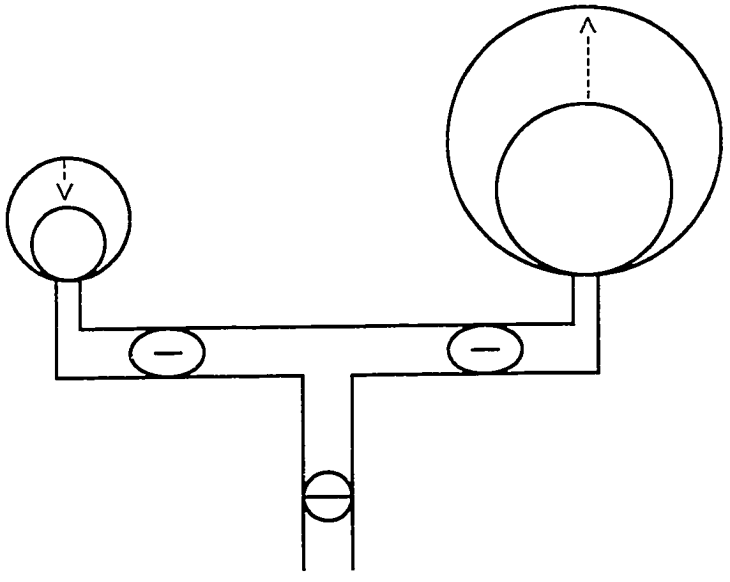

3.1 Introduction

A foam is a dispersion in which a large number of gas bubbles are present in a continuous liquid phase, with a thin film of liquid separating each pair of gas bubbles. The surface energy of the liquid phase is high, and a foaming agent or agents must be added to lower the interfacial tension between the liquid and the gas. Since the bubbles in the resulting foam are fragile, other additives are often used to give the foam the elasticity needed to stabilize it against mechanical shock. Proteins can serve as foam stabilizers by unfolding at the interface and thus increasing surface viscosity. In general, the two main functions of a surfactant or a combination surfactant/stabilizer (in foams or emulsions) are: (1) to lower the interfacial free energy in order to facilitate the formation of the dispersion; and (2) to stabilize the resulting dispersed system.

Besides the foaming properties of the initial solution and the stability of the lamellae, a crucial factor to consider when analyzing the stability of foams is disproportionation or Ostwald ripening. Disproportionation is a coarsening process arising from interbubble gas transport caused by pressure differences between bubbles (but also dependent upon the permeability of the adsorbed surface film). This pressure difference may be a consequence of a difference in size, as, according to Laplace's Law (see Appendix 4), the pressure in a smaller bubble is higher than the pressure in a larger bubble, assuming that the surface tensions of the two

bubbles are equal. Thus the larger bubble will grow at the expense of the smaller one, and the smaller bubble will eventually disappear. The consequence is a coarsening of the foam, leading eventually to its collapse.

Lemlich[16,17] presented a theory for the change in the distribution of bubble sizes that results from the diffusion of gas between bubbles of liquid foam. The theory begins with the application of the classical Law of Laplace and Young to the pressure difference between a bubble and its surrounding liquid, and involves a concept of gas transfer to and from an effective fictitious intermediate bubble.

Lemlich ignored any contribution to the processes of diffusional disproportionation from changes in the gas-liquid surface tension due to the effect of surface area changes upon the dilational properties of the surface. In the case of solutions of proteinaceous materials, where denaturation may inhibit desorption, or in the case of phospholipids, appreciable changes in surface tension may occur as bubbles shrink.

The concept of adding a second insoluble compound to the dispersed phase (liquid droplets in the case of emulsions) to stabilize an emulsion has been suggested by various authors.

Davis, Round, and Purewal[18] concluded that Ostwald ripening is important for emulsion systems having small particle size and made with a **pure** oil of significant solubility in the continuous phase. A small amount

---

[16] Lemlich, R., *Ind. Eng. Chem. Fund.* **17**, 89 (1978)
[17] Ranadive, A.Y., and Lemlich, R., *J. Colloid Interf. Sci.* **70**, 392 (1979)
[18] Davis, S.S., Round, H.P. , and Purewal, T.S., *J. Colloid Interface Sci.* **80**, 508 (1981)

of additive (or impurity) of lower vapor pressure (solubility) than the dispersed phase will give rise to stabilization.The phenomenon will apply equally to O/W and W/O emulsion systems. For the latter category, water will pass from water drop to water drop. Consequently, the phenomenon may be considered as an osmotic process with the oil phase acting as a semipermeable membrane. The addition of a small quantity of electrolyte to the dispersed phase will provide the necessary stabilizing effect.

Kabalnov and Schukin[19] confirmed that Ostwald ripening is the cause of emulsion degradation more often than previously presumed. **Weers, Ni, Tarara, Pelura, and Arlauskas**[20]; and **Weers and Arlauskas**[21] used field flow fractionation to study Ostwald ripening in fluorocarbon emulsions containing two dispersed phase components. To counteract emulsion growth they used the approach developed by **Higuchi and Misra**[22], which uses a second dispersed phase component (a small amount of perfluorodecyl bromide (PFDB) was added to perfluorooctyl bromide (PFOB); PFDB is practically insoluble in the continuous phase). Significant partitioning of the two dispersed phase components between different sized droplets was observed, with the less water-soluble component concentrated in the smaller droplets. The important result reported is that controlling Ostwald ripening resulted in the preparation of much stabler and finer dispersions.

---

19 Kabalnov, A.S., and Schukin, E.D., *Adv. Colloid Interface Sci.* **38,** 69 (1992)
20 Weers, J.G., Ni, Y., Tarara, T.E., Pelura, T.J., and Arlauskas, R.A, *Colloids Surf.* **84,** 81 (1994)
21 Weers, J.G. and Arlauskas, R.A., *Langmuir* **11,** 477 (1995)
22 Higuchi, W.I. and Misra, J., *J. Pharm. Sci.* **51,** 459 (1962)

Kabalnov, Weers, Arlauskas, and Tarara[23] tried to explain the lower ripening rates observed in phospholipid-stabilized emulsions. In my opinion the most probable explanation lies in the insolubility of phospholipids in water and in perfluorocarbon oils: as soon as the droplet area decreases, the phospholipids will reach a high collapse pressure with a resultant very low interfacial tension. Another factor could be the reduction of the rate of diffusion by the monolayer itself (the use of monolayers to reduce the rate of evaporation of water is a familiar technique). Ostwald ripening may be negligible at very low interfacial tensions or when the interfacial film acts as a barrier to diffusion.

Falls, Lawson, and Hirasaki[24] have shown that the lifetime of foams made from condensable gases, like steam foams, is limited by condensation and evaporation. Water condenses on the inside of the smaller bubble and evaporates into the larger one, and one of two mechanisms can govern how fast bubbles collapse: heat transfer or transport of surfactant. When noncondensable gases, such as nitrogen or methane, are added to the steam in an amount sufficient to make a third mechanism, the diffusion of the noncondensable gas, the governing factor in the collapse of the bubbles, bubble lifetime and consequently the foam lifetime are increased.

Weaire and Pageron[25] have shown that an insoluble gaseous component will theoretically inhibit foam evolution even for a very small concentration of insoluble gas. In fact, a small fraction of even a relatively insoluble gas effectively inhibits rapid coarsening of a liquid gas foam:

---

[23] Kabalnov, A.S., Weers, J.G., Arlauskas, R.A., and Tarara, T.E., *Langmuir* **11,** 2966 (1995)
[24] Falls, A.H., Lawson, J.B., and Hirasaki, G.J., *JPT*, Jan., 95 (1988)
[25] Weaire, D., and Pageron V., *Phil. Mag. Lett.*, **62**, 417 (1990)

they offer the example of adding a few percent of N_2 into CO_2-containing beer foams.

Monsalve and Schechter[26] have shown the importance of the initial bubble size distribution in determining the rate of foam surface area reduction due to bubble disproportionation by diffusion. They concluded that foam surface area decreases as a bilinear exponental function of time. One of the two characteristic time constants appears to be related to a gravity mechanism, while the second one is determined by the rate of gas diffusion between bubbles.

The present study seeks to show that it is possible to counterbalance Ostwald ripening in a foam by adding to the gas phase a compound that is insoluble in the continuous phase. I begin with a theoretical explanation of the stabilizing effect.

3.2 Theory

Let us consider two gaseous solutes: gas 1, which is insoluble in water, and gas 2, which is soluble. Let us study the equilibrium between two bubbles a and b of radius r_a and r_b containing a mixture of gases 1 and 2. The pressure P_i inside a bubble of radius r is given by the Gas Law:

$$P_i=(n_1+n_2)RT/(4/3\pi r^3)$$

---

[26] Monsalve, A., and Schechter, R.S., *J. Colloid Interface Sci.* **97**, 327 (1984)

where n_i is the number of moles of component i, R the gas constant, and T the temperature.

Furthermore, using the Laplace equation, given the outside pressure P_O and the surface tension γ, we have the following equation:

$$P_i - P_O = 2\gamma / r.$$

Then

$$P_i = P_O + 2\gamma/r = (n_1+n_2)RT/(4/3\pi r^3) = p_1+p_2$$

where p_i is the partial pressure of component i.

Since gas 1 does not diffuse, n_1 is a permanent characteristic of each bubble, while n_2 is variable. At equilibrium between two bubbles a and b, $p_{2a} = p_{2b}$, since gas 2 diffuses.

The difference between the total inside pressures is

$$\begin{aligned} P_{ia} - P_{ib} &= 2\gamma(1/r_a - 1/r_b) \\ &= (p_{1a}+p_{2a}) - (p_{1b} + p_{2b}) \\ &= p_{1a} - p_{1b} \\ &= (3RT/4\pi)*(n_{1a}/r_a^3 - n_{1b}/r_b^3) \end{aligned}$$

Let $\Gamma = 8\pi\gamma / 3RT$.

Therefore,

$$\Gamma(1/r_a - 1/r_b) = n_{1a}/r_a^3 - n_{1b}/r_b^3 \qquad [3.1]$$

Let $v=r_a/r_b$, $\theta= \Gamma\, r_a^2/n_{1a}$ (dimensionless, energy/energy), and $y=n_{1b}/n_{1a}$. y is the most useful parameter to characterize the system as n_{1a} and n_{1b} remain constant for each bubble. Then Equation [3.1] gives

$$\theta\,(v - 1) = yv^3-1. \qquad [3.2]$$

Equation [3.2] was solved for various values of θ and y. Y was restricted to values between 0 and 1, since a radius is always positive and cases in which y>1 can be treated by reversing the roles of a and b. Furthermore, for y<1 the acceptable solution of v for Equation [3.2] is v<1, as the smaller bubble decreases in size and the larger one increases in size. Since $\theta = \Gamma\, .r_a^2/\, n_{1a}$, the larger n_{1a}, the smaller θ will be. Moreover, $y = n_{1b}/n_{1a} \sim (r_b\text{initial}/r_a\text{initial})^3$ (assuming we have two bubbles with the same concentration of gas 1).

Figure 3.1a shows r_a/r_b equilibrium vs r_a/r_b initial, calculated for values of θ between 0.2 and 1.0 using Equation [3.2]. We may conclude that if the initial bubbles are equal in size for any values of θ no change in size occurs, i.e., no disproportionation occurs. When the two bubbles are of unequal size and a sufficient amount of nondiffusible vapor is present, θ is small enough (for example $\theta = 0.2$) that there is no appreciable difference between initial and equilibrium sizes. When the amount of nondiffusible vapor is insufficient ($\theta = 1.0$), the effect of the disproportionation is important. The obvious conclusion is that if a sufficient amount of insoluble vapor is present in the gas droplet disproportionation disappears. Moreover, the theory predicts (see the graph in Figure 3.1b of θ versus v for values of $\theta > 1$) that the foam may

be polydispersed (i.e., that there may be two solutions for r_a/r_b equilibrium). With the theory of Lemlich in mind, the two solutions for r_a/r_b at equilibrium can be related to the two separate equilibria between each of the two real bubbles and the fictitious bubble considered by Lemlich. This shows the possibility of a bimodal distribution in a real foam. Bimodal distributions have been observed in emulsions. My reasoning has been in terms of two gas bubbles, whereas in reality a foam is an aggregate of bubbles of various diameters. For example, in the case of three bubbles, one smaller and another larger in diameter than the average bubble, it will be necessary to consider simultaneous equilibrium, and a polydispersed system will result.

The present approach has ignored the role played by the permeability of the interbubble lamellae during the lifetime of the foam. When the gas permeability is low compared to the life of the foam, disproportionation may be considered as playing a minor role on the stability of the foam.

3.3 Experimental part

3.3.1 Materials

The foaming agents used are Pluronic F68 (a block copolymer of ethylene oxide and propylene oxide condensate) from Alliance Pharmaceutical Corporation (San Diego), Sodium dodecyl sulfate (SDS) from Sigma (+99%), and two milk proteins, "Alapro" from New Zealand Milk Products (North America Inc.) and "Non-Fat Dry Milk" (NFDM) from Kraft Foods. The required solutions were prepared by diluting the

surfactant with distilled water. Four commercial shampoo formulations (A, B, C, and D) were also used as foaming agents. Lauryl alcohol (LOH) from Sigma was used as a foam booster with SDS, and xanthan gum (XG) was used as hydrosoluble polymer. N_2 and CO_2 were bubbled into either water, Perfluorohexane (PFH), or any of several species of Fluorinert (linear perfluo molecules). Perfluorohexane (PFH) was provided by PCR, and Fluorinert FC77, FC104, FC40, and FC70 by 3M (see Table 3.1).

3.3.2 Methods

Figure 3.2 shows the experimental setup used to produce foam by bubbling and to measure the drainage of a standing foam. The experimental setup consisted of a sintered glass disc located at the bottom of a thermostatted graduated glass column having a diameter of 4.0 cm and a capacity of 250 ml. The column is initially filled with 50ml of a foaming solution. Foam is formed by bubbling air, CO_2, or N_2 (alone or containing a solvent vapor), at a fixed volumetric flow rate through the porous frit into the surfactant solution. Foam is formed at the gas-liquid interface and moves up at a rate that depends on the superficial gas velocity. Once the foam reaches the required height, the gas supply in the cylinder is turned off. The gas is allowed to flow into the lower part of the tube to provide enough back pressure to prevent the liquid from seeping down through the fritted disc. The liquid coming out of the foam is monitored vs. time until an equilibrium is practically reached. I used foam surface velocities (rates of foam formation) that varied from 39.60 cm/min (497.4 cm^3/min) to 1.20 cm/min (15.1 cm^3/min). The gas (CO_2 or N_2) jet used to form the

foam contained various vapors: water, perfluorohexane (PFH), and Fluorinert FC77, FC104, FC40, and FC70.

3.4 Results and Discussion

3.4.1 Influence of the gas composition in the bubble

Figure 3.3 shows a typical result of an experiment on liquid drainage when the air used as the gas phase is saturated with water or with a vapor of perfluorohexane (PFH). The y-axis represents the percentage of water retained in the foam at any time t. This percentage is obtained by the following expression:

$$\% \text{ of liquid in the foam} = \frac{V_o - v(t)}{V_o} * 100$$

V_0 represents the initial volume of the foaming solution, and v(t) the volume of liquid at time t (volume of drained solution + volume of liquid at t=0).

This experiment has a good reproducibility for a certain range of rates of foam formation. We notice a striking difference between the two sets of experiments. When the air used to produce the foam is saturated with water, there is less than 10% of water retained in the foam after 10min, whereas when the air is saturated by PFH, more than 20% of liquid is retained in the foam.

Following foam formation, experimentally the rate of drainage of the liquid from many foams obeys a first-order kinetic equation. I thus began by analyzing the data v(t) as a first-order kinetic. v(t) fits the following mathematical expression for a certain range of time (in most cases for the first 10min):

$$v(t) = V_x(1-e^{-kt})$$

$$\mathrm{Ln}\left(\frac{V_x - v(t)}{V_x}\right) = -kt$$

V_x is varied and $\mathrm{Ln}\left(\frac{V_x - v(t)}{V_x}\right)$ is plotted as a function of time t. The slope of the straight line gives k. When analyzing the data by a first-order kinetic approach, we see that when water vapor is used in the gas, V_x is the initial volume of liquid V_o, whereas when PFH vapor is used we need to set V_x at $0.8V_o$. If we assume that free water drains in between the gas bubbles, V_x can be written as V_o-V_b, where V_b represents the volume of water retained in the foam after a long time (>20 min).

My second approach made use of the suggestion of **Monsalve and Schechter**[27] and **Yu and Damodaran**[28] to consider the drainage of the experiment with PFH as following a biphasic first-order kinetic. Thus the percentage of liquid draining out of the foam can be computed with the following expression:

---

[27] Monsalve, A., and Schechter, R.S., *J. Colloid Interface Sci.* **97,** 327 (1984)
[28] Yu, M., and Damodaran, S., *J. Agric. Food Chem.* **39,** 1555 (1991)

$$\% \text{ calc} = Q_g \exp(-t/\tau_g) + Q_d \exp(-t/\tau_d)$$

where τ_g and τ_d are first-order time constants for the gravitational drainage and gas diffusion, and Q_g and Q_d are the amplitude parameters of the two kinetic phases. In the experiment with PFH (Figure 3.3), the drainage has a time constant of around 200s, while the gas diffusion has a time constant one order of magnitude higher at around 4200s. The experiment without PFH followed a biphasic first-order kinetic with the gas diffusion drainage being the rate-limiting step. The gas diffusion is thus faster than the drainage.

I repeated the experiment replacing PFH by several other species of Fluorinert having different boiling points (Figure 3.4). Observing the physical characteristics of these fluorocarbons makes it clear that if the boiling point is not too high, there is sufficient vapor pressure to stabilize the foam, and the curve obtained is the same as with PFH.

I also investigated the effect of the initial insoluble vapor percentage of FC104 in the CO_2-generating gas on the liquid drainage of a 1g/L Pluronic solution. The percentage of FC104 vapor in CO_2 can be calculated if the vapor pressure of FC104 versus temperature is known (see Figure 3.5 and Table 3.2). Figure 3.5 clearly shows that from 0.42% and above the drainage curves are the same. Below this value the drainage curves tend to catch up with the drainage curve without insoluble vapor. Furthermore, visual observation of these systems reveals two kinds of bubbles: large

bubbles surrounded by smaller ones. This leads me to conclude that this is a case of bimodal distribution.

These results are in agreement with the formula of **Kabalnov and Shchukin** enabling the calculation of the molar fraction of the insoluble solute required to counterbalance the effect of the Laplace pressure (Equation [5] in ref. [29]) :

$$x_{0_{FC104}} > \frac{2\gamma V_m}{3RT\overline{r_0}} \qquad [3.3]$$

where γ is the surface tension, V_m the molar volume of the dispersed phase (here the soluble gas), R the gas constant, T the temperature, and $\overline{r_0}$ the average initial radius of the droplets or bubbles. If the condition [3.3] is not met, the distribution of bubbles cannot attain equilibrium. Ostwald ripening will proceed as in the absence of the second component. Since the second component is insoluble in the dispersion medium, however, the size distribution is represented by a bimodal distribution function. Using 0.125mm for an initial average gas droplet radius, γ of 50 mN/m at 25°C, the molar fraction of FC104 must be larger than 0.26%. Figure 3.6, the photograph at 1900 seconds of a foam containing 3.75% of FC104 in a CO_2-generating gas, shows a homogeneous foam composed of fine bubbles. Figure 3.7, the photograph at 220 seconds of a foam containing 0.203 % FC104 in the CO_2-generating gas, clearly shows that with an FC104 concentration below the stabilization level we see many large bubbles surrounded by smaller bubbles.

---

[29] Kabalnov, A.S., Pertzov, A.V. and Schukin, E.D., *Colloids Surf.* **24,** 19 (1987)

I considered the possible effect of vapor condensation on foam stability during the shrinkage of the bubbles in the foam, but concluded that such an effect was improbable. Reasoning by analogy with the effect of salts on the stability of W/O emulsions, we see that gas condensation in foam bubbles would lead to the erroneous conclusion that emulsion stability results from solute saturation in the dispersed phase!

If CO_2 is substituted for N_2, we notice (Figure 3.8) a large increase in the rate of drainage. This is to be expected, as CO_2 is much more soluble in water than N_2. Nevertheless, PFH can stabilize the foam as well as in the case when the gas is N_2.

Doing the experiment at different temperatures with the same rate of foam formation, and plotting the difference between the percentage of liquid retained in the foam as shown in Figure 3.9, reveals the effect of the interbubble gas diffusion on the drainage. The initial slope of the curve enables us to estimate the rate of Ostwald ripening. We notice that disproportionation starts to act quickly below 100s and that it increases with the temperature. An Arrhenius plot of the initial slope of the curves gives an activation energy of 4.6 kcal/mol.

3.4.2 Influence of the structure and permeability of the liquid lamella

Most of my experiments were done using solutions of F68, and the surface tension was assumed to be constant -- an assumption that is not

always valid. Moreover, the structure of the liquid lamella separating gas bubbles can act as a barrier to gas diffusion. For example, with the "Alapro" milk protein at room temperature there is little difference between an experiment with PFH and one without. In contrast, at 80°C there is a great difference due to the increase of the diffusion with the temperature, as can be seen in Figure 3.10a and 3.10b. If we use air saturated with water vapor, the foam coarsens very fast and the foam collapses completely after 10 minutes. If we use a vapor of PFH we still have 80% of the initial foam height after 10 minutes. Another phenomenon that comes into play is the denaturation of the protein and the resultant formation of a solid foam. In the case of a solution of NFDM, even if we use air saturated with PFH vapor, it is not possible to stabilize the foam. This observation can be attributed to the fact that the lamellae are not stable and coalescence is the major factor that prevents the formation of a stable foam.

Foam stability is widely considered an important selling point in commercial shampoo products, despite its debatable relevance to a given shampoo's actual cleansing capacity: a "good head of suds" that persists over time serves as a strong visual symbol that the product is at work. Foam *decay*, then, is something to be minimized. Foam stability of four 1% aqueous solutions of commercial shampoos were studied using CO_2, saturated with either water or a sparingly insoluble vapor of perfluorohexane (PFH). Ostwald ripening appears to destabilize the foams of formulations A, B, and C 1% solutions, but is hindered to some extent by the presence of PFH. Figures 3.11a-3.14a show the results of parallel experiments, with and without PFH, using the commercial shampoo

formulations. Foams produced with formulations A, B, and C are stabilized by adding PFH vapor to CO_2-generating gas, since in each case the drainage curve with PFH is above the one with water. In contrast, the formulation D solution produced a foam less sensitive to the presence of PFH. In the case of formulation D, there seems to be practically no difference between the two drainage curves. This result suggests that interbubble gas diffusion is minimal for formulation D. Comparing foam heights (Figures 3.11b-3.14b), we see that formulation D is not affected by the presence of PFH vapor in CO_2. Plotting the difference in the percentage of liquid retained in the foam, as shown in Figure 3.15, reveals the effect of the interbubble gas diffusion on the drainage. The initial slope of the curve enables us to estimate the rate of Ostwald ripening. We notice that disproportionation starts to act quickly (below 150 seconds) for formulation A, B, C, and pluronic F68, whereas for formulation D practically no change is noticed.

Brown, Thuman, and McBain[30,31] showed that high foam stability depends on the adsorbed film's having low permeability to air and high surface viscosity, and both of these effects may result from special solute pairs. **Princen and Mason**[32] also stated that the permeability of monolayers on both sides of the film plays an important role in the rate of transport. **Ronteltap, Damste, De Gee, and Prins**[33] showed that when gas composition is uniform throughout the foam the rheological behavior of the bubble surface is the main parameter determining the

---

30 Brown, A.G., Thuman, W.C., and McBain, J.W., *J. Colloid Interface Sci.* **8**, 491 (1953)
31 Brown, A.G., Thuman, W.C., and McBain, J.W., *J. Colloid Interface Sci.* **8**, 508 (1953)
32 Princen, H.M., Overbeek, J.TH.G., and Mason, S.G., *J. Colloid Interface Sci.* **24**, 125 (1967)
33 Ronteltap, A.D., Damste, B.R., De Gee, M. and Prins, A., *Colloids and Surfaces* **47**, 269 (1990)

disproportionation rate. Lauryl alcohol is probably the best-known, classic example of a foam stabilizer or suds booster. Figure 3.16 shows drainage curves for foams produced from a solution of sodium dodecyl sulfate (SDS) alone or in combination with lauryl alcohol (LOH). From these curves we notice that the presence of perfluorohexane stabilizes the SDS foam considerably. The combination of SDS and LOH markedly reduced the drainage rate as expected and consecutively yielded a very stable foam. But furthermore, the addition of perfluorohexane to the CO_2-generating gas increased the stability of the SDS/LOH foam slightly. This confirms that when the adsorbed film has both a low permeability to the foam-generating gas and high surface viscosity, disproportionation is markedly reduced.

Sarma, Pandit, and Khilar[34] showed that the stability of aqueous foams can be significantly enhanced by the addition of a small amount of water-soluble polymers. Such enhancement is attributed to the retardation both in the rate of drainage and in the rate of interbubble gas diffusion. Addition of water-soluble polymer increases the bulk viscosity and thereby decreases the rate of drainage. It also decreases the gas permeability of liquid lamellae and as a result the rate of interbubble gas diffusion is retarded. Figure 3.17 shows drainage curves for foams produced from solution of sodium dodecyl sulfate alone or with xanthan gum (XG). The drainage curve with XG can be seen as composed of two stages: the first characterized by a slow drainage rate and the second by fast drainage. XG initially decreases the gravitational drainage due to an increase in the bulk viscosity of the foaming solution, but then drainage

---

[34] Sarma, D.S.H.S.R., Pandit, J., and Khilar, K.C., *J. Colloid Interface Sci.* **124,** 339 (1988)

shows a marked increase due to thinning of the films and interbubble gas diffusion. The addition of perfluorohexane to the CO_2-generating gas enables us to determine the importance of the gas diffusion in the second part of the drainage curve.

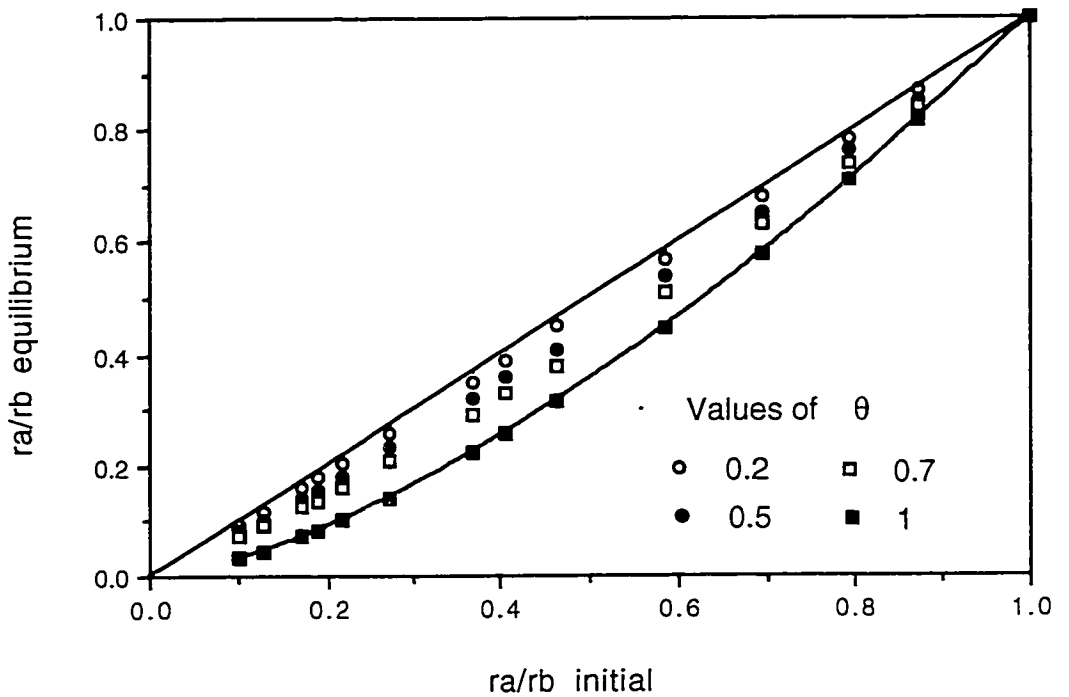

Figure 3.1a : Calculated ra/rb at equilibrium versus r_a/r_b initial for various values of θ.

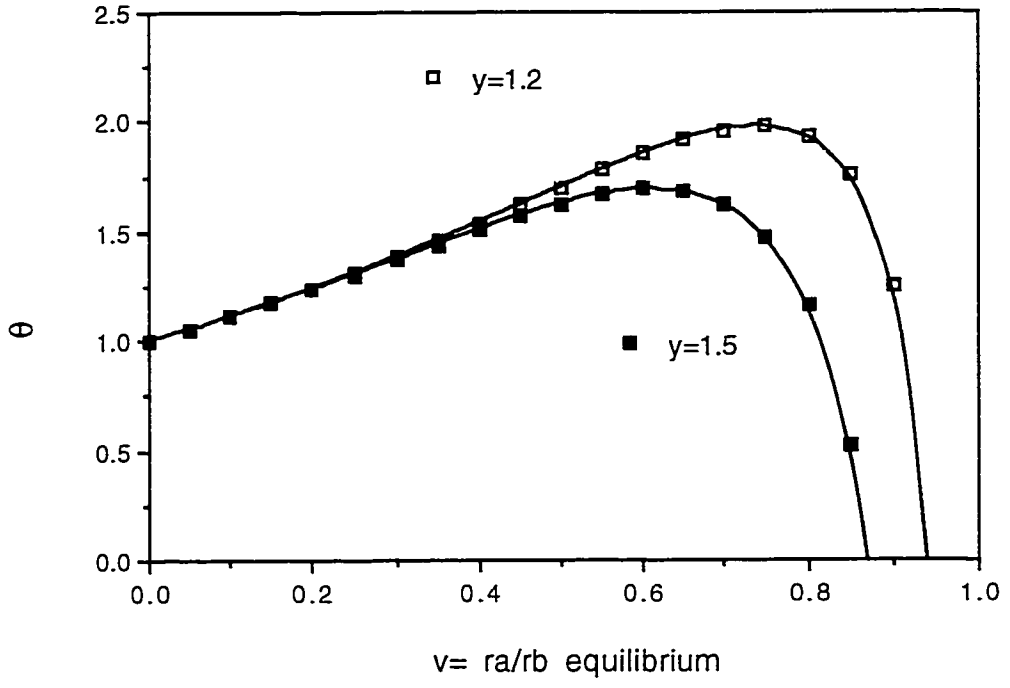

Figure 3.1b : Graph of θ versus v for y=1.5 and 1.2.

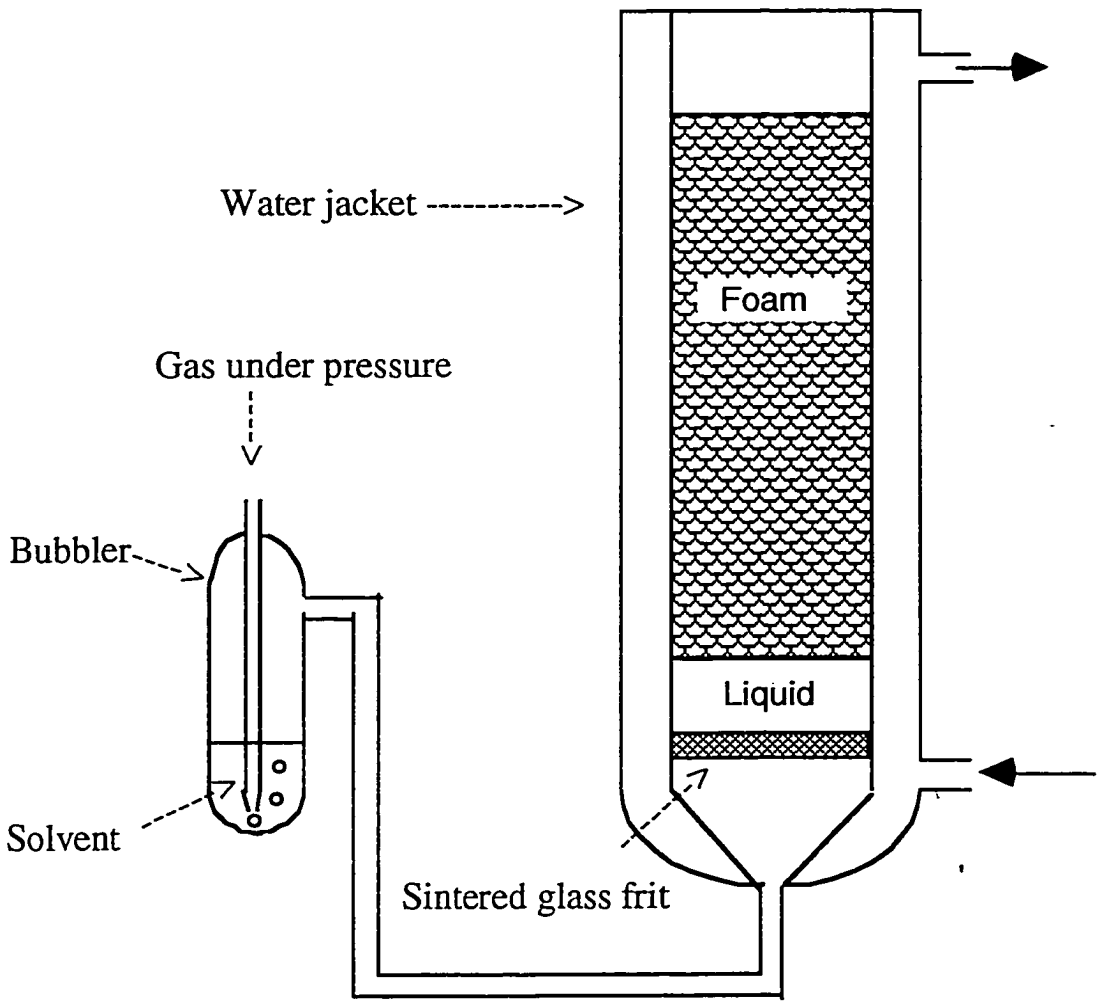

Figure 3.2 : Experimental setup to study the drainage of a standing foam.

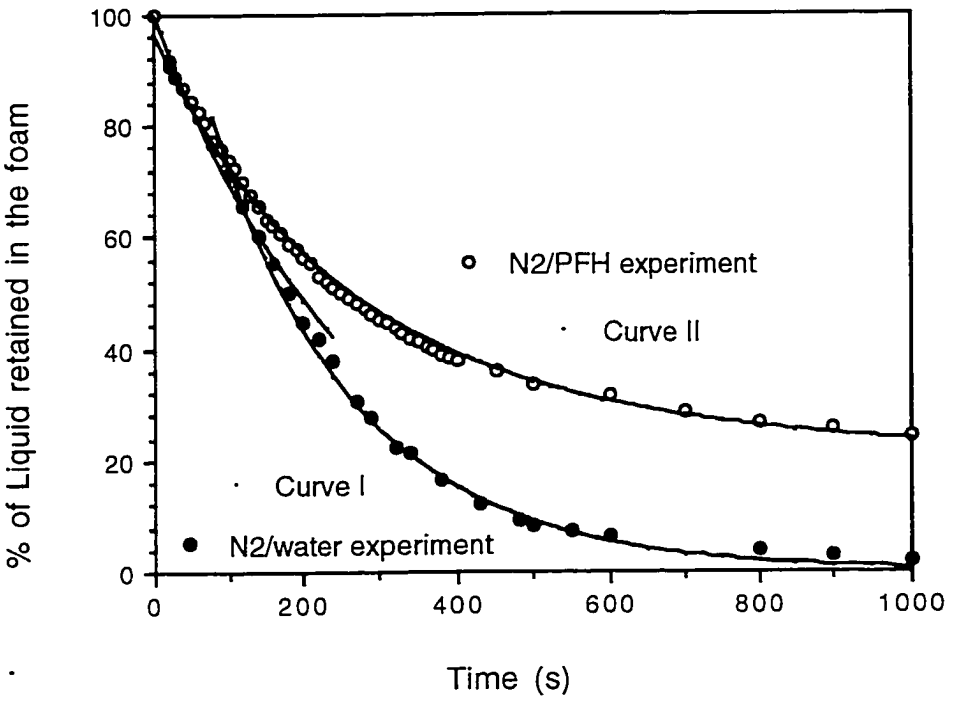

Figure 3.3 : Typical result of a drainage experiment and interpolation by a biphasic first-order kinetic equation. Solution : 1g/L of Pluronic F68. N_2 saturated with water or with PFH, Foam surface velocity=0.22 cm/s, V_O=50ml, Temperature=30°C. Curve I: Correlation by a biphasic first-order kinetic equation (τ_g=276s and τ_d=190s). Curve II: Correlation by a biphasic first-order kinetic equation (τ_g=243s and τ_d=4203s).

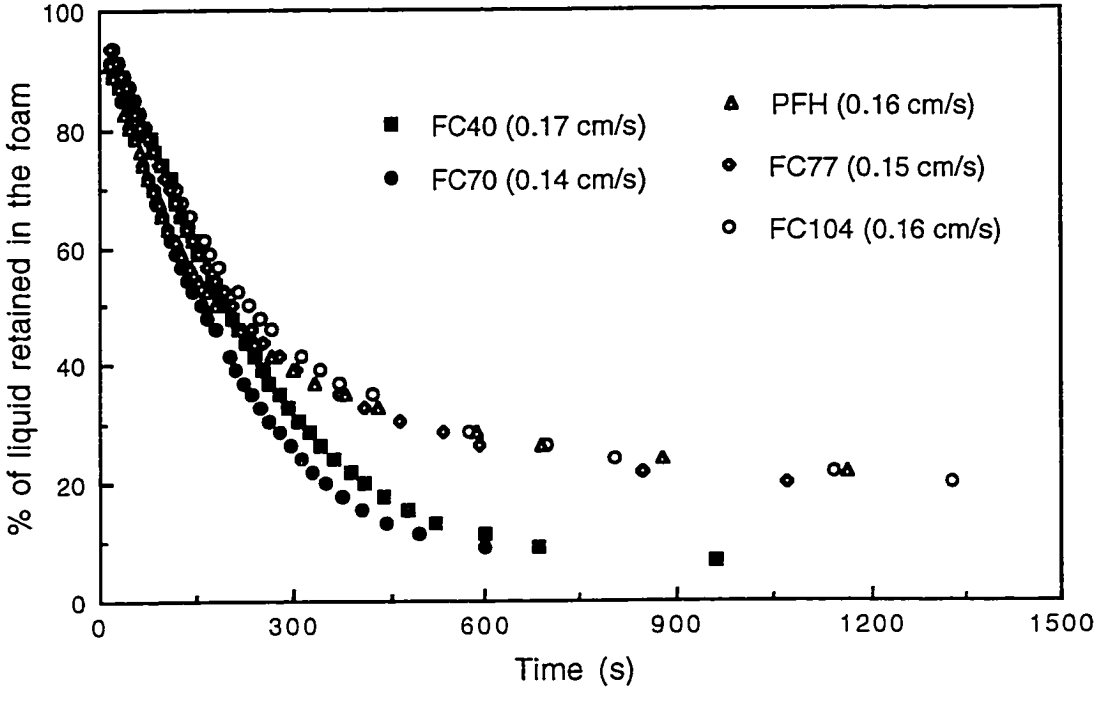

Figure 3.4 : Effect of the addition of various perfluorocarbon vapors to the air of the bubbles. Solution : 1g/L of Pluronic F68.
V_O=50ml, Temperature=20°C.

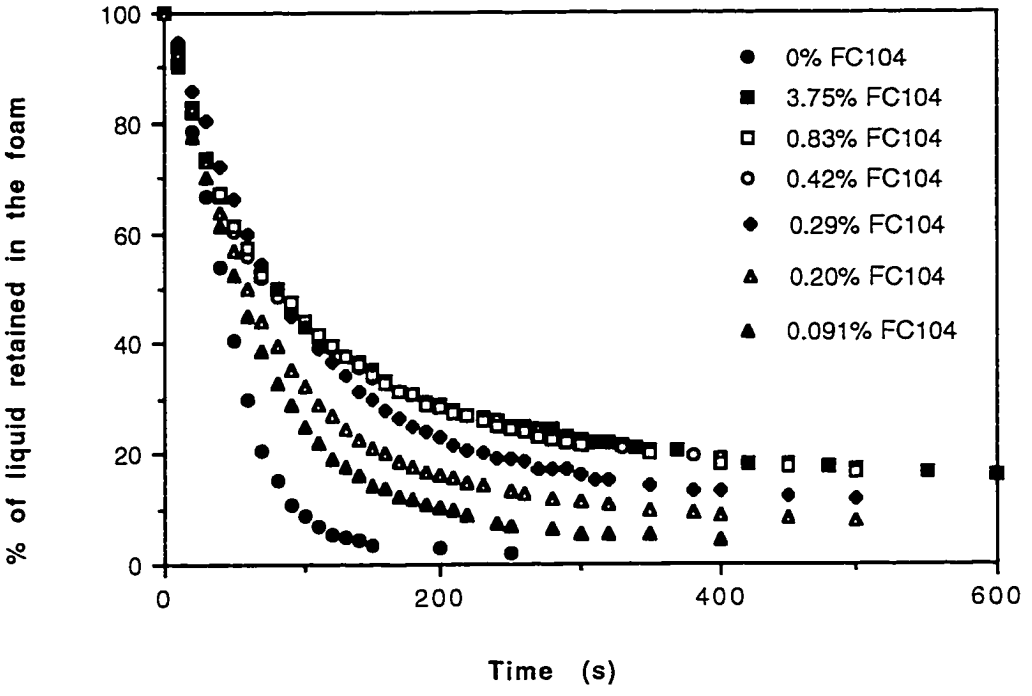

Figure 3.5 : Effect of initial insoluble vapor percentage (FC104) in the CO_2 Foam-generating gas on liquid drainage.

Solution : 1g/L of Pluronic F68.

V_O=50ml, Temperature=25°C, Rate of foam formation=0.22 cm/s.

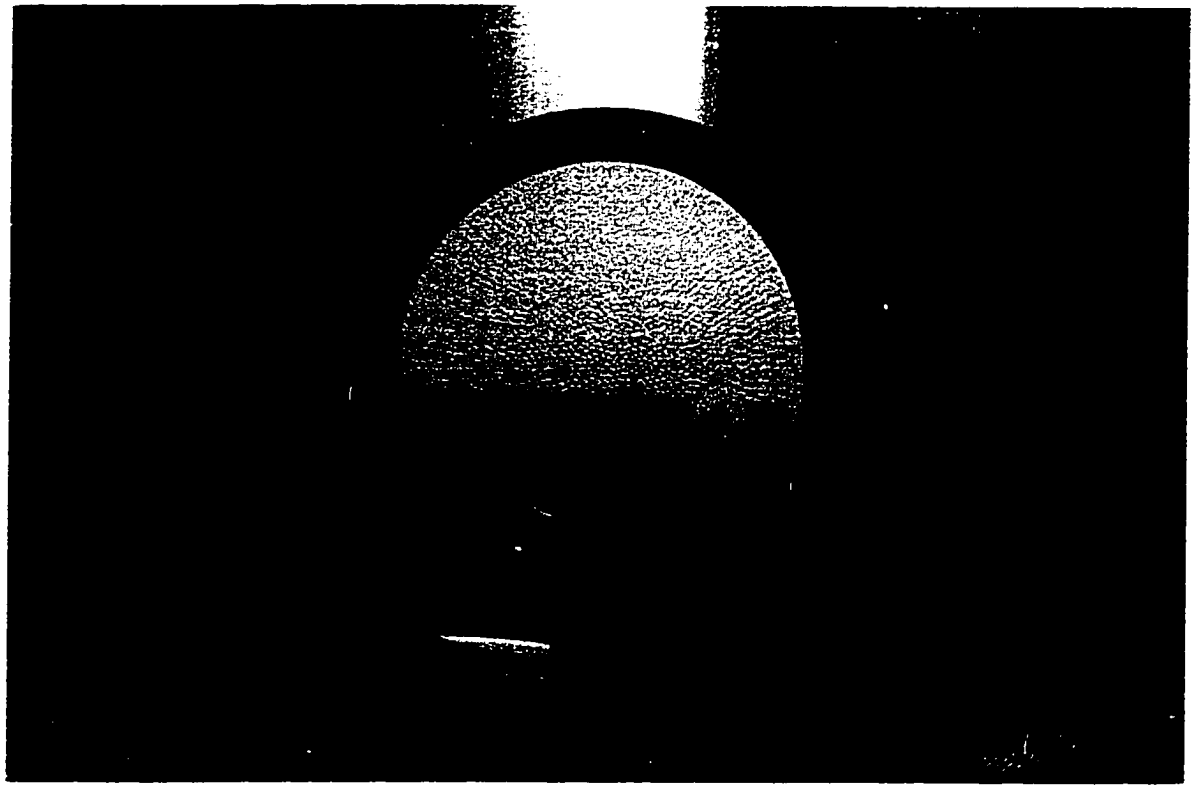

Figure 3.6 : Photograph at 1900 seconds of a foam containing 3.75% of FC104 in a CO_2-generating gas

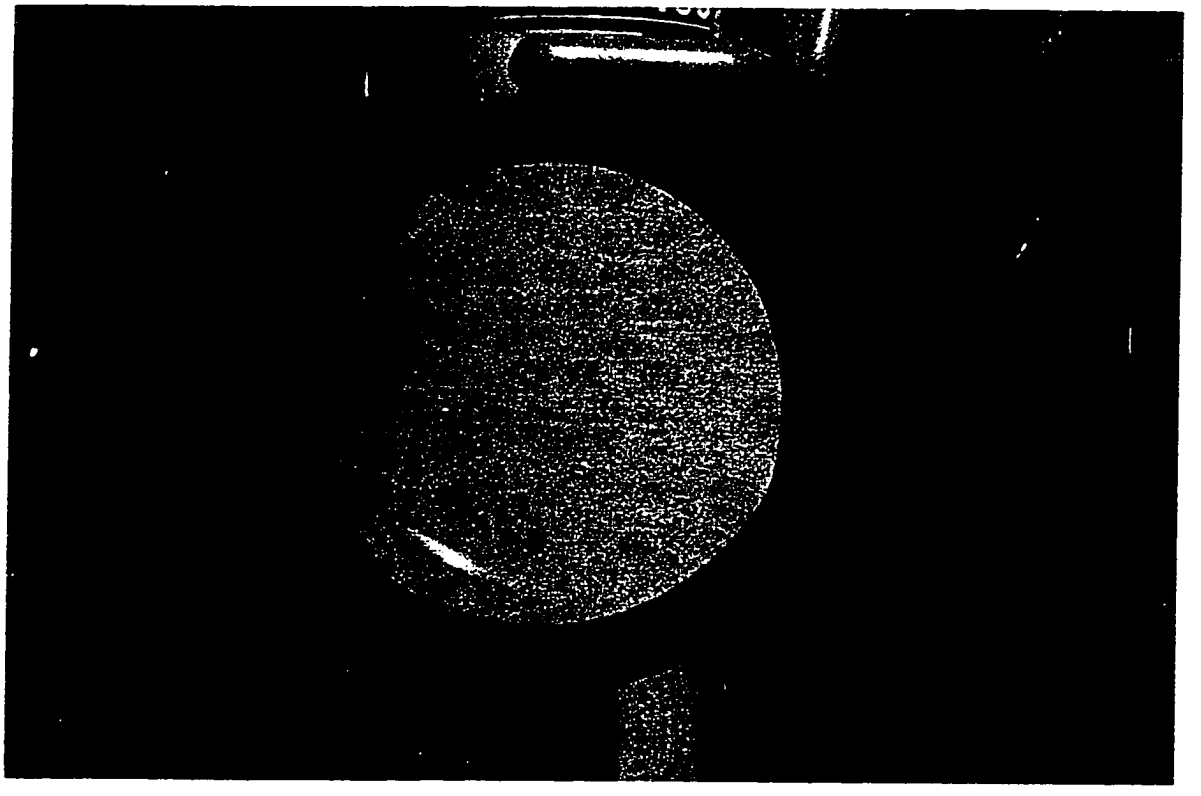

Figure 3.7 : Photograph at 220 seconds of a foam containing 0.203 % FC104 in the CO_2-generating gas

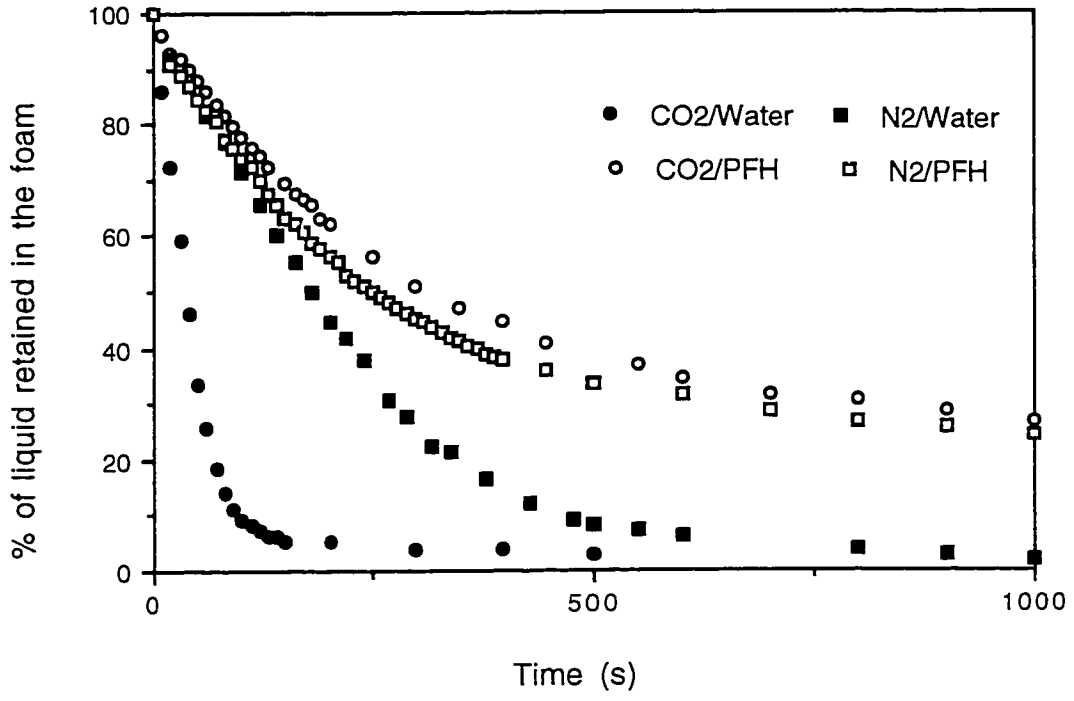

Figure 3.8 : Comparison between two gases, CO_2 and N_2, with and without PFH. Solution : 1g/L of Pluronic F68. V_O=50ml, Temperature=30°C, Rate of foam formation=0.22 cm/s.

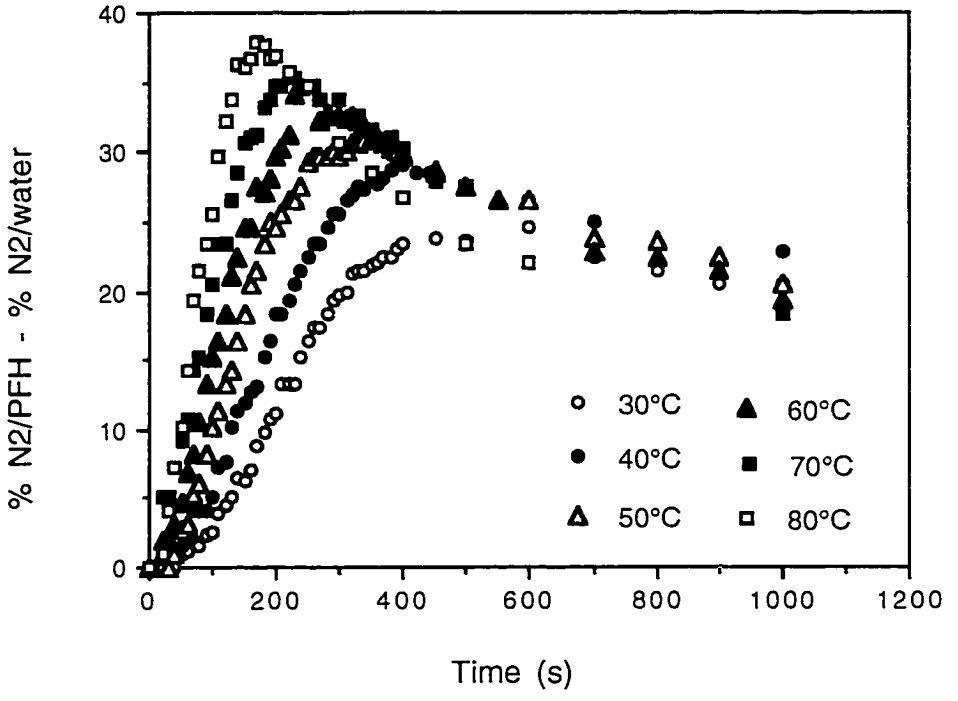

Figure 3.9 : Difference between the % of water retained in the foam in experiments with and without PFH at various temperatures. Solution: 1g/L of Pluronic F68. V_O=50ml, Rate of foam formation=0.22 cm/s.

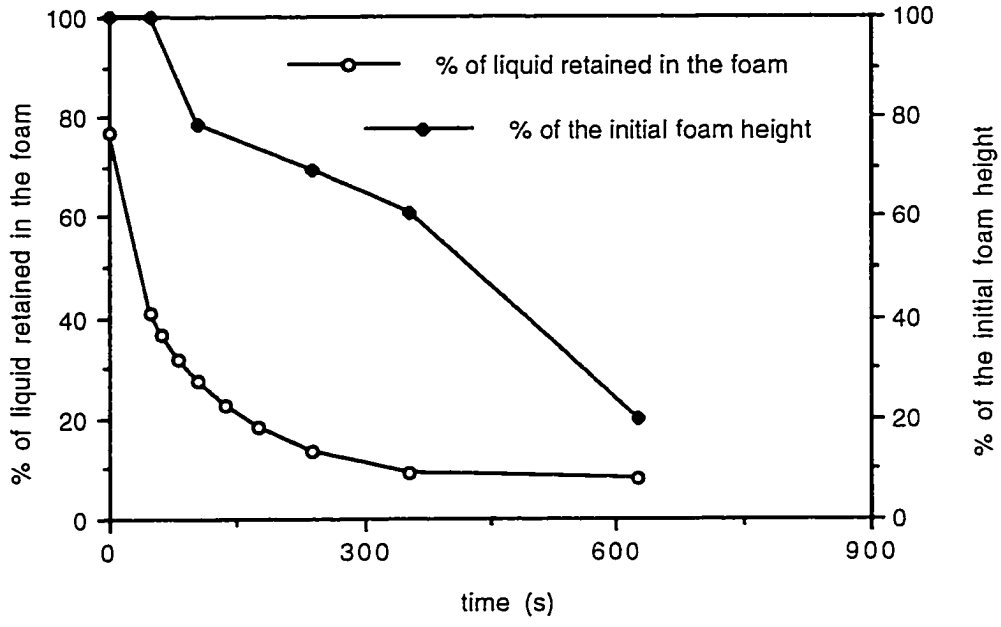

Figure 3.10a : Drainage curve and foam height of a milk protein foam as a function of time, when the foam generating gas is air.
Solution: Alapro milk protein 0.5%, V_O=50ml, Temperature= 80°C

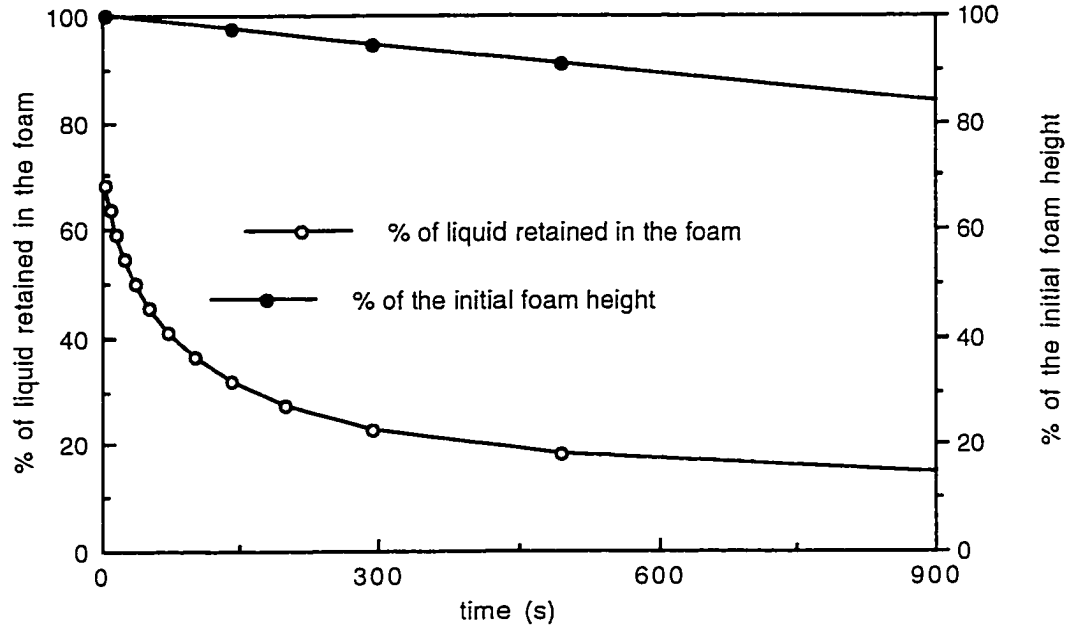

Figure 3.10b : Drainage curve and foam height of a milk protein foam as a function of time, when the foam generating gas is air with PFH.
Solution: Alapro milk protein 0.5%, V_O=50ml, Temperature= 80°C

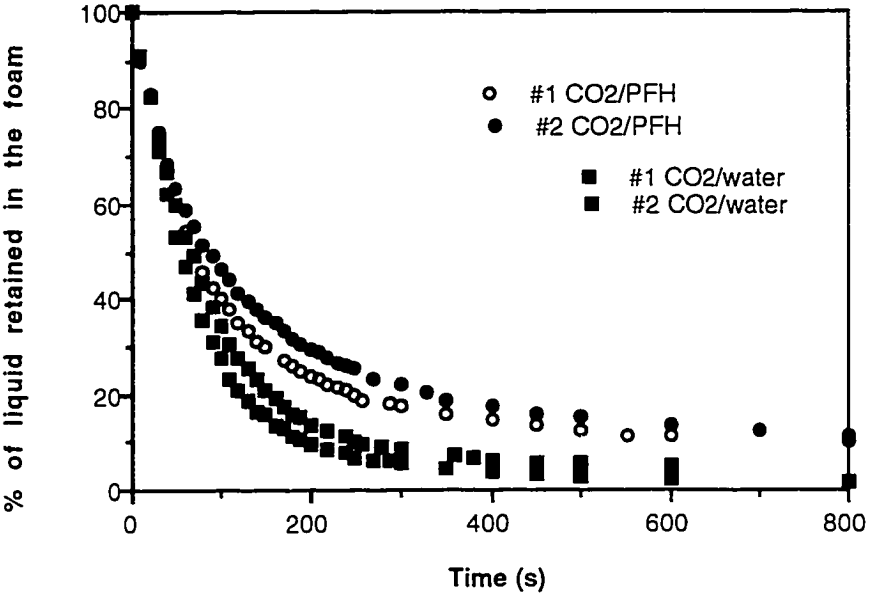

Figure 3.11a : Results of drainage experiments for formulation A.

Solution : 1g/100ml of formulation A

CO_2 saturated with water or with PFH, Foam surface velocity=0.35 cm/s

V_o=50ml, Temperature=21°C

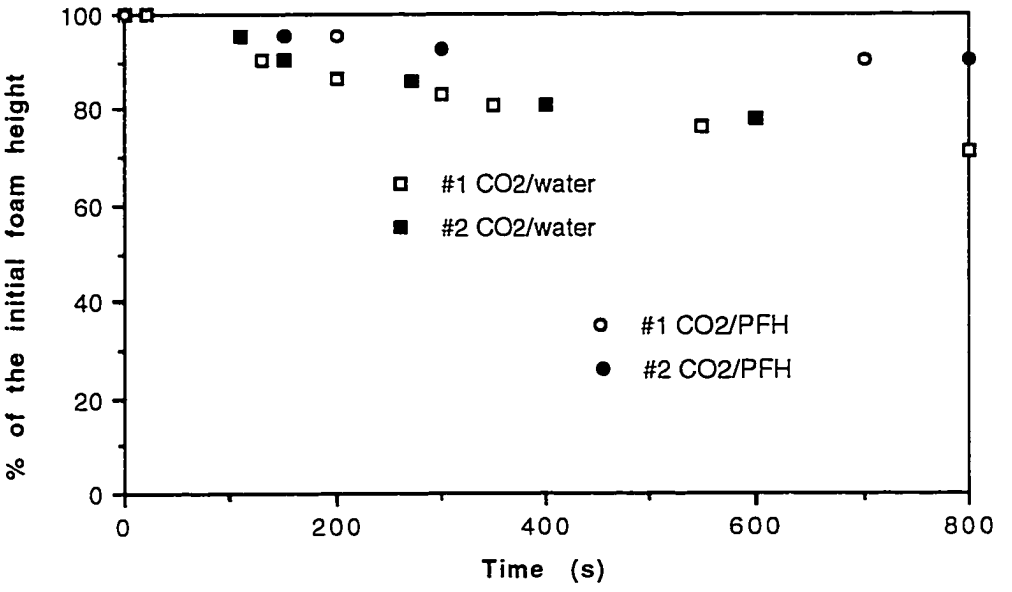

Figure 3.11b : Foam heights of drainage experiments for formulation A.

Solution : 1g/100ml of formulation A

CO_2 saturated with water or with PFH, Foam surface velocity=0.35 cm/s

V_O=50ml, Temperature=21°C

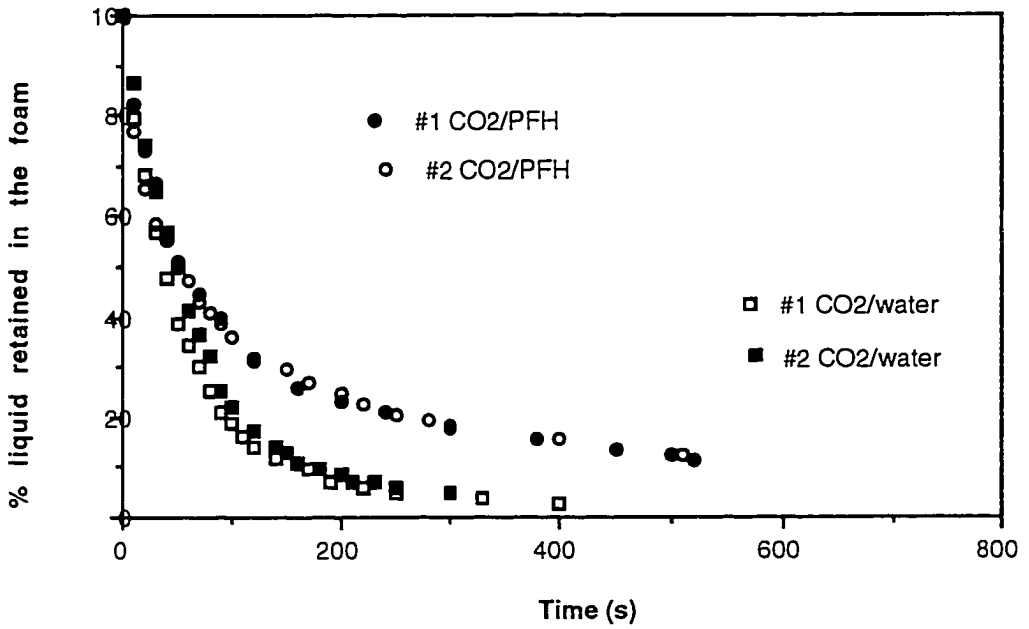

Figure 3.12a: Results of drainage experiments for formulation B.

Solution : 1g/100ml of formulation B

CO_2 saturated with water or with PFH, Foam surface velocity=0.35 cm/s

V_O=50ml, Temperature=21°C

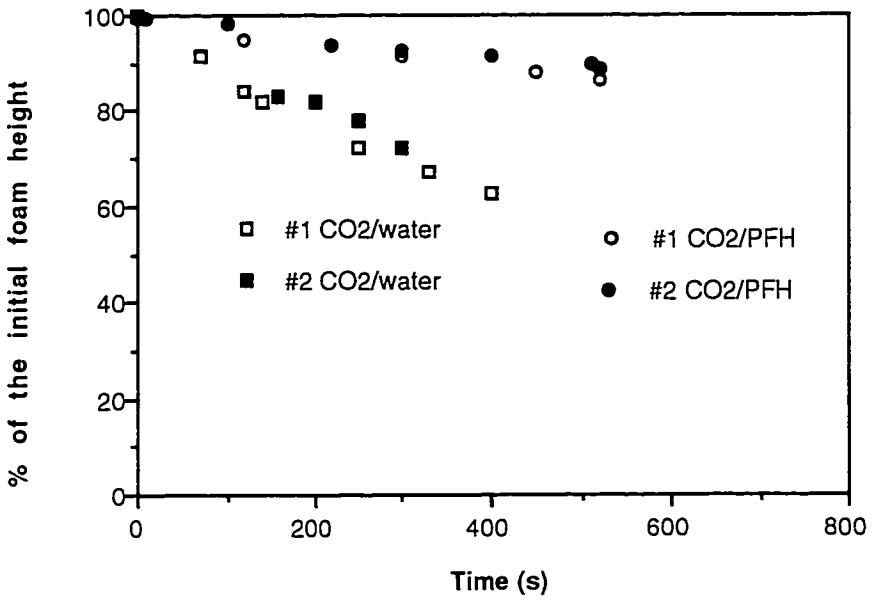

Figure 3.12b : Foam heights of drainage experiments for formulation B.

Solution : 1g/100ml of formulation B

CO_2 saturated with water or with PFH, Foam surface velocity=0.35 cm/s

V_O=50ml, Temperature=21°C

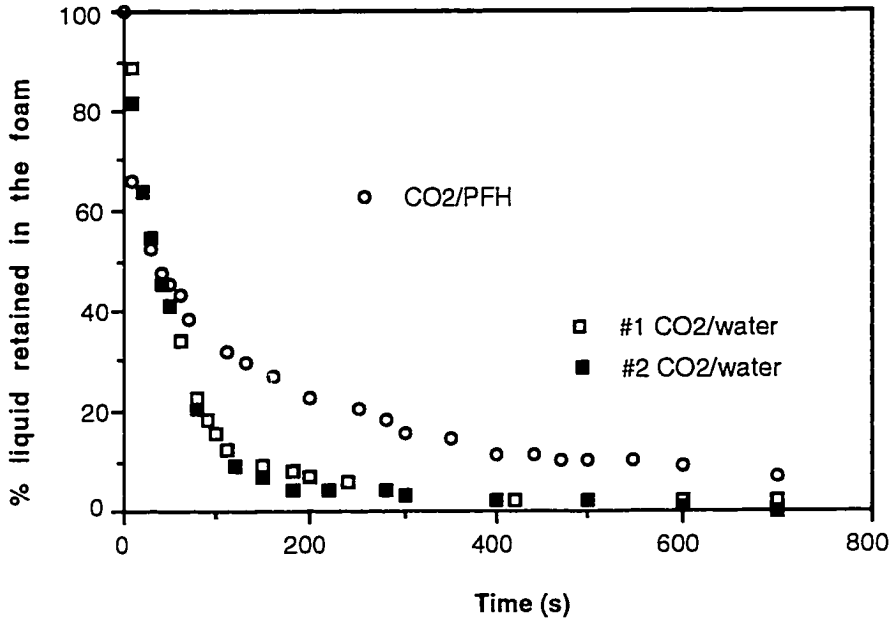

Figure 3.13a : Results of drainage experiments for formulation C.

Solution : 1g/100ml of formulation C

CO_2 saturated with water or with PFH, Foam surface velocity=0.35 cm/s

V_O=50ml, Temperature=21°C

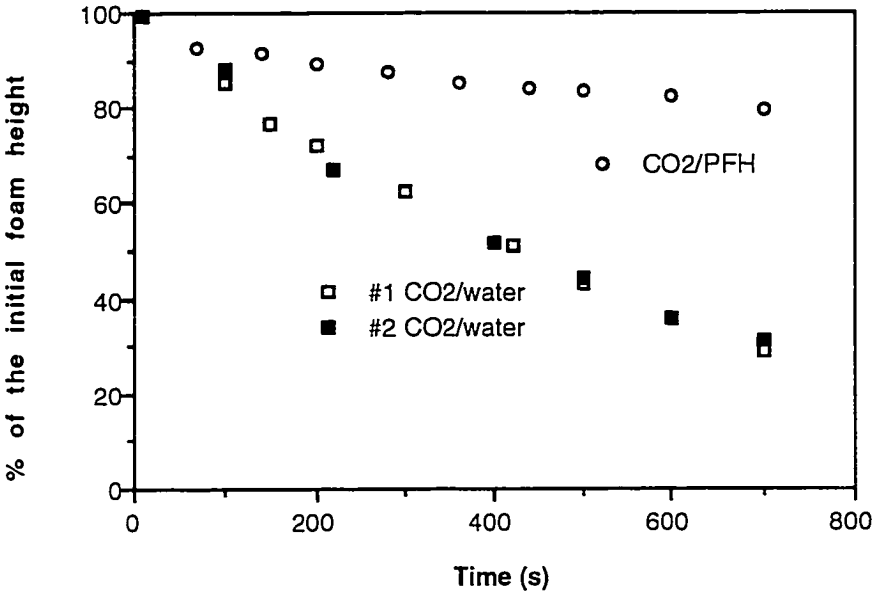

Figure 3.13b : Foam heights of drainage experiments for formulation C.

Solution : 1g/100ml of formulation C

CO_2 saturated with water or with PFH, Foam surface velocity=0.35 cm/s

V_O=50ml, Temperature=21°C

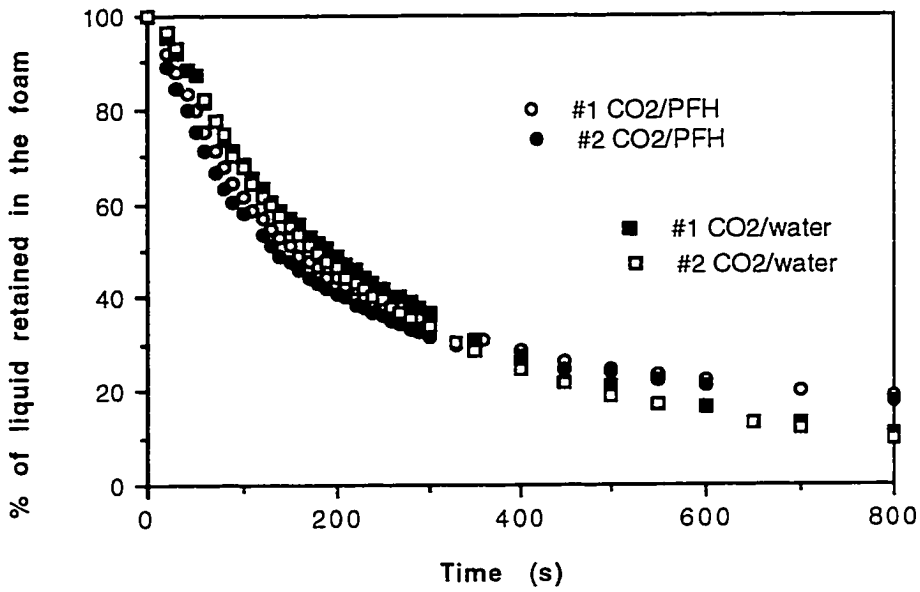

Figure 3.14a : Results of drainage experiments for formulation D.

Solution : 1g/100ml of formulation D.

CO_2 saturated with water or with PFH, Foam surface velocity=0.35 cm/s

V_0=50ml, Temperature=21°C

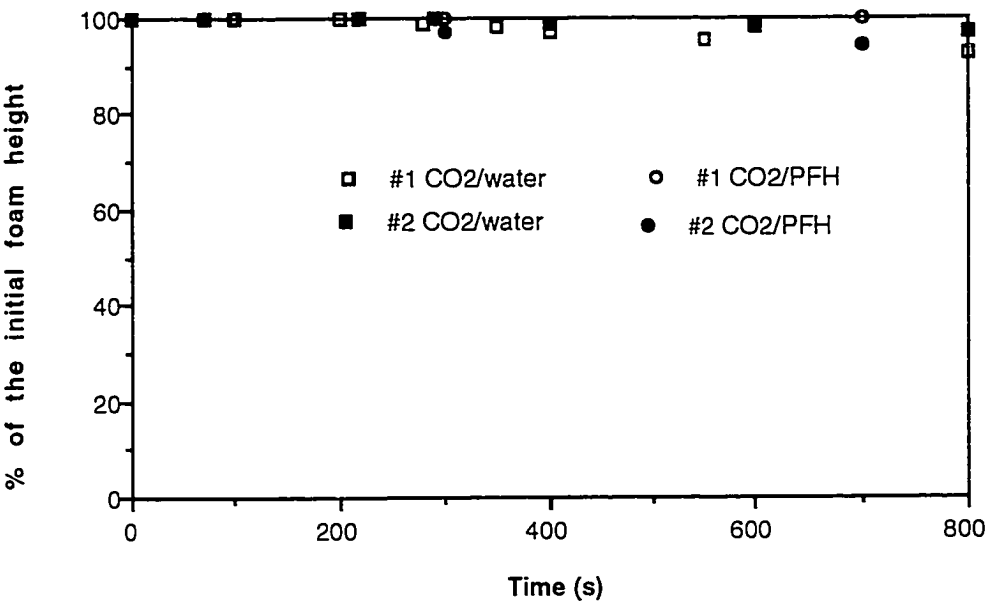

Figure 3.14b : Foam heights of drainage experiments for formulation D.

Solution : 1g/100ml of formulation D.

CO_2 saturated with water or with PFH, Foam surface velocity=0.35 cm/s

V_O=50ml, Temperature=21°C

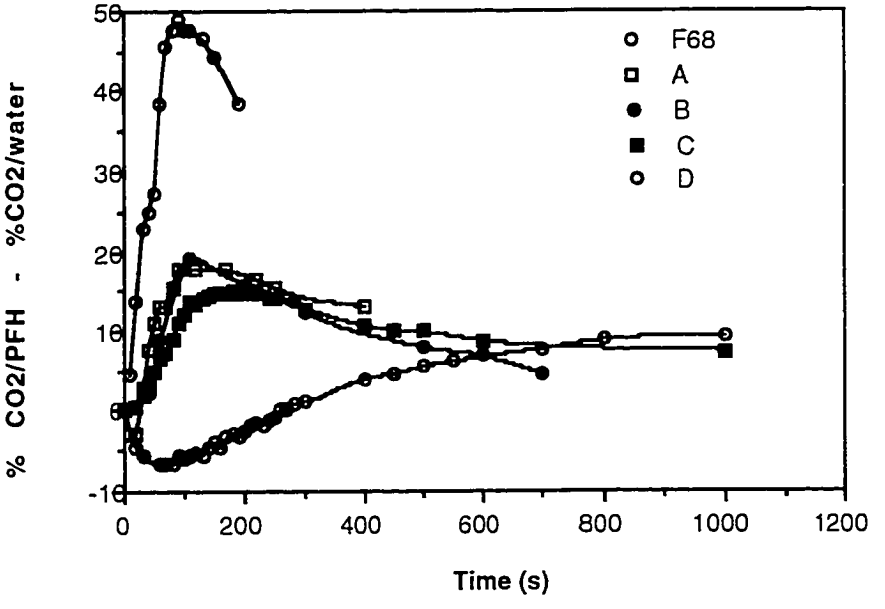

Figure 3.15: Difference between the % of water retained in the foam in experiments with and without PFH.

Solutions : 1g/100ml of Pluronic F68, formulation A, B, C and D.

V_O=50ml, Rate of foam formation=0.35 cm/s, Temperature=21°C

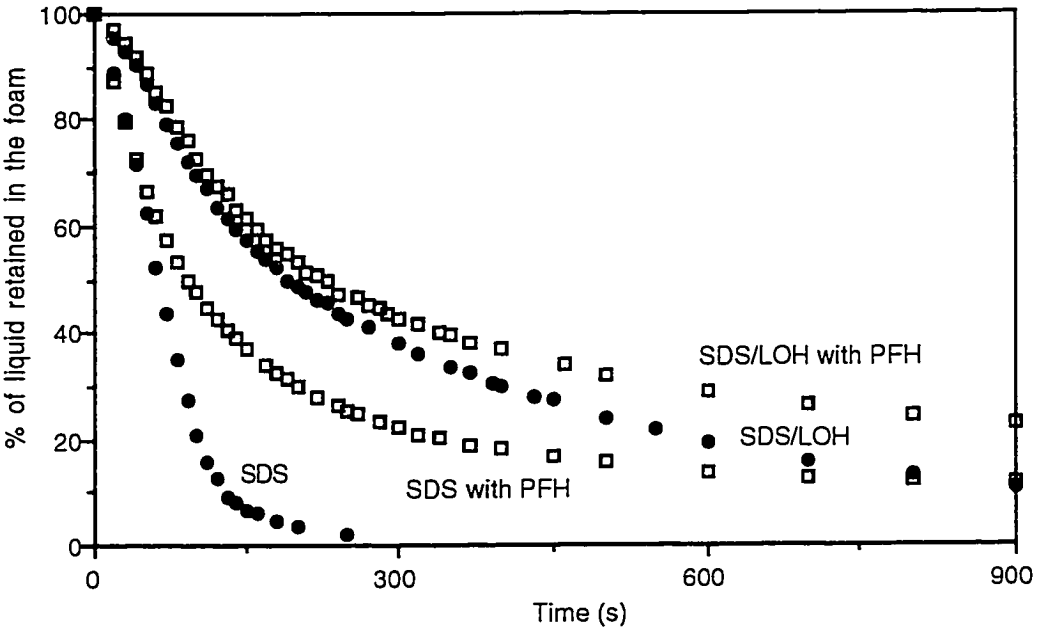

Figure 3.16 : Drainage curves for Sodium dodecyl sulfate (0.2% w/v) alone and with Lauryl alcohol (0.012% w/v)
Vo=50ml, Rate of foam formation 0.44 cm/sec, T=25°C, CO_2 foam.

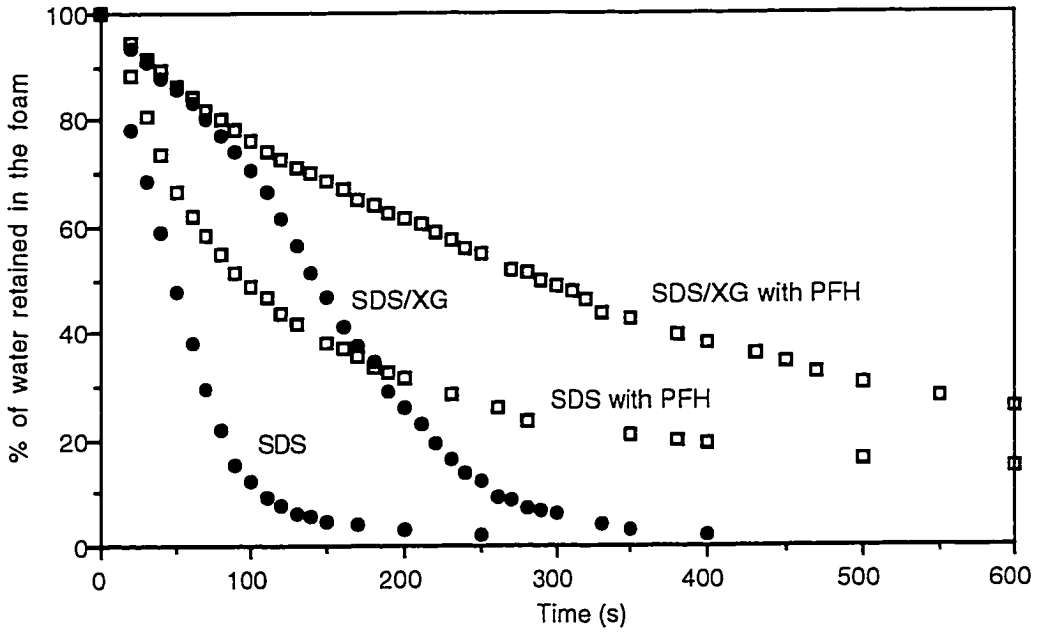

Figure 3.17 : Drainage curves for Sodium dodecyl sulfate (0.2% w/v) alone and with Xanthan Gum (0.025% w/v).
Vo=50ml, Rate of foam formation 0.44 cm/sec, T=25°C, CO_2 foam.

Fluorinert	Boiling point (°C)	Vapor Pressure at 25°C, (torr)	Molecular Weight
PFH	56	232	340
FC77	97	42	415
FC104	101	29	435
FC40	155	3	650
FC70	215	<0.1	820

Table 3.1: Physical characteristics of Fluorinert.

Temperature (°C)	Vapor Pressure (torr)	Initial % of FC104 in foam
25	28.53	3.75
0	6.35	0.835
-10	3.21	0.423
-15	2.24	0.295
-20	1.54	0.203
-30	0.696	0.0915

Table 3.2: Vapor pressure of FC104 as a function of the temperature.

Chapter 4

Models for the Behavior of Bubbles Containing a Gas Insoluble in the Continuous Phase

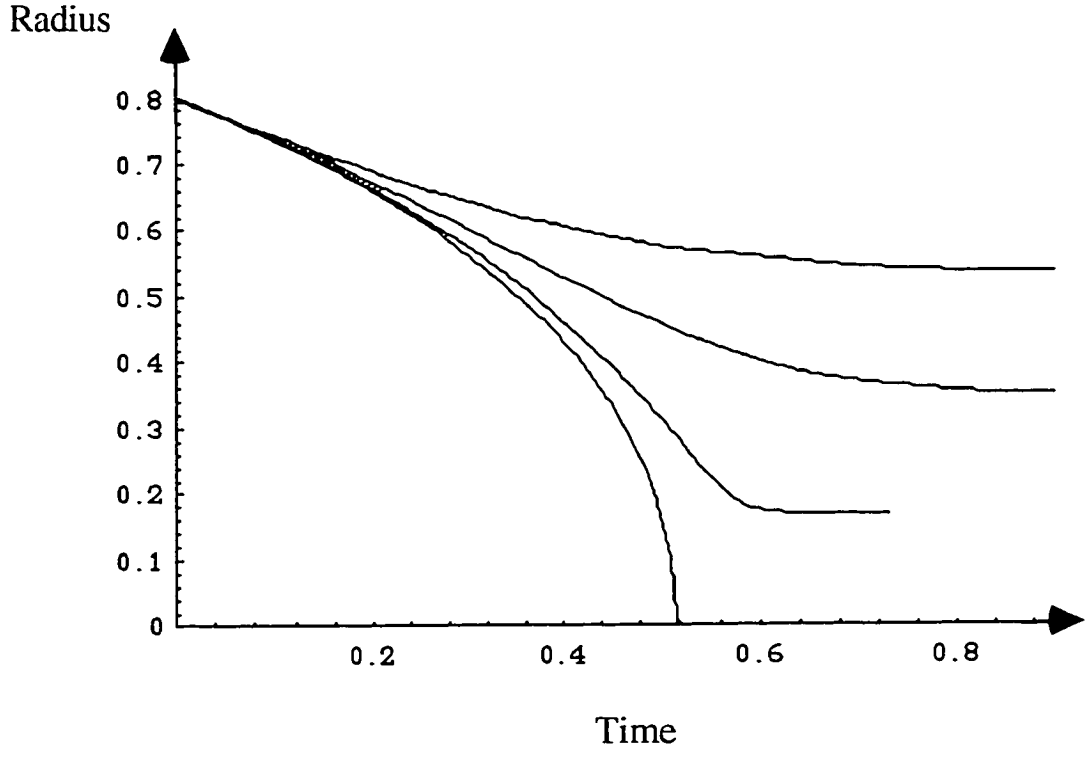

4.1 Predicting Changes in Bubble-Size Distribution due to Interbubble Gas Diffusion in Foams : Lemlich's Theory

At least two distinct spontaneous phenomena can change an existing distribution of bubble sizes in a liquid foam: one involves the rupture of the lamellae between bubbles, another the transfer of gas between bubbles by diffusion. While some liquid foams are extremely resistant to the first phenomenon, i.e., to rupture, none are immune to the second. The following treatment of interbubble gas diffusion and resultant change in bubble-size distribution builds on the work of **Lemlich**[35]. Lemlich's approach, instead of viewing the gas as diffusing directly from bubble to bubble, sees it as first diffusing into the liquid region midway between the bubbles. The concentration of gas in this liquid can be considered as being equivalent (through Henry's law) to a gas pressure in the liquid. Then, by virtue of the law of Laplace and Young, this gas-pressure equivalent can be considered to be the gas pressure that would exist within a fictitious spherical bubble of radius ρ. Thus the pressure difference ΔP_{Lap} between a bubble of any radius r and the liquid is

$$\Delta P_{Lap} = 2\gamma\left(\frac{1}{\rho} - \frac{1}{r}\right) \qquad [4.1]$$

where γ is the surface tension.

---

35 Lemlich, R., *Ind. Eng. Chem. Fund.*, 17, 89 (1978)

The molar rate of gas transfer S(r,t) from a bubble to the liquid is assumed to be given by :

$$S(r,t) = -JA\Delta P_{Lap} \qquad [4.2]$$

where J is the effective permeability of the continuous phase to the transfer and A is the surface area through which the transfer takes place. If n is the number of moles of gas in the bubble, by the conservation of moles we have $S(r,t) = -\frac{dn}{dt}$

and if we approximate A by $4\pi r^2$, Equations [4.1] and [4.2] yield

$$\frac{dn}{dt} = 8\pi J\gamma\left(\frac{r^2}{\rho} - r\right) \qquad [4.3]$$

By assuming conservation of gaseous moles throughout the foam as a whole, $\sum_i \frac{dn}{dt} = 0$. The summation is taken over all the bubbles. Using [4.3], we get

$$\sum_i n_i\left(\frac{r_i^2}{\rho} - r_i\right) = 0 \qquad [4.4]$$

where n_i is the number of bubbles of radius r_i. Equation [4.4] was first proposed by **Clark and Blackman**[36].

---

[36] Clark, N.O., Blackman, M., *Trans. Faraday Soc.*, **44**, 1 (1948)

Lemlich carried this approach further and considered an average effective ρ, independent of r but varying with time. Thus, [4.4] gives

$$\rho = \frac{\sum_i n_i r_i^2}{\sum_i n_i r_i} \quad \text{or} \quad \rho = \frac{\int_0^\infty r^2 F(r,t)dt}{\int_0^\infty rF(r,t)dt} \equiv r_{21} \qquad [4.5]$$

where F(r,t) is the frequency distribution function of r at time t.

Furthermore, as the pressure in a bubble is only slightly higher than the surrounding pressure P_a , which is typically the atmospheric pressure, from the ideal gas law and the formula for the volume of a sphere

$$n = \frac{4\pi P_a r^3}{3R_g T} \qquad [4.6]$$

where R_g is the ideal gas constant and T is the absolute temperature.

Combining Equations [4.3], [4.5], and [4.6] Lemlich deduced that the rate of change of the radius of a bubble over time is given by

$$\frac{dr}{dt} = \frac{2J\gamma R_g T}{P_a}\left(\frac{\int_0^\infty rF(r,t)dt}{\int_0^\infty r^2 F(r,t)dt} - \frac{1}{r}\right) \qquad [4.7]$$

or more succinctly

$$\frac{dr}{dt} = K\left(\frac{1}{r_{21}} - \frac{1}{r}\right) \qquad [4.8]$$

where $K = \frac{2J\gamma R_g T}{P_a}$. Thus bubbles with $r > r_{21}$ grow in size, whereas bubbles with $r < r_{21}$ shrink in size and eventually disappear.

For the sake of generality and utility in simulations, Equation [4.8] is recast in a dimensionless form as

$$\frac{dR}{dY} = \left(\frac{1}{R_{21}} - \frac{1}{R}\right) \qquad \text{with} \qquad R = \frac{r}{r_c} \qquad Y = \frac{Kt}{r_c^2}$$

where r_C is some convenient characteristic radius such as the average initial radius of the distribution.

4.2 Bubbles containing a gas insoluble in the continuous phase: Lemlich's theory modified

If the gas bubbles initially contain a certain amount of gas totally insoluble in the continuous phase, then as the bubbles change in size an osmotic pressure will develop between them. If we consider the phenomenon with two bubbles of different initial radius, initially the concentration of the insoluble vapor is constant and only the Laplace

pressure acts. Thus the smaller bubble shrinks and the larger one increases in size. As a consequence of the changes in size, the concentration of insoluble gas increases in the smaller bubble and decreases in the larger one, giving rise to an osmotic pressure opposite the Laplace pressure.

The osmotic pressure difference ΔP_{osm} that drives a flux of the soluble gas opposite the flux driven by the Laplace pressure difference can be written as:

$$\Delta P_{osm} = R_g T \Delta m$$

where R_g is the gas constant, T the absolute temperature, and Δm the difference in concentration of the insoluble gas between the fictitious bubble of radius ρ and a bubble of radius r.

Using m_o as the initial concentration of insoluble gas, and r_o and ρ_o as the initial radii of the bubble and the fictitious bubble, respectively, we get

$$\Delta P_{osm} = m_o R_g T \left(\left(\frac{r_o}{r} \right)^3 - \left(\frac{\rho_o}{\rho} \right)^3 \right) \qquad [4.9]$$

Recalling Equation [4.2], we have

$$S(r,t) = -JA\left(\Delta P_{Lap} + \Delta P_{Osm} \right) \qquad [4.10]$$

The conservation of the total number of moles of the soluble gas gives

$$\sum_i n_i\left(\frac{r_i^2}{\rho}-r_i\right)+\frac{m_o R_g T}{2\gamma}\sum_i n_i\left(\frac{r_{io}^3}{r_i}-\frac{\rho_o^3}{\rho^3}r_i^2\right)=0 \qquad [4.11]$$

Assuming that ρ is independent of r but varies with time, [4.11] would yield a cubic equation for ρ as a function of the initial radius and at time t. Without pursuing this line of reasoning, we note only that ρ is initially equal to r_{21}, and for the purpose of the following discussion we will assume that ρ has this value.

From [4.9] and [4.10], following Lemlich, we derive the rate of change of the radius with time:

$$\frac{dr}{dt}=\frac{2J\gamma R_g T}{P_a}\left[\frac{1}{r_{21}}-\frac{1}{r}+\frac{m_o R_g T}{2\gamma}\left(\left(\frac{r_o}{r}\right)^3-\left(\frac{r_{21o}}{r_{21}}\right)^3\right)\right] \qquad [4.12]$$

For the sake of generality and utility in simulations, Equation [4.12] is recast in a dimensionless form as

$$\frac{dR}{dY}=\frac{1}{R_{21}}-\frac{1}{R}+\Phi\left(\left(\frac{R_o}{R}\right)^3-\left(\frac{R_{21o}}{R_{21}}\right)^3\right) \qquad [4.13]$$

with $\quad R=\frac{r}{r_c} \qquad Y=\frac{2J\gamma R_g T}{P_a}\frac{t}{r_c^2} \qquad \Phi=\frac{m_0 R_g T r_c}{2\gamma}$

where r_C is some convenient characteristic radius, such as the average initial radius of the distribution.

4.3 Numerical simulation

4.3.1 Values for R_{21} and Φ

For values typically found in familiar liquid foams -- m_O = 0.01 mol/L, γ = 30 dynes/cm, T = 298 °K, and r_C = 1μm -- we have Φ = 0.4. With this example in mind, we see that a reasonable range of values to investigate for Φ is between 0.01 and 1.

Beginning with the empirical distribution of de Vries and the Maxwell-Boltzmann-like distribution of Bayens, we can determine the following initial values of R_{21}: 1.48 for the distribution of de Vries and 1.18 for the distribution of Bayens (Figures 4.1 and 4.2).

4.3.2 Curves of dR/dY as a function of R

Using Equation [4.13], and assuming that R_{21} is a constant equal to its initial value, we can plot dR/dY as a function of R if we know the initial value of the radius of a bubble . Figure 4.3 shows one such plot for $R_o < R_{21}$. We start with an initial radius (R_o) of 0.6. At this radius dR/dY is negative, so the radius will decrease. This initial decrease is due to the Laplace pressure; as the minimum value of dR/dY is reached, the osmotic pressure becomes more significant, equalling and then exceeding the Laplace pressure, with a resultant rapid decrease in dR/dY to a value of 0.

This equilibrium is a stable one, because if the bubble continues to shrink, dR/dY becomes positive and the radius increases again.

Figure 4.4 shows the difference in the initial rate of shrinkage for bubbles with different initial radius. We see that the smaller the bubble, the greater the Laplace pressure. For initial radii of 0.6, 0.9, and 1.3, the equilibrium radii are 0.107, 0.204, and 0.378, respectively.

4.3.3 Influence of the amount of insoluble gas

Figure 4.5 shows the effect of increasing the osmotic pressure on dR/dY. As can be seen, as we increase Φ we reduce the effect of the Laplace pressure,while the equilibrium radius increases as well. Figure 4.6 shows that an increase in Φ also leads to an equilibrium radius closer to the initial radius.

4.3.4 Variation of the radius as a function of time

As **Monsalve and Schechter**[37] showed, if we assume R_{21} to be constant, then the equation of Lemlich [4.8] (which is Equation [4.12] with $\phi = 0$), can be integrated to give :

$$Y = R_{21}\left(R - R_o + R_{21} \mathrm{Ln}\left(\frac{R - R_{21}}{R_o - R_{21}} \right) \right)$$

[37] Monsalve,A. and Schechter, R.S., *J. Colloid Interface Sci.*, **97**, 327 (1984)

We can then plot Y as a function of R (or vice versa R as a function of Y), as shown in Figure 4.7.

If we wish to take into consideration the contribution of an osmotic pressure (i.e., Φ not = 0), we integrate the equation numerically (using Mathematica) and plot R as a function of time Y: see Figure 4.7. This figure shows clearly that adding a small amount of insoluble compound prevents the bubble from disappearing, and an equilibrium radius is attained.

4.3.5 Is the hypothesis of constant R_{21} reasonable ?

As can be seen from Figure 4.8, a change in R_{21} has very little effect on the curves for dR/dY. Thus, the hypothesis of constant R_{21} is tenable, at least for $R_o < R_{21}$.

4.3.6 Stable equilibrium condition

The conditions necessary for one bubble of radius r to reach a stable equilibrium are (i) that $\frac{dr}{dt} = 0$ and (ii) that $\frac{d^2r}{dt^2} \leq 0$.

Let us expand the second condition, taking into consideration the fact that r_{21} is a function of time.

$$\frac{d^2r}{dt^2} = K\left(-\frac{1}{r_{21}^2} + 3\frac{m_o R_g T}{2\gamma}\left(\frac{r_{21o}}{r_{21}}\right)^3 \frac{1}{r_{21}}\right)\frac{dr_{21}}{dt}$$

$$\text{As } \frac{dr_{21}}{dt} \geq 0, \text{ the condition } \frac{3m_o R_g T r_{21_o}^2}{2\gamma} \leq r_{21}^2$$

must be fulfilled.

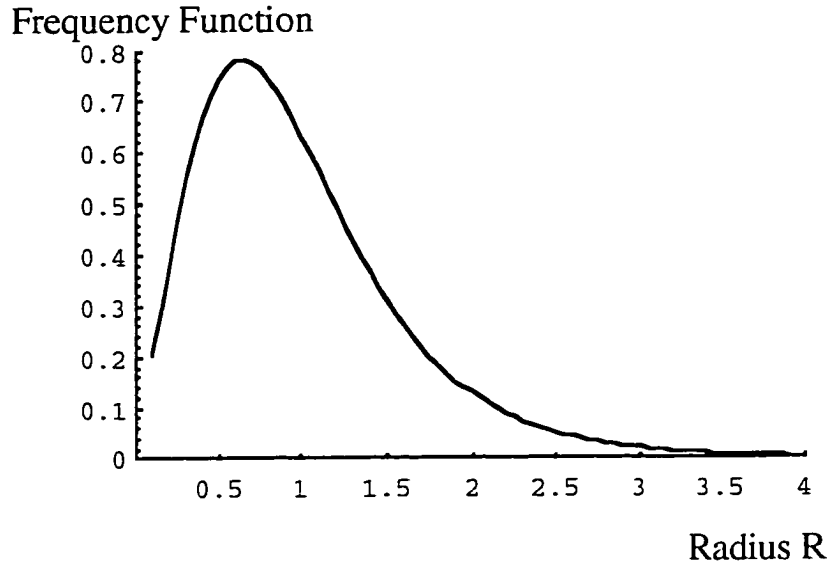

Figure 4.1 : Distribution of de Vries.

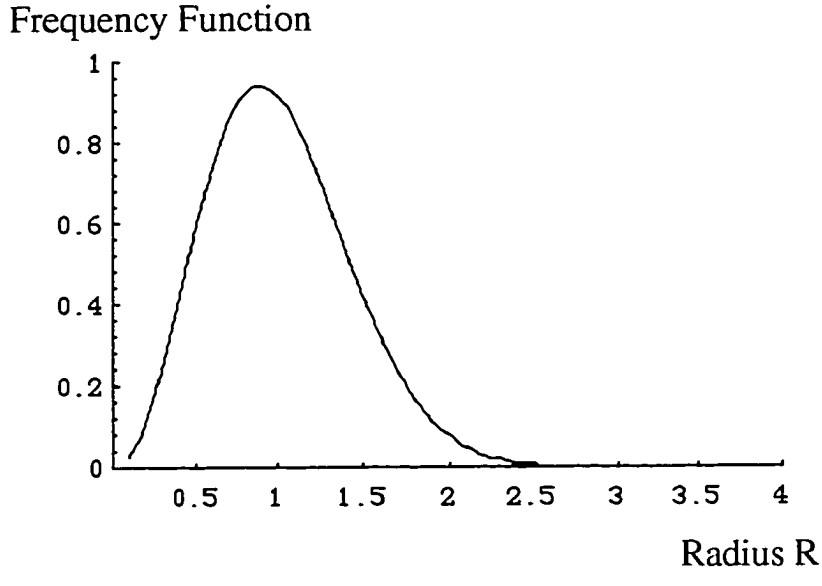

Figure 4.2 : Distribution of Bayens.

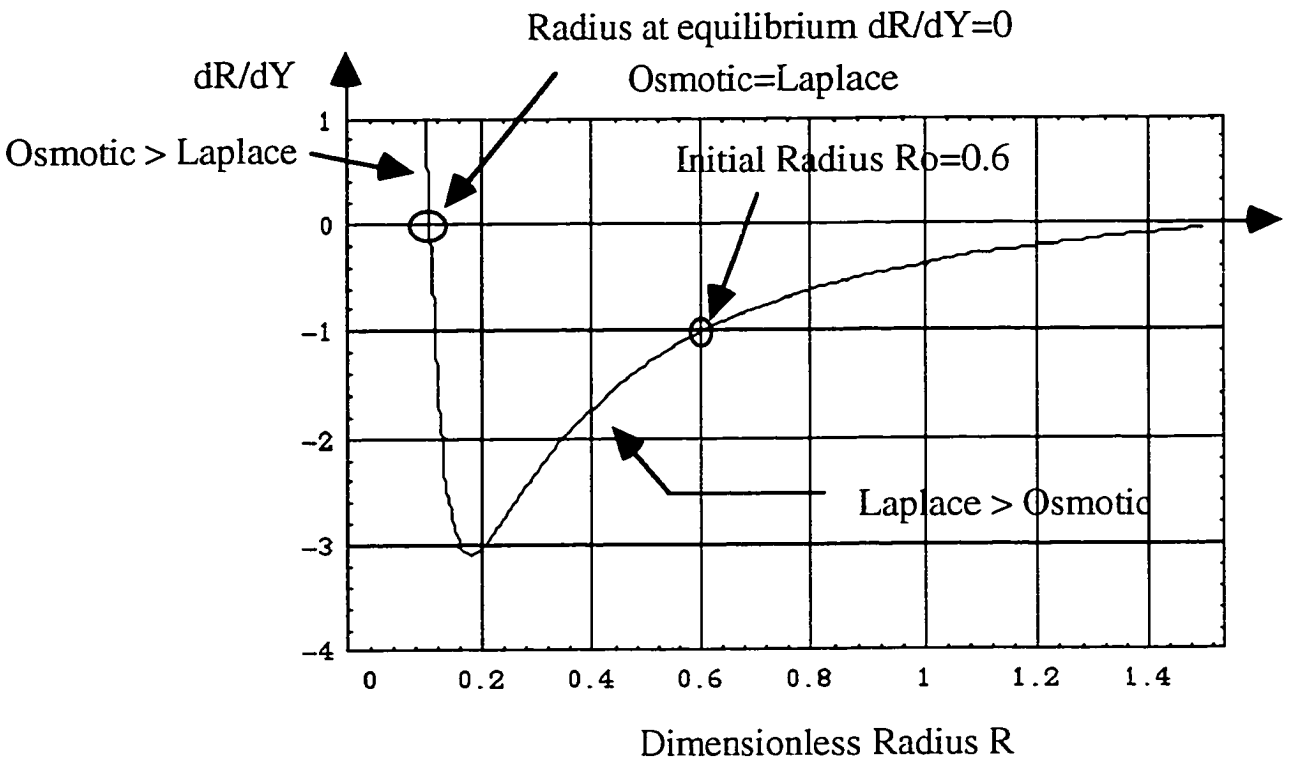

Figure 4.3 : Plot of dR/dY as a function of the radius R for

$\Phi = 0.05$, $R_{21} = 1.5$, $R_o = 0.6$

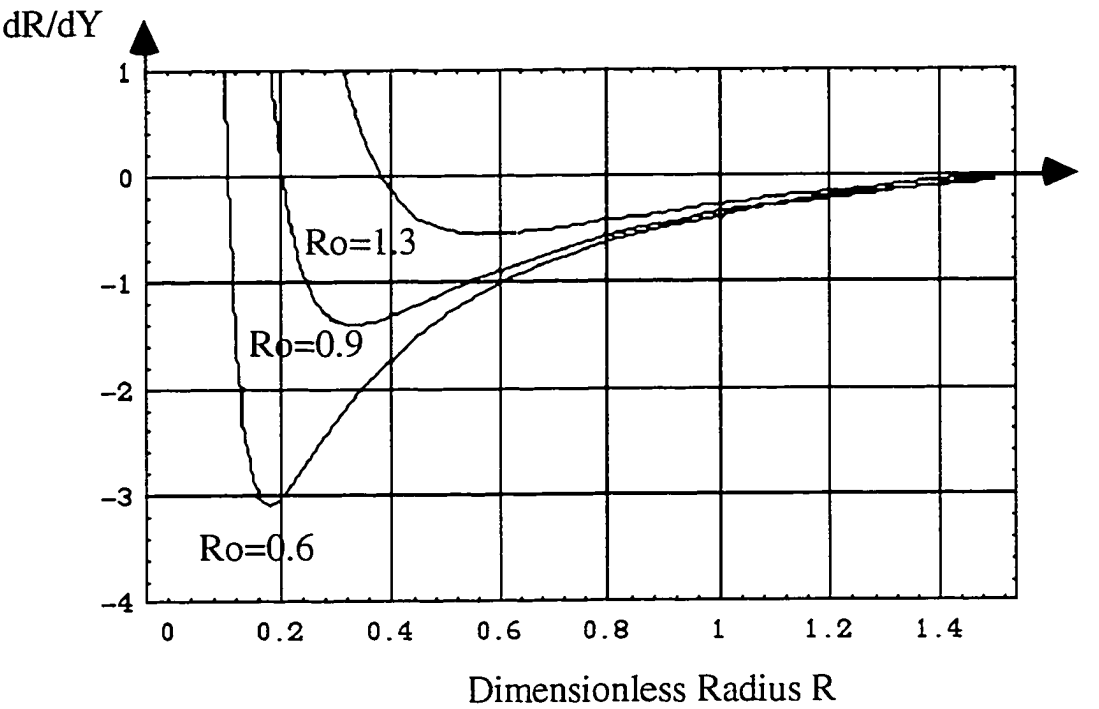

Figure 4.4 : Plot of dR/dY for several initial radii (R_o) and with $\Phi = 0.05$, $R_{21} = 1.5$.

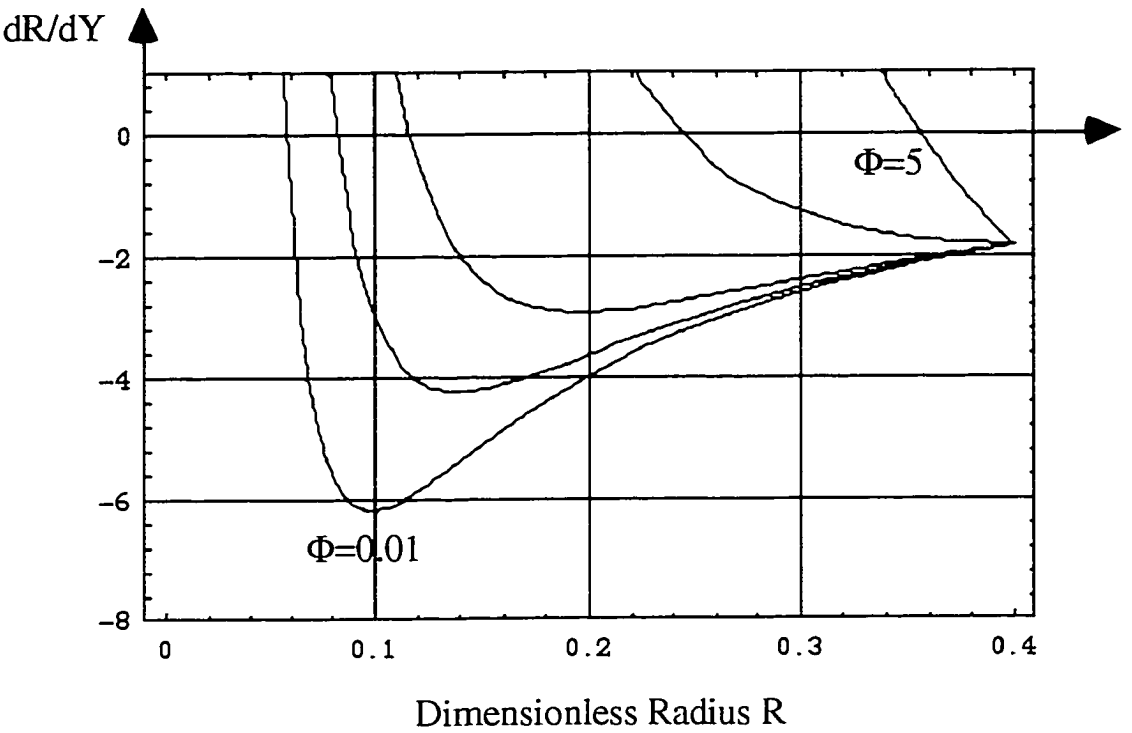

Figure 4.5 : Effect of increasing the osmotic pressure (Φ = 0.05, 0.1, 0.2, 1, 5) for R_{21} = 1.5 and R_o = 0.4.

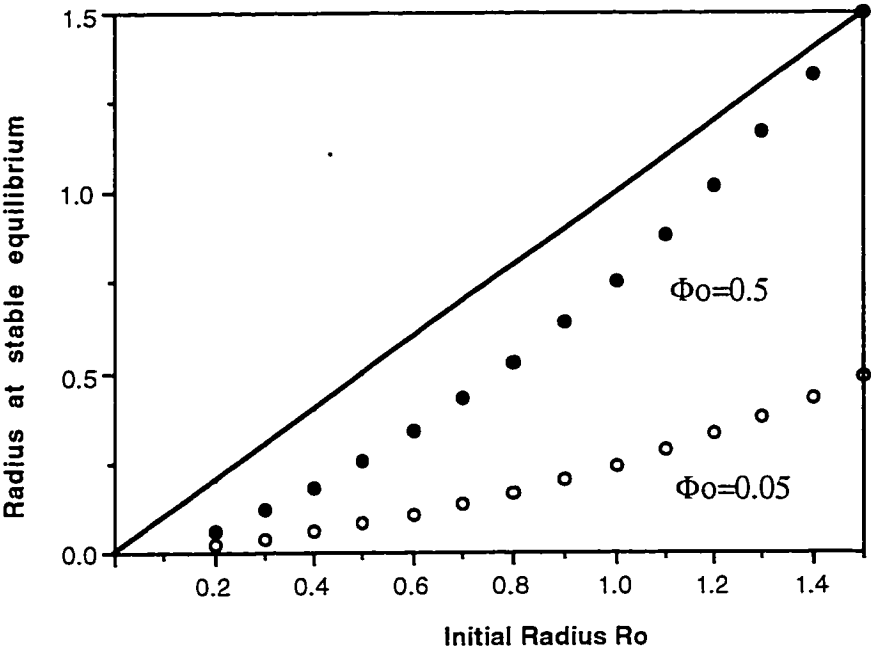

Figure 4.6 : Radius at equilibrium versus initial radius R_o

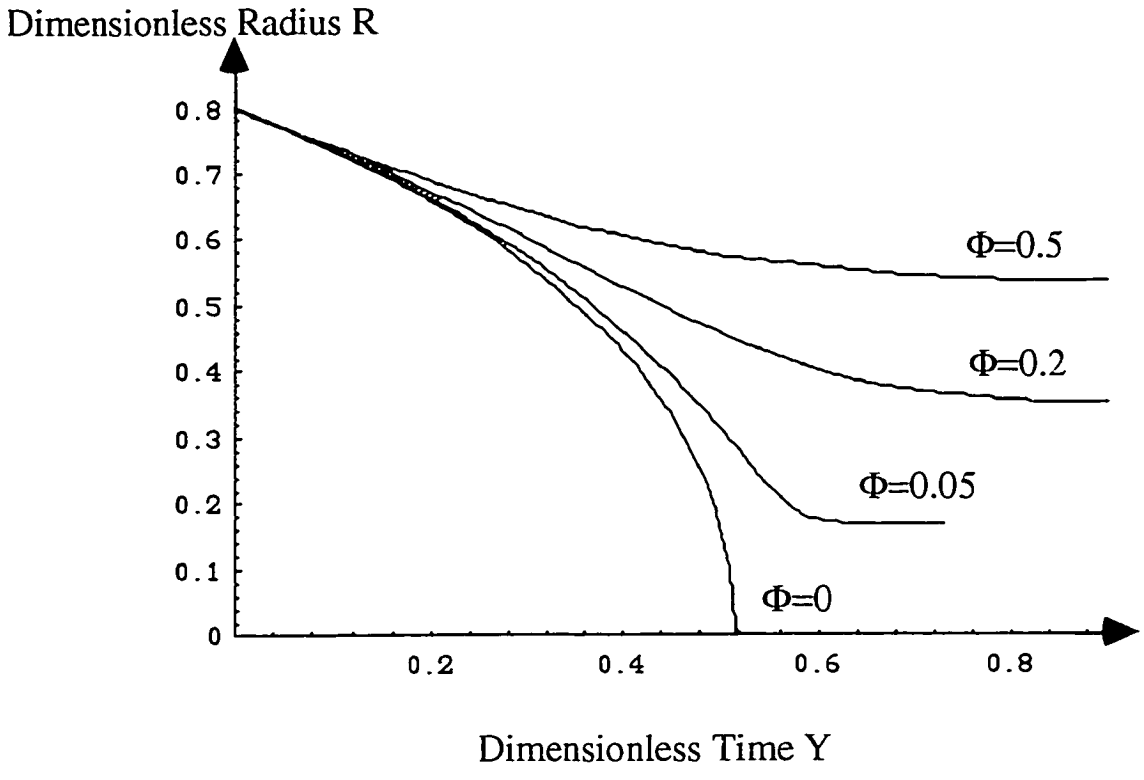

Figure 4.7 : Curves of radius versus time for a bubble with and without an osmotic pressure, with $R_0 = 0.8$, $R_{21} = 1.5$ and $\Phi = 0, 0.05, 0.2, 0.5$

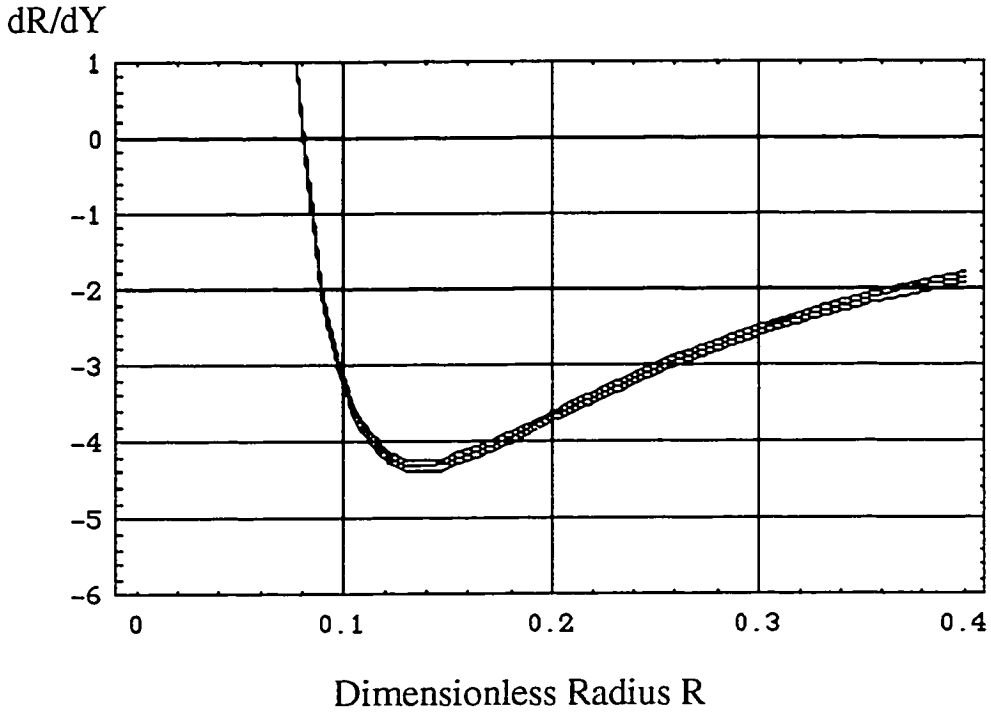

Figure 4.8 : Plot of dR/dY for different R_{21} (1.5, 1.7, 2) and $\Phi = 0.05$, $R_o = 0.5$, and $R_{21o} = 1.5$.

CONCLUSION

Our scanning electron microscope study showed that both the shape and the size of solid microspheres obtained by spray drying depend on the composition of the initial solution and on the spray-drying process itself. The particles observed in the micrographs ranged in diameter from 10 μm to 300 μm, with shapes including both regular and collapsed blood cell like spheres and with surfaces both smooth and flaky. Most internal structures resemble thin or thick shelled hollow spheres. When the microspheres were obtained by foam spray-drying, the internal structure contained either a large cavity with a thick wall containing small voids or was full of voids separated by plateau borders thus resembling a dry foam. All these micrographs showed that these microspheres entrapped gas which could be released by dissolution in an aqueous phase.

The tensiolaminometric technique enables us to determine the surface tension of the initial solution and its ability to form a liquid lamella. Using this technique, we noticed the interaction between Non-fat dry milk and sugar ester. Furthermore, one way to increase the foamability of the non fat dry milk solution was to use a polymer such as carboxy methyl cellulose which increases the viscosity of the solution and reduces the rate of drainage of the water in the film.

Our theoretical work shows that when two bubbles are of unequal size and sufficient amount of nondiffusible vapor is present, disproportionation is limited. These results are not surprising; the literature on emulsions provides ample evidence that adding to the droplets a compound that is insoluble in the continuous phase results in considerable reduction of Ostwald ripening. In the case of foams, liquid drainage from the foam due to interbubble gas diffusion (as distinct from that due to gravitation) can therefore often be greatly reduced by adding a water-insoluble vapor to the foam-generating gas: the presence of such a vapor counterbalances the Ostwald ripening, thus stabilizing the system. The theory also predicts that the foam may be polydispersed or may be a bimodal system. Strong evidence of this point has been observed experimentally.

The contributions of the structure and the interbubble permeability (or lack of gas diffusion) of the lamella were demonstrated by comparing two systems: in the first one the diffusion was prevented by adding perfluorohexane to the foam generating gas and in the second one the diffusion was not prevented. Systems containing a mixture of surfactants, hydrosoluble polymers and certain proteins were much less affected by gas diffusion due to the properties of the film.

APPENDIX

Appendix 1

Relationship between the position of the frame and the angle at the top of the meniscus

Let us consider the plane of the main section of a liquid meniscus, perpendicular through the middle of the horizontal frame of unit width.

A very small element dS (Figure 1) is on this section in equilibrium under the action of the capillary and the hydrostatic forces, so:

$$pdS+\gamma d\theta=0 \qquad [1]$$

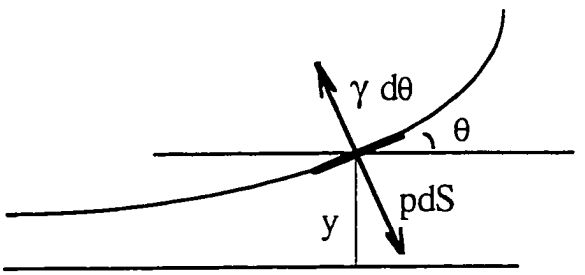

Figure 1 : Schematic of the forces at the interface.

As p is the hydrostatic pressure, we can write $p=\rho gy$, with ρ the density of the liquid, y the vertical position of dS above the horizontal surface, and g the gravitational constant. Thus Equation 1 gives:

$$\rho gy = \frac{d\theta}{dS} \qquad [2]$$

but as $\tan\theta = \frac{dy}{dx} = y' \quad \Rightarrow \quad d\theta = \frac{y''}{1+y'^2}dx$

and $dS = \sqrt{dx^2 + dy^2} = dx\sqrt{1+y'^2}$

we get by substitution in Equation 2:

$$\frac{\rho g y}{\gamma} = \frac{y''}{(1+y'^2)^{\frac{3}{2}}} \qquad [3]$$

To resolve this differential equation, let us set $u = \frac{dy}{dx} = y'$

Then $\frac{d^2y}{d^2x} = y'' = \frac{du}{dy}\frac{dy}{dx} = u\frac{du}{dy}$

Now Equation 3 becomes: $\frac{\rho g y}{\gamma} = \frac{u}{(1+u^2)^{\frac{3}{2}}}\frac{du}{dy}$

By integrating Equation 3

$$\int \frac{\rho g y}{\gamma} dy = \int \frac{u}{(1+u^2)^{\frac{3}{2}}} du$$

we get $\frac{\rho g y^2}{2\gamma} = \text{constant} - \frac{1}{\sqrt{1+u^2}}$

For y=0, u=0; thus constant=1. Furthermore, as $\frac{1}{\sqrt{1+u^2}} = \cos\theta$, we finally obtain the relationship between y and θ:

$$y = \sqrt{\frac{2\gamma}{\rho g}(1-\cos\theta)}$$

Appendix 2

Shape and equation of the liquid meniscus

The equation $y = \sqrt{\frac{2\gamma}{\rho g}(1-\cos\theta)}$ can be written as: $\frac{dy}{dx} = \frac{y\sqrt{(2h^2 - y^2)}}{h^2 - y^2}$.

By integrating, we get the relationship between x and y.

$$x = x_0 - \sqrt{(2h^2 - y^2)} + \frac{h}{\sqrt{2}} \mathrm{Ln}\left(\frac{h\sqrt{2} + \sqrt{(2h^2 - y^2)}}{y}\right)$$

For y=h, x=0; thus $x_0 = h\left(1 - \frac{1}{\sqrt{2}}\mathrm{Ln}\left(1+\sqrt{2}\right)\right) \approx 0.377h$.

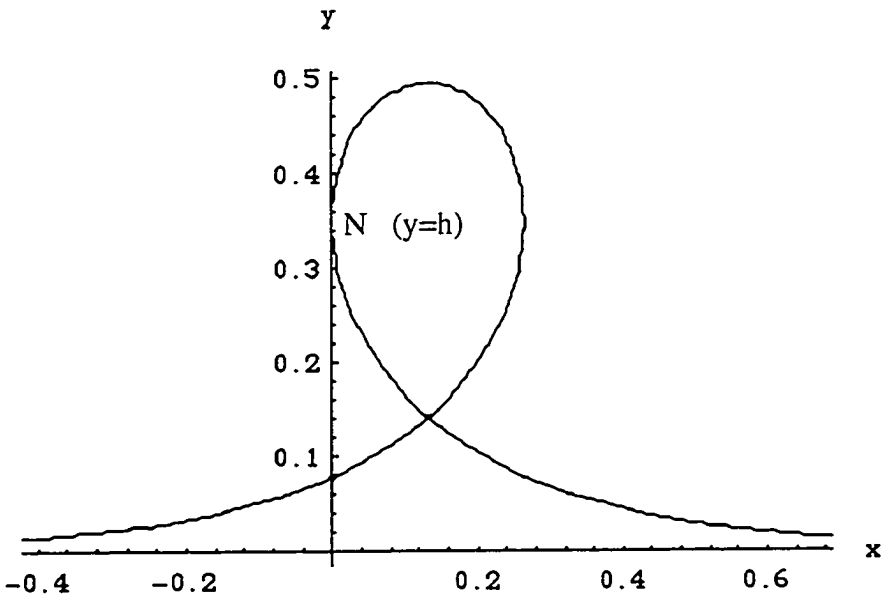

Figure 2 : Shape of the meniscus.

Appendix 3

Work necessary to lift the frame from the bulk of the solution

The work W necessary to lift the frame is: $W = \int_0^y F dy$

Thus:

$$W = \int_0^y F dy = \int_0^\theta 2\gamma \sin\theta d\left(h\sqrt{(1-\cos\theta)}\right)$$

$$= \int_0^\theta 2\gamma \sin\theta \frac{h\sin\theta d\theta}{2\sqrt{(1-\cos\theta)}} = \int_0^\theta \gamma h \sin\theta \sqrt{(1+\cos\theta)} d\theta$$

$$= 4\gamma h\sqrt{2}\int_0^\theta \cos^2\frac{\theta}{2} d\left(\cos\frac{\theta}{2}\right) = \frac{4}{3}\sqrt{2}\gamma h\left(1-\cos^3\frac{\theta}{2}\right)$$

(For the integration we use the fact that when θ=0, W=0.)

The work P against gravity for raising the liquid into the meniscus is calculated as follows:

$$P = 2\int_0^\infty \frac{1}{2}\rho g y^2 dx = \int_0^\infty \rho g h^2 (1-\cos\theta) dx$$

$$= \int_0^\theta \rho g h^2 (1-\cos\theta) \frac{h\cos\theta d\theta}{2\sqrt{(1-\cos\theta)}}$$

$$= \int_0^\theta \rho g h^3 \sqrt{(1-\cos\theta)} \frac{\cos\theta d\theta}{2}$$

$$= \gamma h \int_0^\theta \sqrt{(1-\cos\theta)} \cos\theta d\theta$$

$$= 2\sqrt{2}\gamma h \int_0^\theta \sin\frac{\theta}{2}\left(2\cos^2\frac{\theta}{2}-1\right) d\frac{\theta}{2}$$

$$= 2\sqrt{2}\gamma h\left(-\frac{2}{3}\cos^3\frac{\theta}{2}+\cos\frac{\theta}{2}-\frac{1}{3}\right)$$

(For the integration we use the fact that when θ=0, P=0.)

The work S against the surface cohesion of the liquid while increasing the liquid-air interface is given by: $S = 2\gamma\int_0^{\theta}(dS - dx)$

Using the relations

$$dx = \frac{h\cos\theta d\theta}{2\sqrt{(1-\cos\theta)}} \text{ and } dy = \frac{h\sin\theta d\theta}{2\sqrt{(1-\cos\theta)}}$$

and

$$dS = \sqrt{x^2 + y^2}$$

we calculate S:

$$\begin{aligned} S &= \gamma h\int_0^{\theta}\sqrt{(1-\cos\theta)}d\theta \\ &= 2\sqrt{2}\gamma h\int_0^{\theta}\sin\frac{\theta}{2}d\frac{\theta}{2} \\ &= 2\sqrt{2}\gamma h\left(1-\cos\frac{\theta}{2}\right) \end{aligned}$$

(For the integration we use the fact that when θ=0, S=0.)

By comparing W, P, and S, we observe that W=P+S.

Appendix 4

The Laplace Equation.

In the absence of force fields (the gravitational field, for example), a soap bubble is spherical, this being the shape of minimum surface area for a given enclosed volume. Consider a soap bubble of radius r; its total surface free energy is $8 \pi r^2 \gamma$ and if the radius were to decrease by dr, then the change in surface free energy would be $16 \pi r \gamma$ dr. Since shrinking decreases the surface energy, the tendency to do so must be balanced by a difference in pressure across the film ΔP. The work against this pressure difference $\Delta P\ 8 \pi r^2$ dr is just equal to the decrease in the surface free energy. Thus,

$$\Delta P\ 8\pi r^2\ dr = 16 \pi r \gamma\ dr$$

or

$$\Delta P = \frac{2\gamma}{r}$$

which is the Laplace equation for spheres.

The **General Laplace equation** is:

$$\Delta P = \gamma\left(\frac{1}{r_1} + \frac{1}{r_2}\right)$$

where r_1 and r_2 are orthogonal radii of curvature. In the case of a sphere we have $r_1 = r_2 = r$.

We thus arrive at the important conclusion that the smaller the bubble, the greater the pressure inside compared to that outside. This conclusion is easily verified experimentally by arranging two bubbles with a common air connection, as illustrated in Figure 3. The arrangement is unstable, and the smaller of the two bubbles will shrink while the other grows.

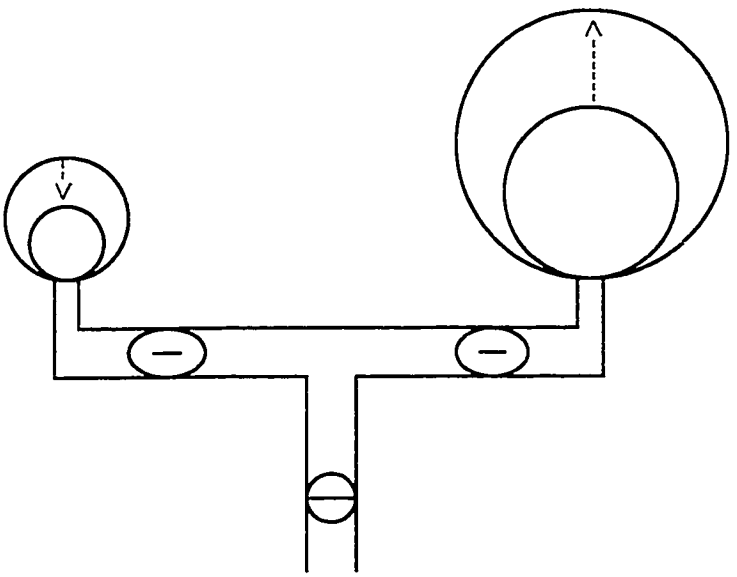

Figure 3: Illustration of the equation of Laplace

BIBLIOGRAPHY

Brown, A.G., Thuman, W.C., and McBain, J.W., *J. Colloid Interface Sci.* **8**, 491 (1953)

Brown, A.G., Thuman, W.C., and McBain, J.W., *J. Colloid Interface Sci.* **8**, 508 (1953)

Buma, T.J., *Neth. Milk Dairy J.*, **25**, 33, (1971)

Buma, T.J. and Henstra S., *Neth. Milk Dairy J.*, **25**, 75, (1971)

Clark, N.O., Blackman, M., *Trans. Faraday Soc.*, **44**, 1 (1948)

Crosby, E.J. and Weyl, R.W., *AIChE Symp. Ser.*, **73**, 82 (1977)

Davis, S.S., Round, H.P., and Purewal, T.S., *J. Colloid Interface Sci.* **80,** 508 (1981)

Eydt, A.J. and Rosano, H.L., *Journal of the American Oil Chemists Society*, **45**, 607, (1967)

Fäldt, P. and Bergenståhl, B., *Colloids Surfaces A: Physicochem. Eng. Aspects*, **90**, 183, (1994)

Fäldt, P. and Bergenståhl, B., JAOCS, **72**, n° 2, 171, (1995)

Frey, D.D. and King, C.J., *Ind. Eng. Chem. Fundam.*, **25**, 723 (1986)

Falls, A.H., Lawson, J.B., and Hirasaki, G.J., *JPT*, Jan., 95 (1988)

Higuchi, W.I. and Misra, J., *J. Pharm. Sci.* **51,** 459 (1962)

Kaláb, M., Caric, M. and S. Milanovic, *Food Struct.*, **10**, 327, (1991)

Kaláb, M., *Food Struct.*, **12**, 95 (1993)

Kabalnov, A.S., and Schukin, E.D., *Adv. Colloid Interface Sci.* **38,** 69 (1992)

Kabalnov, A.S., Weers, J.G., Arlauskas, R.A., and Tarara, T.E., *Langmuir* **11,** 2966 (1995)

Kabalnov, A.S., Pertzov, A.V. and Schukin, E.D., *Colloids Surf.* **24,** 19 (1987)

Lemlich, R., *Ind. Eng. Chem. Fund.* **17**, 89 (1978)

Masters, K., Spray Drying Handbook, 5th ed., John Wiley & Sons Inc., New York (1991)

Mistry, V.V. and Hassan, H.N., *J. Dairy Sci.*, **11**, 3716, (1991)

Mistry, V.V., Hassan, H.N. and Robison, D.J., *Food Struct.*, **11**, 73, (1992)

Monsalve, A., and Schechter, R.S., *J. Colloid Interface Sci.* **97,** 327 (1984)

Princen, H.M., Overbeek, J.TH.G., and Mason, S.G., *J. Colloid Interface Sci.* **24**, 125 (1967)

Ronteltap, A.D., Damste, B.R., De Gee, M. and Prins, A., *Colloids and Surfaces* **47**, 269 (1990)

Sarma, D.S.H.S.R., Pandit, J., and Khilar, K.C., *J. Colloid Interface Sci.* **124,** 339 (1988)

Ranadive, A.Y., and Lemlich, R., *J. Colloid Interf. Sci.* **70**, 392 (1979)

Verhey J.G.P., *Neth. Milk Dairy J.*, **26**, 186, (1972)

Verhey J.G.P., *Neth. Milk Dairy J.*, **26**, 203, (1972)

Weers, J.G., Ni, Y., Tarara, T.E., Pelura, T.J., and Arlauskas, R.A, *Colloids Surf.* **84,** 81 (1994)

Weers, J.G. and Arlauskas, R.A., *Langmuir* **11,** 477 (1995)

Weaire, D., and Pageron V., *Phil. Mag. Lett.*, **62**, 417 (1990)

Yu, M., and Damodaran, S., *J. Agric. Food Chem.* **39,** 1555 (1991)

IMAGE EVALUATION TEST TARGET (QA-3)

150mm

6"

APPLIED IMAGE . Inc
1653 East Main Street
Rochester, NY 14609 USA
Phone: 716/482-0300
Fax: 716/288-5989